STUDIES ON DEVELOPMENT OF MgB_2 SUPERCONDUCTING WIRES FOR CRYOGEN FREE MAGNET APPLICATION

Thesis submitted to
Cochin University of Science and Technology (CUSAT)
in partial fulfilment of the requirements for the award of the degree
of
Doctor of Philosophy in **Physics**
Under the **Faculty of Science**

By

Rahul S

under the supervision of

Dr. Manoj Raama Varma & Dr. U Syamaprasad

National Institute for Interdisciplinary Science and Technology
(Council of Scientific and Industrial Research)
Thiruvananthapuram-695019

November 2017

STUDIES ON DEVELOPMENT OF MgB_2 SUPERCONDUCTING WIRES FOR CRYOGEN FREE MAGNET APPLICATION

Ph.D. Thesis

November 2017

Author:

Rahul S

Materials Science and Technology Division,
CSIR-National Institute for Interdisciplinary Science and Technology,
Thiruvananthapuram – 695019.

Supervising guide:

Dr. Manoj Raama Varma

Senior Principal Scientist
Material Science and Technology Division
National Institute for Interdisciplinary Science and Technology (CSIR)
Trivandrum-695019
Email: manojraamavarma@niist.res.in
Tel: 0471 2515377

Co-Guide:

Dr. U. Syamaprasad

Former Chief Scientist
Material Science and Technology Division
National Institute for Interdisciplinary Science and Technology (CSIR)
Trivandrum-695019
Email: syamcsir@gmail.com
Tel: 0471 2741830

To my family

DECLARATION

I, Rahul S, hereby declare that the thesis entitled **"STUDIES ON DEVELOPMENT OF MgB_2 SUPERCONDUCTING WIRES FOR CRYOGEN FREE MAGNET APPLICATION"** is a bona fide record of the research work carried out by me in the Materials Science and Technology Division of CSIR-National Institute for Interdisciplinary Science and Technology, Thiruvananthapuram under the combined supervision of Dr. Manoj Raama Varma [Senior Principal Scientist] and Dr. U. Syamaprasad [Chief Scientist (Retired)] and no part of this thesis has been submitted previously for the award of any degree in any other university.

Thiruvananthapuram Rahul S

01 November 2017

November 01, 2017

CERTIFICATE

This is to certify that the thesis entitled **"STUDIES ON DEVELOPMENT OF MgB_2 SUPERCONDUCTING WIRES FOR CRYOGEN FREE MAGNET APPLICATION"** is an authentic record of the research work carried out by **Mr. Rahul S**, under our supervision in partial fulfilment of the requirement for the degree of Doctor of Philosophy of the Cochin University of Science and Technology and the same has not been submitted elsewhere for any other degree.

Dr. U. Syamaprasad
(Co-guide)

Dr. Manoj Raama Varma
(Research guide)

ACKNOWLEDGEMENT

I express my sincere thanks and respect to my supervisors Dr. U. Syamaprasad and Dr. Manoj Raama Varma, for their able guidance, valuable suggestions, constructive ideas and immense co-operation throughout the programme of this work.

I sincerely thank Dr. A. Ajayaghosh, Director, NIIST, Dr. Suresh Das and Dr. B. C. Pai former directors of NIIST, for providing me the necessary facilities to carry out this work.

I would like to express my heartfelt thanks to Mr. P. Guruswamy, former Technical Officer, Applied Superconductivity Lab, NIIST**,** for his help and co-operation for the successful completion of this work.

I owe special and wholehearted gratitude to Prof. M. V. George for his inspiring support and constant encouragement.

I express my gratitude to Dr. Prabhakar Rao, Head, Materials Science and Technology Division, Dr. M. L. P Reddy, Dr. M. T. Sebastian and Dr. K. G. K. Warrier, former heads of the division, for their help and support.

My sincere thanks also go to my labmates Dr. K. M. Devadas, Syju Thomas, Dr. Neson Varghese, Dr. K.Vinod, M. Maheshkumar, Dinesh Jose, S. L. Vinu, K. T. Jackson, A. Sivaprakash, S. Santhoshkumar, M. Firozkhan, G. R. Anuraghi, V. F. Rinu, A. Nazeer, Dr. R. Shabna, Dr. P. M. Sarun, Dr. S. Vinu, S.S. Surya, Dr. J. B. Anooja, and Dr. P. M. Aswathi for their encouragement in words and deeds.

I thank Dr. A. Sundaresan, Jawaharlal Nehru Centre for Advanced Scientific Research, Bangalore, Dr. S. B. Roy, Raja Ramanna Centre for Advanced Technology, Indore and Dr. S. Pradhan, Institute for Plasma Research, Gandhinagar, for collaboration.

I thank Prof. K. P. Vijayakumar, Department of Physics, Cochin University of Science and Technology, for his valuable and constructive suggestions during the development of this work.

I thank Mr. M. R. Chandran, Ms. Soumya, Mr. Robert Philip and Mr. Kiran Mohan for extending facilities such as SEM, TEM and EDS.

Many thanks to Mr. Kiran J. S., Dr. Retheesh Krishnan, Dr. Manu Jose, Dr. Vinayak M. V., Dr. Krishnan Kartha, Dr. Kavitha S Kumar, Mr. Akhil S Karun, Ms. Arya Das and Ms. Jeen Maria Mathews who have supported me to complete this work.

At this juncture, I express my indebtedness to my parents and sisters for their support throughout my study.

I sincerely acknowledge Council of Scientific and Industrial Research (CSIR) for providing the research fellowship.

Preface

Since the discovery of superconductivity in 1911, scientists have been trying to develop large electromagnets capable of producing very high fields and yet would consume no power. A superconductor can transport large DC currents with no measurable resistive loss when it is kept below three critical parameters, critical temperature (T_C), critical field (H_C) and critical current density (J_C). The superconductors discovered in the beginning had very low H_C values and were not suitable for making magnets. A breakthrough happened in the 1950s and early 60s when a new class of superconductors was discovered. These materials known as type II superconductors could retain their superconductivity at higher magnetic fields and were capable of carrying large current densities. Soon after, superconducting wires for magnet construction were commercially produced and by 1961 small magnets made from niobium zirconium were available. Then came niobium tin, an intermetallic compound with excellent superconducting properties but its brittle nature made its fabrication difficult. Niobium-titanium was first produced in 1965 and this ductile, easy to fabricate alloy soon became the standard 'work horse' for superconducting magnet industry. The low transition temperatures of niobium superconductors made it necessary to operate them at low temperatures, close to the boiling point of helium. Helium is a natural resource available in poor quantity and hence very costly. The high cost and difficulties in maintaining such low temperatures are the major bottlenecks to the widespread use of superconducting materials.

Discovery of High Temperature Superconductors (HTS) in the mid-80s raised hopes of using a less expensive cryogen, LN_2, as the cooling source. Unfortunately, the current density of HTS falls drastically with increasing temperature and field. In addition, the high complexity and cost of HTS are hindering their widespread use. Recently discovered Fe-As based materials show promising superconducting properties but the presence of toxic arsenic and the difficulties in making good quality wires/tapes are hampering their development. We shift our attention to MgB_2, an intermetallic known since the 1950s but only in 2001 discovered to be superconducting below 39 K. MgB_2 has an advantage in T_C over any of the Low Temperature Superconductor. This makes it suitable for operation in 20-30 K range using a cryocooler. The simple crystal structure, low anisotropy, weak-link free grain boundaries and large coherence length are favourable properties for the development of long conductors with excellent superconducting properties. The well-established Powder In Tube process can be employed for the preparation of MgB_2 wires/tapes and the raw materials are inexpensive and abundant. The

main drawback of MgB_2 is its drastically decreasing J_C in an applied magnetic field due to weak flux pinning.

The aim of the present work is to develop MgB_2 wires with improved transport critical current density at higher fields and characterize them under cryogen free conditions. To achieve this target, a three stage research plan was executed and is detailed in the thesis. The thesis is organized into 6 chapters. Chapter 1 gives a brief introduction to superconductivity and discusses in detail the features and relevance of MgB_2. An insight into the main properties, preparation techniques, challenges, in-field property improvement and applications of MgB_2 are given in this chapter. The preparative techniques and characterizations used for the present work are discussed in chapter 2. Chapter 3 details the studies to improve the in-field critical current density of MgB_2 in bulk form through chemical doping. Effects of mono as well as co-doping of n-SiO_2 and nano diamond on the structural and superconducting properties of MgB_2 are discussed. An issue, which is limiting the effectiveness of chemical doping in the normal preparation techniques is the agglomeration of nano dopants. To address this issue a novel synthesis route using Mg-Si alloy with uniformly distributed Mg_2Si particles, prepared using casting technique is proposed. Chapter 4 details the development of MgB_2 wires in mono and multifilamentary geometry and their characterization under cryogen free condition. Effects of heat treatment temperature and duration on the structural and superconducting properties of undoped monofilamentary wires are discussed in the first section of this chapter. In MgB_2 conductors, sheath materials play an important role. A comparison of commonly used sheath materials regarding their reactivity with the precursor powder, influence on superconducting properties, strain tolerance, mechanical workability, cost etc. are done. Chapter 5 discusses the efforts to replicate the good properties obtained in MgB_2 bulk to wire samples. Transport critical current densities on a par with the best samples reported internationally are achieved through chemical doping. Also, we have shown that Burned Rice Husk (BRH), an indigenously developed dopant by our group is a cheaper alternative for n-SiC, the best dopant reported so far in MgB_2. Finally, chapter 6 summarises the work with main conclusions and future scope and directions of work in the area.

TABLE OF CONTENTS

List of figures

List of tables

Abbreviations

B & R	Bent & Reacted
BCS	Bardeen Cooper and Schrieffer
BRH	Burned Rice Husk
CHPD	Cold High Pressure Densification
DC	Direct Current
FCL	Fault Current Limiter
FWHM	Full Width at Half Maximum
GLAG	Ginsburg, Landau, Abrikosov and Gorkov
GPIB	General Purpose Interface Board
HIP	Hot Isostatic Pressing
HPCVD	Hybrid Physical-Chemical Vapour Deposition
HPS	High Pressure Sintering
HTS	High Temperature Superconductor
ICDD	International Centre for Diffraction Data
ID	Inside Diameter
IMD	Internal Mg Diffusion
LHe	Liquid Helium
LN_2	Liquid Nitrogen
LTS	Low Temperature Superconductor
MCG	Magneto–Cardiology
MEG	Magneto–Encephalography
Mg-RLI	Mg-Reactive Liquid Infiltration
MRI	Magnetic Resonance Imaging
MSI	Magnetic Source Imaging
OD	Outside Diameter
OFHC	Oxygen Free High Conductivity
PC	Personal Computer
PDF	Powder Diffraction File
PIST	Powder In Sealed Tube
PIT	Powder In Tube
PPMS	Physical Property Measurement System
R & B	Reacted & Bent
SEI	Secondary Electron Imaging
SEM	Scanning Electron Microscopy

SMES	Superconducting Magnetic Energy Storage
SQUID	Superconducting Quantum Interference Device
SS	Stainless Steel
TEM	Transmission Electron Microscopy
Vol %	Volume percentage
VSM	Vibrating Sample Magnetometer
VTI	Variable Temperature Insert
WIT	Wire In Tube
Wt %	Weight percentage
XRD	X-Ray Diffraction
ZFC	Zero Field Cooling

Symbols

a, b	sample dimensions
a, *b*, *c*	lattice parameters
B	magnetic field
B_C	critical field
d	spacing of parallel atomic planes
d	diameter of multifilamentary wire
D	bending diameter
e	electronic charge
F_P	flux pinning force density
G	Gibbs free energy
h	Planck's constant
h, *k*, *l*	Miller indices of crystal planes
H	magnetic field
H_C	critical field
H_{C1}	lower critical field
H_{C2}	upper critical field
H_{irr}	irreversibility field
I	current
I_C	critical current
J_C	critical current density
$J_C(H)$	in-field critical current density
M	magnetisation
ΔM	width of M-H loop
R	resistance
T	temperature
T_C	critical temperature (transition temperature)
ΔT_C	transition width
V	voltage
κ	Ginsburg-landau constant
λ	London penetration depth
λ	wavelength of x-ray
ξ	coherence length
ξ	bending strain
ϕ	magnetic flux
Δ	energy gap

Chapter 1

An introduction to MgB_2 superconductor

1.1 Superconductivity

Superconductivity is an exciting phenomenon whereby certain materials when cooled to very low temperatures suddenly lose their resistivity and become perfect conductors of electricity. Unlike linear change in resistance with temperature shown by a normal metal, the superconducting state appears quite abruptly at a critical temperature (T_C), which is characteristic of the material. Often these temperatures are in the liquid He range. In fact, the development of He liquefaction techniques by Kammerlingh Onnes led to the discovery of superconductivity and it happened in 1911 in Leiden [1] (see figure 1.1), three years after he first liquefied He. Onnes started dreaming about giant electromagnets, capable of producing very high fields and yet would consume no power. But his hopes were dashed quickly when he discovered that superconductors also have a critical field (H_C), above which it reverts back to normal state. Many curious properties of superconductors were discovered in subsequent years and our understanding of this fascinating phenomenon has advanced profoundly [2-5]. The dream of large superconducting magnets showed signs of turning into a reality in the late 1950s and early 60s with the discovery of a new class of high field superconducting alloys [6-8]. These materials were capable of retaining their superconducting state even at very high fields and also capable of carrying large current densities. By the way, the current density carried by a superconductor is capped by a critical value (J_C). T_C, H_C and J_C are related to each other by the critical surface, figure (1.2). A material will be superconducting below this surface and normal above it.

1.2 Basic superconducting properties

1.2.1 Critical temperature

The superconducting state is characterised by a condensation of the conduction electrons into a lower energy state. The theories of Frohlich and of Bardeen, Cooper and Schrieffer (BCS theory) have explained this condensation in terms of an attractive interaction between pairs of electrons, which is transmitted via lattice vibrations in the crystal. The strength of this interaction is maximum when electrons are in a state of opposite spin and having equal

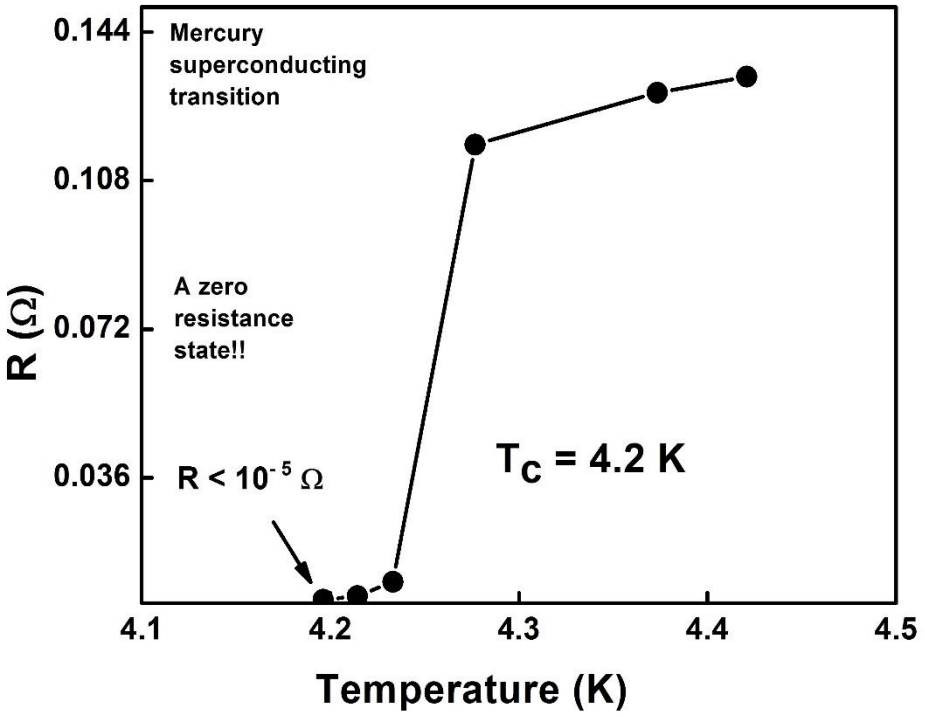

Fig (1.1) When Onnes cooled mercury to 4.25 K, the resistivity suddenly dropped to zero.

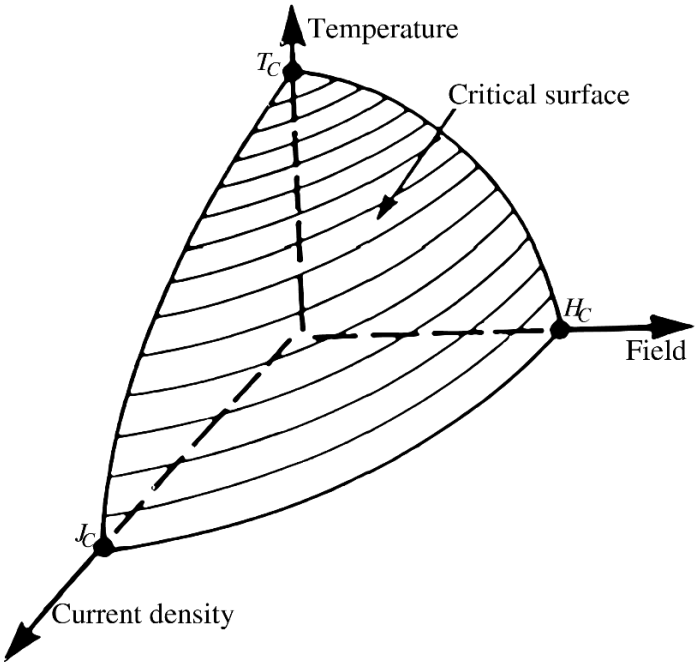

Fig (1.2) Superconducting critical surface

and opposite momentum. The interaction causes the kinetic energy of electrons to increase above that expected in the Fermi distribution and at the same time reducing their potential energy by a greater amount so that the total energy is reduced. The extent of this reduction may be expressed in terms of superconducting energy gap 2Δ, defined as the energy required to break the interaction of a Cooper pair and making the electrons normal again. BCS theory relates energy gap to critical temperature by

$$3.5\ k_B T_C = 2\Delta(0) \qquad (1.1)$$

where k_B is the Boltzmann's constant, $2\Delta(0)$ is the energy gap at absolute zero. Thus it can be seen that T_C is a direct function of the strength of interaction between electrons in the Cooper pair.

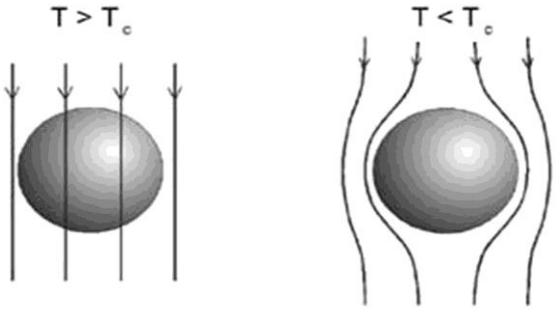

Fig (1.3) Meissner effect- a superconducting sphere in a constant applied magnetic field excludes the magnetic flux.

1.2.2 Critical field

The superconductors discovered in the beginning (e.g. tin, lead and mercury) belong to a class known as 'type I' superconductors. They exhibit Meissner effect, which is the total expulsion of magnetic flux from the interior of the specimen when it enters the superconducting state (figure 1.3). This is a reversible process and it happens, both when a magnetic field is applied to a superconducting specimen and also when a sample in a magnetic field is cooled below its T_C. Condensation of electrons from their normal to superconducting state leads to a reduction in Gibbs free energy from G_n to G_s. When a magnetic field, B is applied to a superconductor, due to flux expulsion its Gibbs free energy increases by $B^2/2\mu_0$ whereas the energy of the normal phase remains unchanged. Therefore at lower fields, superconducting state will be more stable due to lower energy and at higher fields, it would be preferable for the material to admit flux and be in the normal state which would have lower energy. The transition

between normal and superconducting state happens when the Gibbs free energy of the two states become equal and the magnetic field corresponding to this point is called the critical field, B_C. (It is a common practice among workers in superconductivity to denote the critical value of the applied magnetic field as H_C. In the subsequent sections of this thesis critical field will be denoted as H_C). Thus the critical field is given by

$$B_C^2/2\mu_0 = G_n - G_s \qquad (1.2)$$

The Critical field of type I superconductors is very low and therefore they are not very attractive for practical applications. There exists a second category of superconductors known as 'type II' superconductors. Up to a 'lower critical field B_{C1}', they behave just like type I superconductors and exclude magnetic flux completely. Above this B_{C1}, they start to admit flux without losing their superconductivity. Type II superconductors remain superconducting up to a much higher upper critical field B_{C2}. Figure (1.4) shows the behaviour of type I and type II superconductors in an applied magnetic field. All the practically useful superconductors are type II. Ginsburg, Landau, Abrikosov and Gorkov developed the theory of type II superconductors (GLAG theory). According to this theory, the ratio $\kappa = \lambda/\xi$ determines whether a material is type I or type II. Here λ is the London penetration depth and ξ is the coherence length. λ is the depth to which magnetic field can penetrate a superconductor and ξ is the range of the interaction between Cooper pairs. If $\kappa > 1/\sqrt{2}$, the material is type II. Above B_{C1} magnetic field enter the superconductor in the form of discrete flux lines or fluxoids, each carrying one quantum unit of flux, $\phi_o = h/2e$, where h is the Planck's constant and e is the electronic charge, i.e. $\phi_o = 2.0 \times 10^{-15}$Wb [9, 10]. The core of each fluxoid is in the normal state with a radius of $\sim \xi$ and it is enclosed by a circulating vortex of supercurrent of radius $\sim\lambda$. The behaviour of flux lines is similar to Faraday's lines of force, exhibiting line tension and a mutual repulsive force perpendicular to the lines. Inside a homogeneous crystal, flux lines arrange themselves into a triangular lattice (which is the configuration of lowest energy). At an applied field B, spacing between fluxoids is given by

$$d^2 = \sqrt{4/3}\phi_o / B \qquad (1.3)$$

i.e. an increase in magnetic field will push the flux lines closer to each other and finally at upper critical field B_{C2}, the normal cores of flux lines overlap and the material becomes normal. GLAG theory gives the upper critical field of a type II material as

$$B_{C2} = \sqrt{2}\kappa B_C \qquad (1.4)$$

where B_C is the 'thermodynamic critical field' given by equation (1.2).

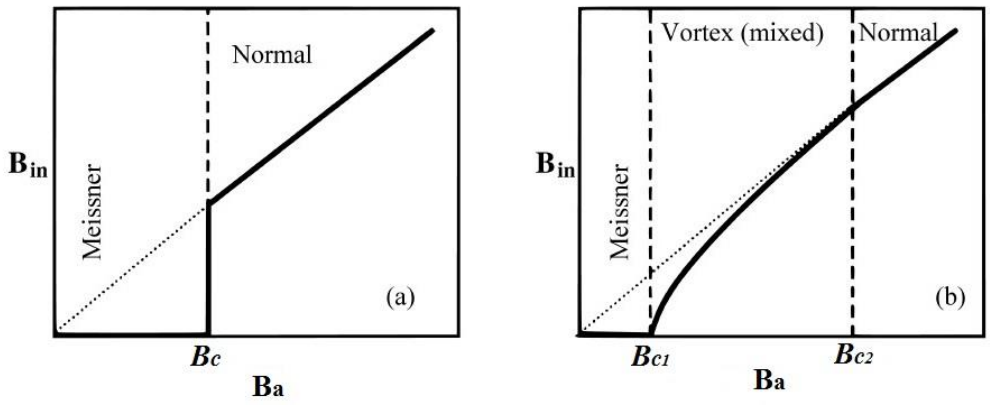

Fig (1.4) Variation of magnetic field inside a (a) type I and (b) type II superconductor with applied field.

1.2.3 Critical current density

Inside a superconducting material if the flux lines form a regular and uniform lattice, the field within the superconductor must also be uniform. In this case since curl B = μ_oJ, no macroscopic current is allowed to flow through the superconductor. Experiments on some very pure type II superconducting samples bear out this prediction. It is only possible to flow supercurrent on the surface of the samples and the resulting critical currents are extremely low. To develop technically useful superconductors capable of carrying large supercurrents through their volume it is required to disturb the distribution of flux lines and make it non-uniform. We can discuss it in a simple way using figure (1.5). In figure (1.5a), it is a uniform array of fluxoids and the supercurrents cancel out on a macroscopic scale. However in figure (1.5b), there is a gradient in fluxoid density and as a result between each row there is a proportion of vortex current which is not cancelled, i.e. there is a macroscopic current density. Because of the repulsive force between fluxoids, the gradient in density gives rise to a net force per unit volume which is proportional to both the density and the gradient.

i.e. $F = \frac{B}{\mu_o}\frac{dB}{dx}$

This could be extended to the more general case of curved flux lines in three dimensions

$$F = \frac{1}{\mu_o} B \times \text{curl } B = B \times J \qquad (1.5)$$

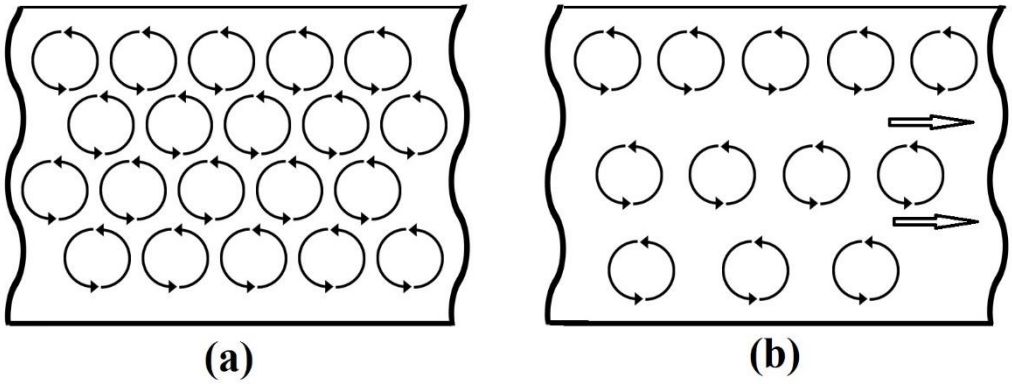

Fig (1.5) (a) A uniform array of vortex currents produces no net current density; (b) a gradient in the density of vortex currents produces a net current.

This is the expression for Lorentz force acting on a current density J. To stop flux lines from moving and allow a current density to be maintained the lattice must provide an equal and opposite 'pinning force' per unit volume F_p. If the Lorentz force exceeds the pinning force, the fluxoids will start to move. The motion of flux lines produces a voltage drop across the specimen and a resistance known as flux flow resistance. Critical current corresponds to the point at which flux line lattice starts to move. Flux pinning in a superconductor is caused by the forces between fluxoids and certain inhomogeneities known as 'pinning centres' in the crystal [10-12]. If the normal core of a fluxoid resides on a non-superconducting point in a crystal, its energy would be lowered because there is no need to drive a previously superconducting region to normal [13]. Lattice defects and inclusions of normal particles in a crystal act as effective flux pinners.

1.3 Applications of superconductors

Introducing a superconductor instead of a conventional conductor is always associated with a significant rise in cost. Therefore a superconductor approach comes into contention when it brings overwhelming cost effectiveness and a unique solution to the need. Some applications of superconductors are mentioned here.

Electric power: Superconductors find applications in generators, transformers, transmission cables, synchronous condensers, magnetic energy storage devices and fault current limiters. The unique properties of superconductors lead to highly powerful, efficient and compact devices [14-19].

Transportation: Transportation facilities for people and goods play a pivotal role in the progress of a country. Superconductors are revolutionising this area with maglev trains, railway

traction transformers and ship propulsion systems. Figure (1.6) shows a maglev train operated by Central Japan Railway [20-25].

Fig (1.6) Maglev train.

Medicine: The most popular application of superconductors is in Magnetic Resonance Imaging (MRI) systems [26-28]. Magneto–Encephalography (MEG), Magnetic Source Imaging (MSI) and Magneto–Cardiology (MCG) are some other systems making use of the unique features of superconductors.

Industry: It is reported that large motors rated at 1000 HP and above consume 25 % of total electricity generated in the USA. Superconducting motors can significantly reduce this energy requirement [29-31]. Also, superconducting magnets for materials purification [32-34] and industrial processing are being demonstrated.

Communications: Superconducting filters are widely used in cellular communication systems. Such filters can enhance the signal to noise ratio [35, 36]. The world is moving from analogue to digital communications and superconducting chips can drastically improve performance in many applications.

Scientific Research: The first ever applications of superconductors were in small scale laboratory experiments. Superconducting magnets are now an essential research tool. Making use of superconducting materials, today's cutting edge scientific research facilities are pursuing breakthroughs that can give us clean, abundant energy from nuclear fusion [37] to supercomputers that are faster than the theoretical limit of silicon technology [38, 39].

1.4 Superconducting Materials

Mercury was the first material discovered to be superconducting. Before 1973 many other metals, alloys and intermetallics were found to be superconducting and the maximum T_C attained was 23.2 K in Nb_3Ge. These were known as Low Temperature Superconductors (LTS). Superconductivity in LTS was well explained by BCS theory. Since 1960s Niobium-Titanium alloy has been the most preferred material for superconducting magnets. Niobium-Tin is a brittle intermetallic material which offered even higher magnetic field strengths. Even today these two superconductors dominate superconducting magnet industry [40-43]. In 1986, J G Bednorz and K A Muller discovered an oxide based ceramic superconductor (LaBaCuO) with a surprisingly high T_C of ~ 30 K [44]. In 1987 C W Chu discovered an Y based cuprate superconductor with T_C above the boiling point of liquid nitrogen, 77 K [45]. Extensive research uncovered many more copper oxide systems with T_Cs well above 100 K. Superconductors with T_C above 23.2 K are generally called High Temperature Superconductors (HTS) [46, 47]. Now a century after the discovery of superconductivity, thousands of materials are known to be superconducting with T_Cs spanning over a wide range of temperatures. Table1.1 gives some of the superconducting materials belonging to different classes.

The discovery of superconductivity in MgB_2 came as a surprise to researchers. The material was known since the 1950s but only in 2001, Jun Akimitsu's group in Japan discovered that it becomes superconducting below 39 K [48]. Though this T_C of 39 K was much cooler than that of copper oxide based superconductors, the excitement it generated among theoreticians and experimentalists was alike since MgB_2 is an inter metallic material unlike cuprates. Recently superconductivity was discovered in Iron based layered compounds with T_Cs comparable and higher than that of MgB_2 [49-51]. T_C above 50 K and H_{C2} of the order of 100 T were reported. The difficulties in handling toxic arsenic and preparation of wires/tapes with good superconducting properties are the bottle-necks in its development. MgB_2 has already surpassed many of the critical properties of LTS and is free from the limitations of HTS.

1.5 Why Magnesium Diboride?

Though there are now thousands of materials exhibiting superconductivity under various conditions, only a handful of them have evolved into practical superconductors. NbTi and Nb_3Sn are still the most widely used superconductors. NbTi has a T_C of 9 K and Nb_3Sn a T_C of 18 K. Both have good H_{C2} values as well (12-29 T). NbTi was first produced in 1965 and

this ductile, easy to fabricate material soon became the standard 'work horse' for superconducting magnet industry. The ability to co-process this with copper made it even more

Table 1.1 Classification of superconductors

Class	Example	T_C (K)
Organic Superconductors	$(BT)_2{}^*I_3$	3.3
	$(BT)_2Cu(NCS)_2$	10.4
A-15 compounds	Ti_3Sb	6.5
	V_3Ga	15.9
Magnetic Superconductors (Chevrel Phases)	$PbMo_6S_8$	15
	$LaMo_6S_8$	7
Heavy Fermion Superconductors	$ZrZn_2$	3
	$YNi_{1.9}B_{1.2}$	14
Oxide Superconductors without Copper	$Ba_{1-x}K_xBiO_3$	31
	NbO, TiO	< 1
Pyrochlore Oxides	$CsOs_2O_6$	3.3
	$RbOs_2O_6$	6.3
Rutheno-Cuprates	$RuSr_2GdCu_2O_{8-\delta}$	16
	$RuSr_2YCu_2O_8$	< 39
High-Temperature Superconductors	$YBa_2Cu_3O_{7-x}$	93
	$(Bi, Pb)_2Sr_2Ca_2Cu_3O_{10}$	110
Rare-Earth Borocarbides	$LuNi_2B_2C$	16
	YPd_2B_2C	23
Silicon-Based Superconductors	$ThSi_2$	1.56
	$CaSi_2$	14
Chalcogens	S	10 (P = 93 GPa)
	Se	4-6 (P = 15-25 GPa)
Carbon Superconductors	Single wall nanotube	15
	K_3C_{60}	19.28
Borides	MgB_2	39
	ZrB_2	5.5
Iron based Superconductors	$NdFeAsO_{1-x}F_x$	53
	$SmFeAsO_{1-x}F_x$	55
Elements	Hg	4.2
	Nb	9.2

*BT = BEDT-TTF [BEDT- bis(ethylenedithio), TTF- tetrathiafulvalene]

attractive. NbTi is mainly used for magnets below 10 T. Nb_3Sn is a brittle material but with excellent superconducting properties. It has a higher T_C and capable of producing higher fields than NbTi. Niobium-tin is more sensitive to strain and difficult to manufacture and hence more expensive than NbTi [52-54]. Niobium superconductors excel for their performance at LHe

temperature. Helium is a natural resource which is available only in poor quantity and hence very costly. Also handling LHe is tricky and hazardous. These are the major bottlenecks to the widespread use of superconducting materials.

The discovery of cuprate high temperature superconductors was the biggest breakthrough in superconductivity research since 1911. The commercially interesting HTS are BSCCO (Bi-2223 and Bi-2212) and YBCO. All these materials have T_Cs well above the boiling point of LN_2 which is cheap and readily available. Upper critical field values of these HTS are above 100 T at 4.2 K. Powder-In-Tube (PIT) method is used for the fabrication of BSCCO tapes and these are known as first generation HTS conductors. Coated conductor technique is adopted for YBCO and these are considered as second generation conductors. The high complexity and cost of HTS are hindering their widespread use. HTS conductor fabrication is difficult and requires expensive Ag as sheath material. Due to high anisotropy, uniaxial / biaxial texturing is necessary for BSCCO / YBCO in order to achieve good J_C. HTS materials have low coherence length and their grains are weakly connected. For YBCO even the modest grain boundary misorientation adversely affect J_C [55-61]. Recently discovered Fe-As based materials show promising superconducting properties but making good quality wires/tapes is extremely difficult.

MgB_2 has a high T_C of 39 K and is suitable for operation in 20-30 K temperature range with cryocoolers where conventional LTS cannot be used. Thus the life cycle costs of MgB_2 are lower than NbTi and Nb_3Sn. A comparison of superconducting properties of MgB_2 with those of LTS has shown that MgB_2 has already attained or even surpassed many of the critical properties of LTS. Figure (1.7) shows a comparison of engineering current density of MgB_2 wires with other practical superconducting materials. Expected fields of application are also highlighted in the figure and potential applications of MgB_2 are represented by squares. MgB_2 has weak-link free grain boundaries and grain boundaries act as good flux pinners [62-68]. Preparation of MgB_2 into long multifilamentary conductors is easy and raw materials are inexpensive. The density of MgB_2 is 2.6 gm/cm^3 which is much lower than other superconductors and copper. Thus it is suitable for light weight applications. MgB_2 can be configured in round as well as rectangular cross sections giving flexibility in coil design and fabrication. MgB_2 can be prepared using a number of inexpensive and easily available sheath materials and the process requires only a lower heat treatment temperature and duration. MgB_2 doesn't necessarily require an inert atmosphere heat treatment. In an industrial point of view, these are significant advantages and hence MgB_2 is considered as the material for next

generation high field magnets [69-72]. Table (1.2) compares the fundamental superconducting properties of practical superconductors.

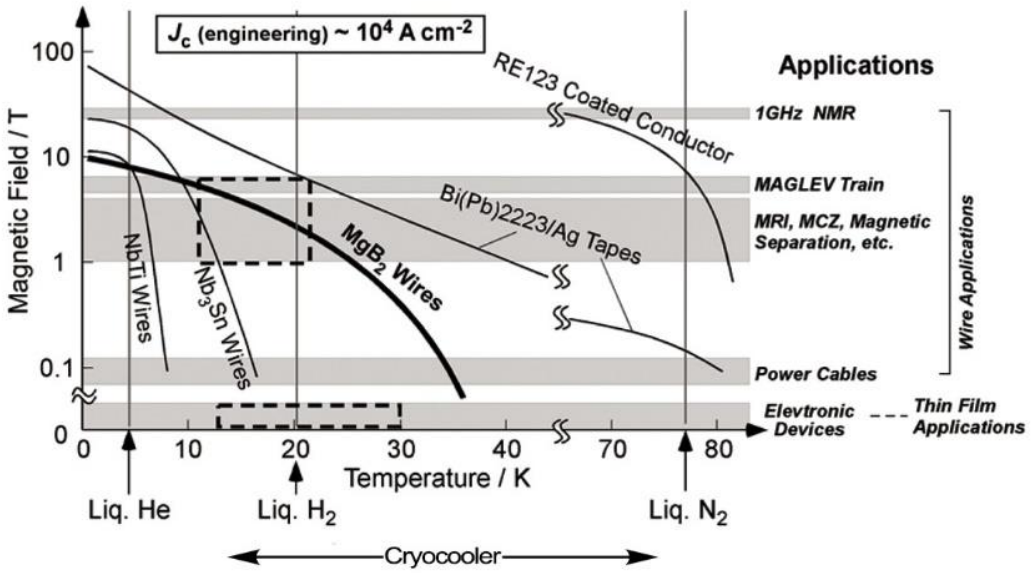

Fig (1.7) Expected fields of application for superconducting materials.

Table 1.2 Properties of practical superconductors

Parameter	NbTi	Nb_3Sn	MgB_2	YBCO	Bi-2223
T_C (K)	9	18	39	92	110
Anisotropy	Negligible	Negligible	1.5-5	5-7	50-200
J_C at 4.2 K (A/cm^2)	~ 10^6	~ 10^6	~ 10^6	~ 10^6	~ 10^7
H_{C2} at 4.2 K (T)	11-12	25-29	30-40	> 100	> 100
H_{irr} at 4.2 K (T)	10-11	21-24	16-20	5-7 (77 K)	0.2 (77 K)
Coherence length $\xi(0)$ (nm)	4-5	3	5-12	1.5	1.5
Penetration depth $\lambda(0)$ (nm)	240	65	100-140	150	150
Resistivity $\rho(T_C)$ ($\mu\Omega$cm)	60	5	0.4	150-800	40-60

1.6 Properties of MgB_2

MgB_2 was known and commercially available during early 1950s [73] but the superconductivity in it was discovered only in the 21st century. This is quite surprising because intermetallic superconductivity was the hot topic during 1960s. We already had binary superconductors like Nb_3Sn and Nb_3Ge then and BCS theory was well established. Specific heat of MgB_2 was measured down to 40 K in 1957 [74] but somehow superconductivity was missed. Two years later scientists predicted two-gap superconductivity [75, 76] but we didn't have a concrete example till 2001 when Akimitsu's group discovered superconductivity in MgB_2. The discovery was greeted with a lot of enthusiasm by researchers all over the world. MgB_2 exhibits a plethora of interesting features.

1.6.1 Crystal structure

MgB_2 has a hexagonal crystal structure with B atoms forming a graphite like honeycomb network and Mg atoms occupying the pores of these hexagons, as shown in figure (1.8). MgB_2 belongs to the space group p6/mmm. In the unit cell, Mg takes the position (0, 0, 0) [Weizkoff symbol 1a] and B takes positions (1/3, 2/3, 1/2) and (2/3, 1/3, 1/2) [Weizkoff symbol 2d]. The coordination polyhedra are ($B_{12}Mg_8$) and (Mg_6B_3) for Mg and B respectively. The lattice parameters are 'a' = 3.084 Å and 'c' = 3.524 Å. Intralayer interatomic distances are: B-B = 1.780 Å, Mg-Mg = 3.084 Å. Interplane B-B distance is almost double that of in-plane B-B distance. Mg-Mg inter-layer distance is 3.524 Å and Mg-B interlayer distance is 2.5 Å [73, 77-79].

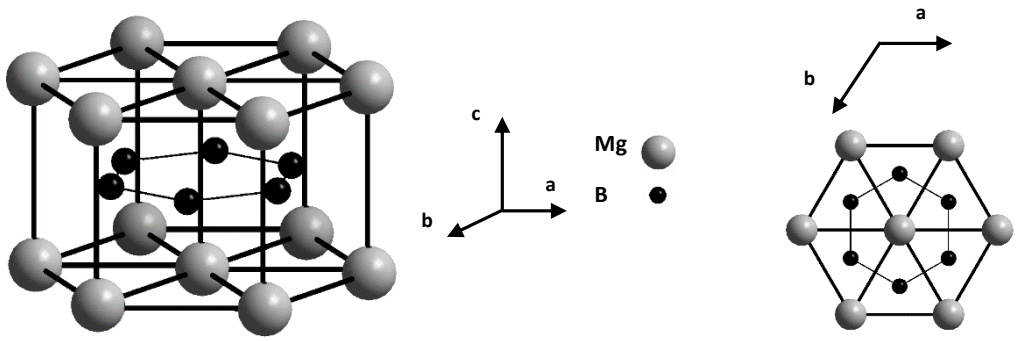

Fig (1.8) Crystal structure of MgB_2.

1.6.2 Basic physical and superconducting properties

MgB_2 is a brittle material like Nb_3Sn and HTS materials. Anisotropy of MgB_2 is 1.5-5 and this is very low compared to HTS [80-82]. This low anisotropy avoids the need of texturing in long wires and tapes of MgB_2 unlike in high T_C cuprates. The coherence length of MgB_2 is 5-12 nm and penetration depth is 100-140 nm [83]. The coherence length of MgB_2 is higher than inter-atomic spacing, therefore grain boundaries of MgB_2 are transparent to supercurrent flow. MgB_2 has a transition temperature of 39 K which is nearly double that of Nb_3Sn and four times that of NbTi [84, 85]. Though this temperature is much cooler than liquid nitrogen temperature, MgB_2 can be cooled to an operational temperature by liquid hydrogen, solid nitrogen or fairly inexpensive closed cycle cryocoolers. MgB_2 has a low room temperature resistivity of about 10 μΩcm and just above T_C, it is about 0.4 μΩcm [86]. Its resistivity is comparable to bulk copper wire. In contrast, room temperature resistivity of Nb_3Sn is 80 μΩcm and 5 μΩcm just above T_C. MgB_2 is a type II superconductor whose mechanism is well explained by BCS theory. Pure MgB_2 has a lower critical field (H_{C1}) of less than 50 mT, and upper critical field (H_{C2}) of 15-20 T and irreversibility field (H_{irr}) of 6-12 T at 4.2 K [83, 86-89]. The depairing current density is approximately 10^7 A/cm^2 which is one order lower than cuprates [90]. MgB_2 has two superconducting gaps, $\Delta 1 \sim$ 5-7 meV and $\Delta 2 \sim$ 1.5-2.0 meV [85, 91].

1.6.3 The high T_C and two gap superconductivity in MgB_2

The unusually high T_C of 39 K puzzled researchers since the discovery of MgB_2 [85]. According to BCS theory, T_C of a material depends on three parameters,

$$k_B T_C = 1.13\, \hbar\omega_D \exp[-1/VN(E_F)] \qquad (1.6)$$

the characteristic phonon energy $\hbar\omega_D$, the electronic density of states $N(E_F)$ and the electron phonon interaction giving rise to V. The phonon energies of MgB_2 are not particularly different from that of other diborides and light element superconductors which have much lower T_C values. Since MgB_2 has no 'd' electrons, $N(E_F)$ is also low. What remains is V, which is a caliper of the strength of electron-phonon interaction. The selective coupling between specific electronic states and specific phonons is the secret behind the interesting properties of MgB_2.

In MgB_2, the Mg ions donate electrons to the conduction bands but Mg orbitals play only a minor role in the superconducting process – it is the B honeycomb planes that determine the electronic properties [92, 93]. To put it simply, let us consider benzene molecule. In

benzene, the sp^2 carbon orbitals overlap and form σ bonds between neighbouring atoms in the plane of the molecule. The carbon p_z orbital extend above and below the plane to form π bonds. The electrons in both bonds are delocalized among the six C atoms in the ring. In MgB_2, boron honeycomb network replaces the carbon ring in benzene and electrons are delocalized throughout the honeycomb. The σ and π bonds in benzene become σ and π bands in MgB_2, with very little electron hopping between them. The π bands connect adjacent B layers through the inert Mg ions and this allows metallic conduction perpendicular and parallel to the B sheets. The σ electrons conduct only in the B plane. Figure (1.9) shows the Fermi surface of MgB_2. The vertical cylinders at the corners are associated with σ bands and the 3D type tunnels and caves in the centre are associated with the π bands. These two nearly non-interacting bands and their sensitivity to phonons play an important role in the superconducting properties of MgB_2. In conventional superconductors, electron-phonon interaction results in Cooper pairs of nearly equal pairing strength, evenly distributed over the Fermi surface. In MgB_2 one high energy phonon (about 570 meV) associated with the in-plane movement of B atoms couples strongly with σ band electrons. The σ band has charge concentrated along the B-B axes, rather than spread throughout the unit cell. When B atoms move in the plane the charge is substantially distorted. This results in the shifting of energy of electronic states and accounts for the large coupling energy [94].

The strong electron-phonon coupling in the σ band and weak coupling in π band lead to the formation of two distinct superconducting gaps in MgB_2 [95]. Though this possibility of two gap superconductivity was proposed earlier, MgB_2 was the first material in which this effect was clearly visible. If the two bands were independent there would have been two

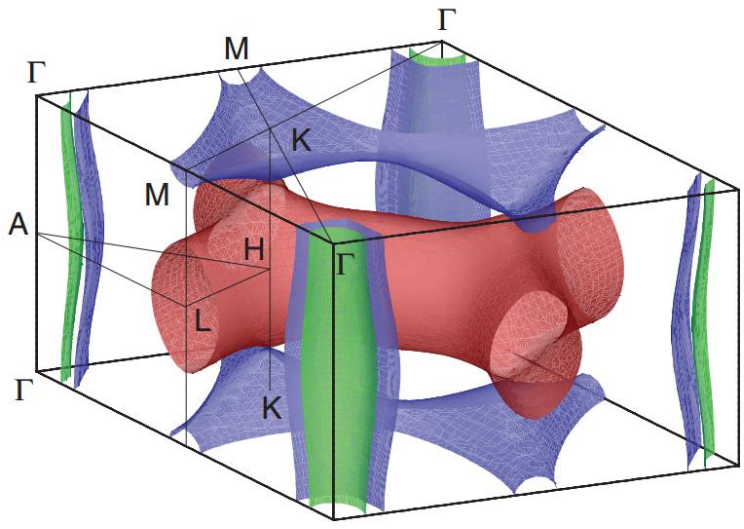

Fig (1.9) The Fermi surface of MgB_2.

superconducting transition temperatures and other distinct properties. But in MgB_2 these two bands interact, though weakly. The interaction is through scattering from states in one band to states in the other and through Coulomb repulsion. This small interaction provides the richness and subtlety to the superconducting properties of MgB_2.

1.7 Synthesis of MgB_2

MgB_2 superconductor is usually prepared in bulk, wire, tape, thin film and single crystal forms. Mainly two approaches are used for the preparation of MgB_2. In *ex-situ* approach pre-reacted MgB_2 power is used for the preparation of the conductor. *Ex-situ* method gives better homogeneity, density and phase purity compared to *in-situ* method. *Ex-situ* requires higher sintering temperatures and longer sintering duration to get good quality conductors. Since the powder is already reacted doping of impurities is not easy in *ex-situ* approach. In *in-situ* method, a stoichiometric mixture of Mg and B powders/sources is used. *In-situ* requires only a lower sintering temperature and duration and is suitable for chemical doping. The density of MgB_2 prepared using *in-situ* approach is very low (usually only 50 % of theoretical density). Volatile Mg loss and the possibility of Mg and/or B reacting with sheath materials are high in *in-situ* approach [96-102].

1.7.1 Bulk samples

MgB_2 in bulk form is very useful and convenient in studying its basic physical and electrical properties. Though both *ex-situ* and *in-situ* approaches could be used for preparing bulk samples, *in-situ* is generally preferred for research purposes. Several synthesis procedures for *in-situ* bulk preparation are reported [103-108]. Mg in powder/flakes/chips and B (amorphous or crystalline) in powder form are the starting materials. Instead of elemental Mg, compounds containing Mg are also sometimes used as starting materials. The starting materials are taken in the desired stoichiometry and enclosed in a metal/quartz tube/foils/ampules and heat treated at 600-900 ^{o}C for 15 min-5 hrs. Heat treatment is preferably done in an inert atmosphere. This is to avoid the oxidation of Mg. Mg is highly volatile and to compensate the potential loss of Mg during heat treatment, sometimes excess Mg is used in the starting powder. Mechanical alloying/ high energy ball milling are found to accelerate MgB_2 phase formation at lower temperatures and improve the superconducting properties [105-108].

High energy ball milling is particularly useful when mixing large quantities of powder. Ball milling can be used to reduce the particle size in MgB_2. Smaller grains provide more grain boundaries which are very good flux pinners and thus suitable for improving high field

performance of the conductor. It should be noted that the quality of the ball milled samples depends on the nature and size of the bowl and balls, powder to ball ratio, speed and milling duration and milling medium [106, 108]. The precursor can get contaminated by bowl, balls and milling media. Agglomeration of particles is another drawback; this could severely dent the advantages of chemical doping in MgB_2.

To improve the density of bulk samples prepared using *in-situ* technique high pressure sintering (HPS) [109, 110], hot isostatic pressing (HIP) [111], and two stage sintering are tried [112]. In HPS and HIP pressure (0.5-5 GPa) is applied to the sample during heat treatment to reduce porosity and cracks and improve density. Extremely high dense samples were prepared using these methods. The technique is mainly suitable for bulk samples but tried to make short wire/tape samples also. EDISON SpA of Italy developed a liquid Mg infiltration technique for producing bulk samples of different shape and high density. In this method, Mg in liquid form is reacted with B powder in a closed metallic container [113].

1.7.2 Wire/Tape samples

Some of the techniques used for the fabrication of LTS and HTS wires/tapes were successfully applied to MgB_2 soon after the discovery of superconductivity in it. Over 50 years of conductor fabrication experience in superconductors propelled the development of MgB_2 wires/tapes at a brisk pace.

Diffusion method: The first MgB_2 wire made was using diffusion method [86]. By diffusing Mg into commercially available B fibres they could be converted into superconducting MgB_2 wires. The phase homogeneity of wires prepared using diffusion method is poor and it is mostly suitable for short samples. A modified version of the diffusion method was developed by Giunchi *et al* known as Internal-Mg-Diffusion (IMD) or Mg-Reactive Liquid Infiltration (Mg-RLI) process [114, 115]. In this process a boron filled tube with Mg rod embedded axially in it is cold worked and then heat treated. Mg gets diffused into B and a layered core is formed. The original IMD method proposed by Giunchi was bettered by Hur *et al* [116] and Togano *et al* [117] and the J_C values shown by samples prepared by this method are very encouraging.

Coating technique: The method is widely used for the manufacture of high T_C second generation superconducting wires of YBCO. Excellent properties shown by hybrid physical-chemical vapour deposited (HPCVD) thin films encouraged researchers to make MgB_2 coated conductors using HPCVD method. Ferrando *et al* [118] coated MgB_2 on SiC fibres. Sputtering and Molten Salts Electroplating are tried to coat MgB_2 on various substrates [119, 120].

Though ceramic substrates are widely used, some metal substrates gave better chemical stability, plasticity and heat conductance. SS, Fe, Cu and Nb are some of the metallic substrates used for coated conductor development [120-123]. Scaling up of this technique for commercial production of MgB_2 conductors is not easy.

Powder-In-Tube (PIT) method: PIT technique was well known for making good quality conductors of BSCCO. In the case of MgB_2 also PIT is the most popular conductor fabrication technique [124-129]. In PIT, precursor powder is filled in a metal tube/sheath, mechanically compacted and rolled/drawn/extruded into desired size and shape. This is followed by heat treatment. Sometimes intermediate annealing is provided to relieve the stress developed during rolling or drawing [130]. The chosen sheath material must be chemically compatible with $Mg/B/MgB_2$, should provide adequate mechanical support to the brittle superconducting core and should be ductile enough to be cold worked. For making multifilamentary conductors, Wire-In-Tube (WIT) method is employed. In WIT, monofilamentary wires are bundled along with some thermal stabilizers such as Cu wires in a suitable tube and then rolled or drawn [131-134]. Multifilamentary conductors can withstand higher uniaxial and bend strains and have better thermal stability than monofilamentary conductors [134-138].

1.7.3 Thin films

Superconducting thin films find important applications in Josephson Junctions and Superconducting Quantum Interference Devices (SQUID). The high volatility and oxygen affinity of Mg and the large difference in the vapour pressures of Mg and B are the major challenges to the development of MgB_2 thin films. Pulsed laser deposition is a common method used for MgB_2 thin film development. A one step (*in-situ*) and a two step (*ex-situ*) preparation techniques are popularly adopted. In *ex-situ*, amorphous boron is deposited on a substrate and then it is heated in a Mg rich vapour. *Ex-situ* approach gives films with better superconducting properties but not suitable for preparing multi-layer films [139, 140]. *In-situ* method produces films with a smoother surface. Zeng *et al* reported MgB_2 thin films prepared using HPCVD [141].

1.7.4 Single crystal

Single crystals of MgB_2 are of particular interest to the research community to explore the intrinsic, especially anisotropic properties of this superconductor. Two different approaches are developed to grow sub-millimetre MgB_2 single crystals; growth by encapsulation and high pressure method. High Mg vapour pressure, formation of MgO, reactivity of Mg in vapour and

melt phases with containers and flux materials, low solubility of MgB_2 in Mg are some of the challenges faced in the preparation of good quality single crystals of MgB_2 [142, 143].

1.8 The challenges

For commercial applications, MgB_2 must be produced in long multifilamentary conductors with good J_C, T_C and H_{C2} values. Thermal stability and uniformity of properties over the whole length are important. Wires should be able to maintain adequate fraction of critical current density when subjected to uniaxial and bend strains. The cost/performance ratio should be low to compete with the well-established Nb based superconductors. Some of the challenges in achieving these goals are described below.

1.8.1 Problems regarding fabrication

Mg is highly volatile and has a strong affinity towards oxygen. This can seriously affect the phase purity and homogeneity of the conductor. Mg loss can result in non-stoichiometry and lead to the formation of higher borides. MgO and higher borides can adversely affect inter-grain supercurrent transport [144, 145]. Adding excess Mg to compensate Mg loss and inert atmosphere heat treatment are some of the ways to tackle this issue. The MgB_2 formed by liquid-solid reaction is highly porous, limiting the active current carrying area. There is a volume reduction when Mg and B react to give MgB_2 phase ($V_{Mg} + V_{2B} > V_{MgB_2}$) [145]. The density of *in-situ* prepared samples is usually only 50 % of the theoretical density. HIP and Cold High Pressure Densification (CHPD) are some techniques to reduce porosity and improve density of MgB_2 [146-150]. Mg reacts with most of the commonly used sheath materials. These reacted secondary phases act as a barrier for current transfer from outer sheath to the inner superconducting core. The highly resistive barrier will increase the current transfer length from sheath to core and affect the thermal stability of the conductor [151]. By introducing a metallic barrier material between sheath and core this problem can be solved but the commonly used barrier materials, Nb and Ta are expensive.

1.8.2 Problems regarding property improvement

MgB_2 has high self-field J_C compared to Nb superconductors at low temperatures but the J_C decreases drastically at higher fields due to insufficient flux pinning and low irreversibility field. Since MgB_2 is a material with a simple crystal structure consisting of only two elements, the density of defects produced during synthesis is too low to provide sufficient flux pinning at higher fields. Grain boundaries are the only flux pinners in pure MgB_2. While

Nb superconductors have an H_{irr} close to H_{C2} (H_{irr}~ 0.8 × H_{C2}), H_{irr} of MgB_2 is only half of H_{C2} (H_{irr}~ 0.5 × H_{C2}). Insufficient current density at higher fields limits the temperature and field range where MgB_2 could be superior to Nb_3Sn. By introducing artificial pinning centres, field performance of MgB_2 could be improved [145, 152, 153]. Though the T_C of MgB_2 is more than double that of Nb_3Sn, it is still much cooler than HTS cuprates. Substitution of B^{11} for B^{10} increased the T_C by 1 K [154], apart from this no other effort has enhanced the T_C significantly. At the same time, chemical doping, application of pressure, irradiation with high energy particles which are found to have a positive effect in enhancing $J_C(H)$ have suppressed T_C to various extent.

1.9 Improving $J_C(H)$ and H_{C2} of MgB_2 through various methods

Although the attempts to improve the T_C of MgB_2 were not very successful, other important properties, $J_C(H)$ and H_{C2} could be improved through various methods. $J_C(H)$ of MgB_2 is closely associated with H_{C2} and flux pinning. H_{C2} is an intrinsic property which could be tailored by turning the inter and intra band scattering rates [155, 156]. As mentioned earlier, grain boundaries are good flux pinners in MgB_2. By reducing the grain size density of grain boundaries could be improved and this will improve the flux pinning. Lowering the synthesis temperature, mechanical alloying, reducing the size of Mg/B powders etc. are tried to reduce the grain size [106,157-161]. Irradiating MgB_2 with high energy particles [protons, neutrons and ions] introduce defects in the crystal structure. These defects act as good flux pinners and scattering centers and improve J_C at higher fields [162-167]. The drawbacks of irradiation are reduction in T_C and low field J_C and its non-suitability to produce long conductors.

Chemical addition/doping, like in LTS superconductors is the most effective method to improve the flux pinning and thus J_C and H_{C2} in MgB_2. Depending on the nature of the dopant, it can cause substitution at Mg/B sites (causing lattice defects/disorders), form secondary phases or remain as such in the MgB_2 matrix. All these can act as flux pinning centres and enhance the H_{C2} and H_{irr} and thereby improve the J_C of MgB_2. A large number of additives/dopants were introduced into MgB_2 to improve its field performance. An overview of such efforts is given here.

Most of the metallic elements were not found to be good dopants to improve J_C of MgB_2. These metallic dopants reacted with Mg/B to form intermetallics, these could only reduce the superconducting volume and grain connectivity. Some metals like Ti and Zr have some positive effects on J_C [168, 169]. Ti is a good grain refiner which absorbs impurities at

grain boundaries and improves grain connectivity. Carbon in various forms (nano carbon- n C, nano diamond-n D, graphite, nanotubes) is highly successful in improving J_C at high fields [170-176]. C is the only element which was found to substitute for B in MgB_2. C substitution strongly alters the σ and π band scattering and enhances J_C and H_{C2}. Due to the smaller covalent radius of C, its entry locally distorts the lattice. The lattice distortions and strains act as good flux pinners. A typical C substituted tape has a $J_C > 10^4$ A/cm^2 at 10-12 T and 4.2 K [177, 178]. A carbon doped MgB_2 fibre showed H_{C2} of ~ 55 T at 1.5 K [118]. The main drawbacks of C doping are significant reduction in T_C and high heat treatment temperatures required (due to the low solubility of C).

The success of Dou *et al* in improving J_C and H_{C2} of MgB_2 by doping n-SiC was, in fact, a significant breakthrough in such efforts [179-181]. They reported that 10% SiC doping has improved J_C by a factor of 32 at 5 K and 8 T. At 20 K and 2 T, J_C of the sample is 2.4×10^5 A/cm^2, which is comparable to the best Ag Bi-2223 tapes. $H_{C2} > 33$ T are reported for SiC doped wire samples at 4.2 K [182]. Unlike n-C, SiC requires only a lower heat treatment temperature. Excellent properties were achieved for samples sintered at temperatures as low as 600 ^{o}C [183]. Also, SiC doesn't affect the T_C much. In MgB_2, SiC decomposes and reacts with Mg to form Mg_2Si and the released C substitutes at B sites. Effect of C substitution for B was explained earlier. Mg_2Si particles dispersed in the MgB_2 matrix act as good flux pinners. Hydrocarbons are another class of excellent dopants. Sugar, malic acid, stearates, toluene, benzene, acetone, paraffin etc. have given good results [150, 184-189]. Easy availability, low cost, low sintering temperatures are some of the advantages of hydrocarbons. They could be coated on the B powder using a suitable solvent, thus enabling better mixing of the dopant. The disadvantage is the presence of oxygen which could increase the amount of MgO. Some silicides, borides, hydrides, rare earth oxides are found to moderately improve flux pinning and J_C. Co-doping of two or more dopants has been found to be very effective in improving the in-field properties of MgB_2 [190-192].

1.10 Applications of MgB_2

The largest commercial market for superconducting wires is in magnetic resonance imaging systems. For the desired image quality high field strength and homogeneity are required. The suitability of a wire depends on the price performance ratio at a given temperature and background field. The low density and low cost of raw materials are favourable factors to reduce the production cost of MgB_2 below NbTi and Nb_3Sn. If the engineering current density

could be increased beyond that of Nb superconductors, MgB_2 could become the wire of choice for MRI systems [193]. MgB_2 has a higher temperature margin compared to LTS which gives the option of solid N_2, conduction or liquid hydrogen cooling systems [194-196]. Persistent MgB_2 joints, which are desirable in MRI systems should be developed first [197].

Together with other superconducting properties, the sharp transition from superconducting to normal state makes MgB_2 an ideal candidate for resistive type fault current limiters (FCL). A stabilized, twisted multifilamentary MgB_2 conductor is a low AC loss superconductor, making it suitable for operation in AC during normal condition. In 20-30 K range, MgB_2 can compete with inductive FCL coils using YBCO. Superconducting transformers have the advantage of reduced size and weight and lower losses compared to conventional transformers. They could reduce the short circuit in the system and lower transformer impedance. A 12.5 kVA MgB_2 superconducting transformer was designed and tested by Hascicek *et al* [198]. Superconducting motors and generators can be power-dense, lightweight, small, highly efficient and reliable. A stator winding using MgB_2 for superconducting motor was tested by Kajikawa *et al* [199]. Hypertech has developed MgB_2 rotor coils for a superconductor generator for NASA [137]. Potential high energy physics applications of MgB_2 are windings of undulator magnet installations and replacement of wiggler magnets in accelerator applications. MgB_2 can also find applications in light source bending magnets and solenoids for muon collider [200]. The low cost and high temperature margin of MgB_2 make it an attractive alternative for NbTi for magnetic separation systems. A 100 MJ superconducting magnetic energy storage (SMES) system using MgB_2 has been conceptualized by Atomura *et al* [201]. NASA is planning to have detectors operating well below 1 K in some of its instruments in space. The temperature will be achieved through adiabatic demagnetization refrigerators. Magnets made of NbTi, Nb_3Sn and MgB_2 are considered for various stages. This is a unique application which requires conductors of very small diameter (0.075-0.20 mm), with an I_C in the range 3-30 A at 15 K and 3-4 T magnetic fields [202].

1.11 Objectives of the present work

Superconductivity, a unique phenomenon of nature, is regarded as one of the greatest scientific discoveries of the 20^{th} century. At the dawn of the 21^{st} century, we are only beginning to exploit its full commercial potential. Among the practical superconductors, MgB_2 has opened new avenues for basic and applied research. The material showcases a plethora of

astonishing features. To exploit its full potential, MgB_2 must be developed into long composite conductors with good mechanical and superconducting properties. Critical current density is one of the yardsticks of a superconductor's suitability for many applications. We have discussed some of the potential applications of MgB_2 in the previous section. The primary factor in materializing many of these is the production of wires with the desired price performance at the targeted field and temperature.

The aim of the present work is to develop MgB_2 wires with improved transport critical current density at higher fields so as to make them suitable for application in cryogen free magnets. To achieve this target, a three stage research plan was made. We have discussed various efforts to improve the $J_C(H)$ of MgB_2. Of these chemical doping is the most effective and scalable technique. In the first stage, we propose to study the effects of chemical doping in improving the in-field properties of MgB_2 in bulk form. *In-situ*, Powder-In-Sealed-Tube (PIST) method will be adopted for the preparation of bulk samples. Effects of mono as well as co-doping effects of n-SiO_2 and nano diamond on the structural and superconducting properties of MgB_2 will be investigated in detail. An issue, which is limiting the effectiveness of chemical doping in the normal methods of preparation, is the agglomeration of nano dopants. To address this issue a novel synthesis route using Mg-Si alloy with uniformly distributed Mg_2Si particles, prepared using casting technique is proposed.

The second stage is the development of MgB_2 in mono and multifilamentary geometries. Effects of heat treatment temperature and duration on the structural and superconducting properties of undoped monofilamentary wires will be examined at this stage. In MgB_2 conductors, sheath materials play an important role. A comparison of commonly used sheath materials regarding their reactivity with the precursor powder, their influence on superconducting properties, strain tolerance, mechanical workability, cost etc. also come under the objectives of the second stage. In the third stage, the main objective is to translate the good superconducting properties achieved in MgB_2 bulk samples in wires and to achieve transport critical current density values on par with the best results reported internationally through chemical doping. Also, we plan to critically analyse the usefulness of Burned Rice Husk (BRH), an indigenously developed dopant by our group as a cheaper alternative for n-SiC, the best dopant reported so far in MgB_2.

Reference

1. "Heike Kamerlingh Onnes - Nobel Lecture: Investigations into the Properties of Substances at Low Temperatures, which Have Led, amongst Other Things, to the Preparation of Liquid Helium". *Nobelprize.org.* Nobel Media AB 2014. Web. 19 Jan 2017. http://www.nobelprize.org/nobel_prizes/physics/laureates/1913/onnes-lecture.html

2. Grassie, A.D.C.: The superconducting state. Chatto and Windus for Sussex University Press, London (1975)

3. Parks, R.D.: Superconductivity: Part 1 (In Two Parts). Taylor & Francis, (1969)

4. Schrieffer, J.R.: Theory of superconductivity. Perseus Books, Reading, Mass (1999)

5. Tinkham, M.: Introduction to superconductivity. Dover Publications, Mineola, NY (2004)

6. Gennes, P.-G.d.: Superconductivity of metals and alloys. Addison-Wesley, Redwood City, Calif. (1989)

7. Wilson, M.N.: Superconducting magnets. Clarendon, Oxford (1986)

8. Huebener, R.P.: Magnetic flux structures in superconductors : extended reprint of a classic text. Springer, Berlin [u.a.] (2001)

9. Schrieffer, J.R., Tinkham, M.: Superconductivity. Reviews of Modern Physics **71**(2), S313-S317 (1999). doi:10.1103/RevModPhys.71.S313

10. Abrikosov, A.A.: Nobel Lecture: Type-II superconductors and the vortex lattice. Reviews of Modern Physics **76**(3), 975-979 (2004). doi:10.1103/RevModPhys.76.975

11. Poole, C.P., Elsevier: Superconductivity. Elsevier, Amsterdam [etc.] (2014)

12. Buzea, C., Yamashita, T.: Review of the superconducting properties of MgB_2. Supercond. Sci. Technol. **14**(11), R115-R146 (2001). doi:10.1088/0953-2048/14/11/201

13. Lee, P.J.: Engineering superconductivity. Wiley-Interscience, New York [u.a.] (2001)

14. Barnes, P.N., Sumption, M.D., Rhoads, G.L.: Review of high power density superconducting generators: Present state and prospects for incorporating YBCO windings. Cryogenics **45**(10-11), 670-686 (2005). doi:10.1016/j.cryogenics.2005.09.001

15. Snitchler, G., Gamble, B., King, C., Winn, P.: 10 MW Class Superconductor Wind Turbine Generators. IEEE Trans. Appl. Supercond. **21**(3), 1089-1092 (2011). doi:10.1109/tasc.2010.2100341

16. Larbalestier, D., Gurevich, A., Feldmann, D.M., Polyanskii, A.: High Tc superconducting materials for electric power applications. Nature **414**(6861), 368-377 (2001). doi:10.1038/35104654

17. Scanlan, R.M., Malozemoff, A.P., Larbalestier, D.C.: Superconducting materials for large scale applications. Proc. IEEE **92**(10), 1639-1654 (2004). doi:10.1109/jproc.2004.833673

18. Hassenzahl, W.V., Hazelton, D.W., Johnson, B.K., Komarek, P., Noe, M., Reis, C.T.: Electric power applications of superconductivity. Proc. IEEE **92**(10), 1655-1674 (2004). doi:10.1109/jproc.2004.833674

19. Paul, W., Baumann, T., Rhyner, J., Platter, F.: Tests of 100 kW high T_C superconducting fault current limiter. IEEE Trans. Appl. Supercond. **5**(2), 1059-1062 (1995). doi:10.1109/77.402734

20. Ono, M., Koga, S., Ohtsuki, H.: Japan's superconducting Maglev train. IEEE Instrum. Meas. Mag. **5**(1), 9-15 (2002). doi:10.1109/5289.988732

21. Lee, H.W., Kim, K.C., Lee, J.: Review of maglev train technologies. IEEE Trans. Magn. **42**(7), 1917-1925 (2006). doi:10.1109/tmag.2006.875842

22. Kamijo, H., Hata, H., Fujimoto, H., Inoue, A., Nagashima, K., Ikeda, K., Iwakuma, M., Funaki, K., Sanuki, Y., Tomioka, A., Yamada, H., Uwamori, K., Yoshida, S.: Tests of superconducting traction transformer for railway rolling stock. IEEE Trans. Appl. Supercond. **17**(2), 1927-1930 (2007). doi:10.1109/tasc.2007.898887

23. Kamijo, H., Hata, H., Fukumoto, Y., Tomioka, A., Bohno, T., Yamada, H., Ayai, Yamasaki, K., Kato, T., Iwakuma, M., Funaki, K., Iop: Development of Low AC Loss Windings for Superconducting Traction Transformer. In: 9th European Conference on Applied Superconductivity, vol. 234. Journal of Physics Conference Series. Iop Publishing Ltd, Bristol (2010)

24. Snitchler, G., Gamble, B., Kalsi, S.S.: The performance of a 5 MW high temperature superconductor ship propulsion motor. IEEE Trans. Appl. Supercond. **15**(2), 2206-2209 (2005). doi:10.1109/tasc.2005.849613

25. Umemoto, K., Aizawa, K., Yokoyama, M., Yoshikawa, K., Kimura, Y., Izumi, M., Ohashi, K., Numano, M., Okumura, K., Yamaguchi, M., Gocho, Y., Kosuge, E., Iop: Development of 1 MW-class HTS motor for podded ship propulsion system. In: 9th European Conference on Applied Superconductivity, vol. 234. Journal of Physics Conference Series. Iop Publishing Ltd, Bristol (2010)

26. Ma, Q.Y., Chan, K.C., Kacher, D.F., Gao, E.Z., Chow, M.S., Wong, K.K., Xu, H., Yang, E.S., Young, G.S., Miller, J.R., Jolesz, F.A.: Superconducting RF coils for clinical MR imaging at low field. Acad. Radiol. **10**(9), 978-987 (2003). doi:10.1016/s1076-6332(03)00110-7

27. Tadic, T., Fallone, B.G.: Design and Optimization of Superconducting MRI Magnet Systems With Magnetic Materials. IEEE Trans. Appl. Supercond. **22**(2) (2012). doi:10.1109/tasc.2012.2183871

28. Razeti, M., Angius, S., Bertora, L., Damiani, D., Marabotto, R., Modica, M., Nardelli, D., Perrella, M., Tassisto, M.: Construction and operation of cryogen free MgB_2 magnets for open MRI systems. IEEE Trans. Appl. Supercond. **18**(2), 882-886 (2008). doi:10.1109/tasc.2008.920661

29. Kajikawa, K., Nakamura, T.: Proposal of a Fully Superconducting Motor for Liquid Hydrogen Pump With MgB_2 Wire. IEEE Trans. Appl. Supercond. **19**(3), 1669-1673 (2009). doi:10.1109/tasc.2009.2017840

30. Oswald, B., Best, K.J., Soell, M., Duffner, E., Gawalek, W., Kovalev, L.K., Krabbes, G., Prusseit, W.: HTS motor program at OSWALD, present status. IEEE Trans. Appl. Supercond. **17**(2), 1583-1586 (2007). doi:10.1109/tasc.2007.897761

31. Ryu, K.S., Jo, Y.S., Park, M.: Overview of the development of the advanced power system by the applied superconductivity technologies programme in Korea. Supercond. Sci. Technol. **19**(3), S102-S108 (2006). doi:10.1088/0953-2048/19/3/014

32. Nishijima, S., Takahata, K., Saito, K., Okada, T., Nakagawa, S., Yoshiwa, M.: Applicability of superconducting magnet to high-gradient magnetic separator. IEEE Trans. Magn. **23**(2), 573-576 (1987). doi:10.1109/tmag.1987.1064909

33. Takeda, S.I., Nishijima, S.G.: Development of magnetic separation of water-soluble materials using superconducting magnet. IEEE Trans. Appl. Supercond. **17**(2), 2178-2180 (2007). doi:10.1109/tasc.2007.899198

34. Kim, T.H., Ha, D.W., Kwon, J.M., Sohn, M.H., Baik, S.K., Oh, S.S., Ko, R.K., Kim, H.S., Kim, Y.H., Park, S.K.: Purification of the Coolant for Hot Roller by Superconducting Magnetic Separation. IEEE Trans. Appl. Supercond. **20**(3), 965-968 (2010). doi:10.1109/tasc.2010.2043521

35. Xu, Z., Wei, B., Cao, B.S., Guo, X.B., Zhang, X.P., Wang, D., Song, X.K., Lu, X.L.: A Compact Superconducting Filter at 6.5 MHz Using Capacitor-Loaded Spiral-in-Spiral-Out Resonators. IEEE Microw. Wirel. Compon. Lett. **24**(4), 242-244 (2014). doi:10.1109/lmwc.2014.2299541

36. Ohsaka, M., Takeuchi, S., Ono, S., Lee, J.H., Saito, A., Akasegawa, A., Yamanaka, K., Kurihara, K., Ohshima, S.: A mechanism for tuning 5 GHz HTS filters. Physica C **468**(15-20), 1966-1968 (2008). doi:10.1016/j.physc.2008.05.180

37. Perkins, F.W., Post, D.E., Uckan, N.A., Azumi, M., Campbell, D.J., Ivanov, N., Sauthoff, N.R., Wakatani, M., Nevins, W.M., Shimada, M., Van Dam, J., Boucher, D., Cordey, G., Costley, A., Jacquinot, J., Janeschitz, G., Mirnov, S., Mukhovatov, V., Porter, G., Putvinski, S., Shimada, M., Stambaugh, R., Wakatani, M., Wesley, J., Young, K., Aymar, R., Shimomura, Y., Boucher, D., Fujisawa, N., Igitkhanov, Y., Kukushkin, A., Mukhovatov, V., Putvinski, S., Rosenbluth, M., Wesley, J.: Chapter 1: Overview and summary. Nucl. Fusion **39**(12), 2137-2174 (1999).

38. Service, R.F.: What It'll Take To Go Exascale. Science **335**(6067), 394-396 (2012).

39. Holmes, S., Ripple, A.L., Manheimer, M.A.: Energy-Efficient Superconducting Computing-Power Budgets and Requirements. IEEE Trans. Appl. Supercond. **23**(3) (2013). doi:10.1109/tasc.2013.2244634

40. Mitchell, N., Devred, A., Libeyre, P., Lim, B., Savary, F., Div, I.M.: The ITER Magnets: Design and Construction Status. IEEE Trans. Appl. Supercond. **22**(3) (2012). doi:10.1109/tasc.2011.2174560

41. Yamamoto, A.: Advances in superconducting magnets for particle physics. IEEE Trans. Appl. Supercond. **14**(2), 477-484 (2004). doi:10.1109/tasc.2004.829700

42. Devred, A., Gourlay, S.A., Yamamoto, A.: Future accelerator magnet needs. IEEE Trans. Appl. Supercond. **15**(2), 1192-1199 (2005). doi:10.1109/tasc.2005.849530

43. Kiyoshi, T., Otsuka, A., Kosuge, M., Yuyama, M., Nagai, H., Matsumoto, F.: Generation of high magnetic fields using superconducting magnets. Fusion Eng. Des. **81**(20-22), 2411-2415 (2006). doi:10.1016/j.fusengdes.2006.07.063

44. Bednorz, J.G., Müller, K.A.: Possible highTc superconductivity in the Ba-La-Cu-O system. Zeitschrift für Physik B Condensed Matter **64**(2), 189-193 (1986). doi:10.1007/bf01303701

45. Wu, M.K., Ashburn, J.R., Torng, C.J., Hor, P.H., Meng, R.L., Gao, L., Huang, Z.J., Wang, Y.Q., Chu, C.W.: Superconductivity at 93 K in a new mixed-phase Y-Ba-Cu-O compound system at ambient pressure. Phys. Rev. Lett. **58**(9), 908-910 (1987). doi:10.1103/PhysRevLett.58.908

46. Burns, G.: High-temperature superconductivity : an introduction. Academic Press, Boston (1992)

47. Tinkham, M., Lobb, C.J.: Physical properties of the new superconductors. Solid State Physics-Advances in Research and Applications **42**, 91-134 (1989).

48. Nagamatsu, J., Nakagawa, N., Muranaka, T., Zenitani, Y., Akimitsu, J.: Superconductivity at 39 K in magnesium diboride. Nature **410**(6824), 63-64 (2001). doi:10.1038/35065039

49. Aswathy, P.M., Anooja, J.B., Sarun, P.M., Syamaprasad, U.: An overview on iron based superconductors. Supercond. Sci. Technol. **23**(7) (2010). doi:10.1088/0953-2048/23/7/073001

50. Liu, X., Zhao, L., He, S.L., He, J.F., Liu, D.F., Mou, D.X., Shen, B., Hu, Y., Huang, J.W., Zhou, X.J.: Electronic structure and superconductivity of FeSe-related superconductors. J. Phys.-Condes. Matter **27**(18) (2015). doi:10.1088/0953-8984/27/18/183201

51. Hosono, H., Tanabe, K., Takayama-Muromachi, E., Kageyama, H., Yamanaka, S., Kumakura, H., Nohara, M., Hiramatsu, H., Fujitsu, S.: Exploration of new superconductors and functional materials, and fabrication of superconducting tapes and wires of iron pnictides. Sci. Technol. Adv. Mater. **16**(3) (2015). doi:10.1088/1468-6996/16/3/033503

52. Krauth, H.: Recent developments in NbTi superconductors at Vacuumschmelze. IEEE Trans. Magn. **24**(2), 1023-1028 (1988). doi:10.1109/20.11402

53. Wada, H.: Fabrication of Nb_3Sn multifilamentary composite superconductors. Cryogenics **35**, S13-S14 (1995). doi:10.1016/0011-2275(95)99824-r

54. Galambos, J.D., Peng, Y.K.M., Lubell, M.S., Dresner, L., Reid, R.L., Miller, J.R.: Comparison of Nb_3Sn and NbTi superconductor magnet ITER Devices. Fusion Technol. **15**(2), 1046-1050 (1989).

55. Sandhage, K.H., Riley, G.N., Carter, W.L.: Critical issues in the OPIT processing of high-J_C BSCCO superconductors. J. Miner. Met. Mater. Soc. **43**(3), 21-25 (1991).

56. Larbalestier, D.C., Cai, X.Y., Feng, Y., Edelman, H., Umezawa, A., Riley, G.N., Carter, W.L.: Position-sensitive measurements of the local critical-current density in Ag sheathed high-temperature superconductor (Bi, $Pb)_2Sr_2Ca_2Cu_3Oy$ tapes - The importance of local microstructure and macrostructure. Physica C **221**(3-4), 299-303 (1994). doi:10.1016/0921-4534(94)90236-4

57. Parrell, J.A., Polyanskii, A.A., Pashitski, A.E., Larbalestier, D.C.: Direct evidence for residual, preferentially-oriented cracks in rolled and pressed Ag-clad BSCCO-2223 tapes and their effect on the critical current density. Supercond. Sci. Technol. **9**(5), 393-398 (1996). doi:10.1088/0953-2048/9/5/010

58. Araki, T., Hirabayashi, I.: Review of a chemical approach to $YBa_2Cu_3O_7$-x-coated, superconductors - metalorganic deposition using trifluoroacetates. Supercond. Sci. Technol. **16**(11), R71-R94 (2003). doi:10.1088/0953-2048/16/11/r01

59. Matsumoto, K., Mele, P.: Artificial pinning center technology to enhance vortex pinning in YBCO coated conductors. Supercond. Sci. Technol. **23**(1) (2010). doi:10.1088/0953-2048/23/1/014001

60. Foltyn, S.R., Civale, L., Macmanus-Driscoll, J.L., Jia, Q.X., Maiorov, B., Wang, H., Maley, M.: Materials science challenges for high-temperature superconducting wire. Nat. Mater. **6**(9), 631-642 (2007). doi:10.1038/nmat1989

61. Malozemoff, A.P., Carter, W., Fleshler, S., Fritzemeier, L., Li, Q., Masur, L., Miles, P., Parker, D., Parrella, R., Podtburg, E., Riley, G.N., Rupich, M., Scudiere, J., Zhang, W.: HTS wire at commercial performance levels. IEEE Trans. Appl. Supercond. **9**(2), 2469-2473 (1999). doi:10.1109/77.784978

62. Vinod, K., Kumar, R.G.A., Syamaprasad, U.: Prospects for MgB_2 superconductors for magnet application. Supercond. Sci. Technol. **20**(1), R1-R13 (2007). doi:10.1088/0953-2048/20/1/r01

63. Xi, X.X.: Two-band superconductor magnesium diboride. Rep. Prog. Phys. **71**(11) (2008). doi:10.1088/0034-4885/71/11/116501

64. Kortus, J.: Current progress in the theoretical understanding of MgB_2. Physica C **456**(1-2), 54-62 (2007). doi:10.1016/j.physc.2007.01.023

65. Patel, D., Al Hossain, M.S., Motaman, A., Barua, S., Shahabuddin, M., Kim, J.H.: Rational design of MgB_2 conductors toward practical applications. Cryogenics **63**, 160-165 (2014). doi:10.1016/j.cryogenics.2014.04.016

66. Vinod, K., Varghese, N., Syamaprasad, U.: Superconductivity of MgB_2 in the BCS framework with emphasis on extrinsic effects on critical temperature. Supercond. Sci. Technol. **20**(10), R31-R45 (2007). doi:10.1088/0953-2048/20/10/r01

67. Blumberg, G., Mialitsin, A., Dennis, B.S., Zhigadlo, N.D., Karpinski, J.: Multi-gap superconductivity in MgB_2: Magneto-Raman spectroscopy. Physica C **456**(1-2), 75-82 (2007). doi:10.1016/j.physc.2007.02.011

68. Ma, Z.Q., Liu, Y.C.: Low-temperature synthesis of MgB_2 superconductors. Int. Mater. Rev. **56**(5-6), 267-286 (2011). doi:10.1179/1743280411y.0000000002

69. Dimitrov, I.K., Zhang, X., Solovyov, V.F., Chubar, O., Li, Q.: Rapid and Semi-analytical Design and Simulation of a Toroidal Magnet Made With YBCO and MgB_2

Superconductors. IEEE Trans. Appl. Supercond. **25**(5) (2015). doi:10.1109/tasc.2015.2448455

70. Ling, J.Y., Voccio, J.P., Hahn, S., Kim, Y., Song, J.B., Bascunan, J., Iwasa, Y.: Construction and Persistent-Mode Operation of MgB_2 Coils in the Range 10-15 K for a 0.5-T/240-mm Cold Bore MRI Magnet. IEEE Trans. Appl. Supercond. **25**(3) (2015). doi:10.1109/tasc.2014.2370105

71. Mine, S., Xu, M.F., Bai, Y., Buresh, S., Stautner, W., Immer, C., Laskaris, E.T., Amm, K.: Development of a 3 T-250 mm Bore MgB_2 Magnet System. IEEE Trans. Appl. Supercond. **25**(3) (2015). doi:10.1109/tasc.2014.2364396

72. Yao, W.J., Bascunan, J., Kim, W.S., Hahn, S., Lee, H., Iwasa, Y.: A solid nitrogen cooled MgB_2 "Demonstration" coil for MRI applications. IEEE Trans. Appl. Supercond. **18**(2), 912-915 (2008). doi:10.1109/tasc.2008.920836

73. Jones, M.E., Marsh, R.E.: The Preparation and Structure of Magnesium Boride, MgB_2. Journal of the American Chemical Society **76**(5), 1434-1436 (1954). doi:10.1021/ja01634a089

74. Swift, R.M., White, D.: Low Temperature Heat Capacities of Magnesium Diboride (MgB_2) and Magnesium Tetraboride (MgB_4). Journal of the American Chemical Society **79**(14), 3641-3644 (1957). doi:10.1021/ja01571a007

75. Suhl, H., Matthias, B.T., Walker, L.R.: Bardeen-Cooper-Schrieffer Theory of Superconductivity in the Case of Overlapping Bands. Phys. Rev. Lett. **3**(12), 552-554 (1959). doi: 10.1103/PhysRevLett.3.552

76. Binnig, G., Baratoff, A., Hoenig, H.E., Bednorz, J.G.: Two-Band Superconductivity in Nb-Doped $SrTiO_3$. Phys. Rev. Lett. **45**(16), 1352-1355 (1980). doi: 10.1103/PhysRevLett.45.1352

77. Oikawa, K., Kamiyama, T., Mochiku, T., Takeya, H., Furuyama, M., Kamisawa, S., Arai, M., Kadowaki, K.: Neutron powder diffraction study on ($Mg^{11}B_2$) synthesized by different procedures. J. Phys. Soc. Jpn. **71**(10), 2471-2476 (2002). doi:10.1143/jpsj.71.2471

78. Margadonna, S., Muranaka, T., Prassides, K., Maurin, I., Brigatti, K., Ibberson, R.M., Arai, M., Takata, M., Akimitsu, J.: Phase inhomogeneities and lattice expansion near Tc in the ($Mg^{11}B_2$) superconductor. J. Phys.-Condes. Matter **13**(35), L795-L802 (2001). doi:10.1088/0953-8984/13/35/101

79. Jorgensen, J.D., Hinks, D.G., Short, S.: Lattice properties of MgB_2 versus temperature and pressure. Phys. Rev. B **63**(22) (2001). doi:10.1103/PhysRevB.63.224522

80. Eltsev, Y., Lee, S., Nakao, K., Chikumoto, N., Tajima, S., Koshizuka, N., Murakami, M.: Anisotropic superconducting properties of MgB_2 single crystals probed by in-plane electrical transport measurements. Phys. Rev. B **65**(14) (2002). doi:10.1103/PhysRevB.65.140501

81. Eisterer, M., Zehetmayer, M., Weber, H.W.: Current percolation and anisotropy in polycrystalline MgB_2. Phys. Rev. Lett. **90**(24) (2003). doi:10.1103/PhysRevLett.90.247002

82. de Lima, O.F., Ribeiro, R.A., Avila, M.A., Cardoso, C.A., Coelho, A.A.: Anisotropic superconducting properties of aligned MgB_2 crystallites. Phys. Rev. Lett. **86**(26), 5974-5977 (2001). doi:10.1103/PhysRevLett.86.5974

83. Finnemore, D.K., Ostenson, J.E., Bud'ko, S.L., Lapertot, G., Canfield, P.C.: Thermodynamic and transport properties of superconducting ($Mg^{10}B_2$). Phys. Rev. Lett. **86**(11), 2420-2422 (2001). doi:10.1103/PhysRevLett.86.2420

84. Calandra, M., Lazzeri, M., Mauri, F.: Anharmonic and non-adiabatic effects in MgB_2: Implications for the isotope effect and interpretation of Raman spectra. Physica C **456**(1-2), 38-44 (2007). doi:10.1016/j.physc.2007.01.021

85. Choi, H.J., Roundy, D., Sun, H., Cohen, M.L., Louie, S.G.: The origin of the anomalous superconducting properties of MgB_2. Nature **418**(6899), 758-760 (2002). doi:10.1038/nature00898

86. Canfield, P.C., Finnemore, D.K., Bud'ko, S.L., Ostenson, J.E., Lapertot, G., Cunningham, C.E., Petrovic, C.: Superconductivity in dense MgB_2 wires. Phys. Rev. Lett. **86**(11), 2423-2426 (2001). doi:10.1103/PhysRevLett.86.2423

87. Takano, Y., Takeya, H., Fujii, H., Kumakura, H., Hatano, T., Togano, K., Kito, H., Ihara, H.: Superconducting properties of MgB_2 bulk materials prepared by high-pressure sintering. Appl. Phys. Lett. **78**(19), 2914-2916 (2001). doi:10.1063/1.1371239

88. Li, S.L., Wen, H.H., Zhao, Z.W., Ni, Y.M., Ren, Z.A., Che, G.C., Yang, H.P., Liu, Z.Y., Zhao, Z.X.: Linear temperature dependence of lower critical field in MgB_2. Phys. Rev. B **64**(9) (2001). doi:10.1103/PhysRevB.64.094522

89. Bud'ko, S.L., Petrovic, C., Lapertot, G., Cunningham, C.E., Canfield, P.C., Jung, M.H., Lacerda, A.H.: Magnetoresistivity and $H_{c2}(T)$ in MgB_2. Phys. Rev. B **63**(22) (2001). doi:10.1103/PhysRevB.63.220503

90. Kunchur, M.N., Lee, S.I., Kang, W.N.: Pair-breaking critical current density of magnesium diboride. Phys. Rev. B **68**(6) (2003). doi:10.1103/PhysRevB.68.064516

91. Iavarone, M., Karapetrov, G., Koshelev, A.E., Kwok, W.K., Crabtree, G.W., Kang, W.N., Choi, E.M., Kim, H.J., Lee, S.I.: STM tunnelling spectroscopy in MgB_2 thin films: the role of band structure in tunnelling spectra. Supercond. Sci. Technol. **17**(5), S106-S111 (2004). doi:10.1088/0953-2048/17/5/003

92. Kortus, J., Mazin, II, Belashchenko, K.D., Antropov, V.P., Boyer, L.L.: Superconductivity of metallic boron in MgB_2. Phys. Rev. Lett. **86**(20), 4656-4659 (2001). doi:10.1103/PhysRevLett.86.4656

93. An, J.M., Pickett, W.E.: Superconductivity of MgB_2: Covalent bonds driven metallic. Phys. Rev. Lett. **86**(19), 4366-4369 (2001). doi:10.1103/PhysRevLett.86.4366

94. Yelland, E.A., Cooper, J.R., Carrington, A., Hussey, N.E., Meeson, P.J., Lee, S., Yamamoto, A., Tajima, S.: de Haas-van Alphen Effect in Single Crystal MgB_2. Phys. Rev. Lett. **88**(21), 217002 (2002). doi: 10.1103/PhysRevLett.88.217002

95. Liu, A.Y., Mazin, II, Kortus, J.: Beyond Eliashberg superconductivity in MgB_2: Anharmonicity, two-phonon scattering, and multiple gaps. Phys. Rev. Lett. **87**(8) (2001). doi:10.1103/PhysRevLett.87.087005

96. Pan, A.V., Zhou, S.H., Liu, H.K., Don, S.X.: Properties of superconducting MgB_2 wires: in situ versus ex situ reaction technique. Supercond. Sci. Technol. **16**(5), 639-644 (2003). doi:10.1088/0953-2048/16/5/317

97. Yamamoto, A., Tanaka, H., Shimoyama, J., Ogino, H., Kishio, K., Matsushita, T.: Towards the Realization of Higher Connectivity in MgB_2 Conductors: In-situ or Sintered Ex-situ? Jpn. J. Appl. Phys. **51**(1) (2012). doi:10.1143/jjap.51.010105

98. Fujii, H., Togano, K., Kumakura, H.: Fabrication of MgB_2 tapes sheathed with carbon steels by ex situ and in situ methods. IEEE Trans. Appl. Supercond. **13**(2), 3217-3220 (2003). doi:10.1109/tasc.2003.812204

99. Zhao, Y., Ionescu, M., Horvat, J., Don, S.X.: Comparative study of in situ and ex situ MgB_2 films prepared by pulsed laser deposition. Supercond. Sci. Technol. **17**(9), S482-S485 (2004). doi:10.1088/0953-2048(04)77115-8

100. Kovac, P., Husek, I., Melisek, T., Martinez, E., Dhalle, M.: Properties of doped ex and in situ MgB_2 multi-filament superconductors. Supercond. Sci. Technol. **19**(10), 1076-1082 (2006). doi:10.1088/0953-2048/19/10/016

101. Kovac, P., Melisek, T., Dhalle, M., den Ouden, A., Husek, I.: Critical currents of MgB_2 wires prepared in situ and ex situ subjected to axial stress. Supercond. Sci. Technol. **18**(10), 1374-1379 (2005). doi:10.1088/0953-2048/18/10/022

102. Alknes, P., Hagner, M., Bjoerstad, R., Scheuerlein, C., Bordini, B., Sugano, M., Hudspeth, J., Ballarino, A.: Mechanical Properties and Strain-Induced Filament Degradation of Ex Situ and In Situ MgB_2 Wires. IEEE Trans. Appl. Supercond. **26**(3) (2016). doi:10.1109/tasc.2015.2509166

103. Yamada, H., Hirakawa, M., Kumakura, H., Matsumoto, A., Kitaguchi, H.: Critical current densities of powder-in-tube MgB_2 tapes fabricated with nanometer-size Mg powder. Appl. Phys. Lett. **84**(10), 1728-1730 (2004). doi:10.1063/1.1667263

104. Kumakura, H., Kitaguchi, H., Matsumoto, A., Hatakeyama, H.: Upper critical fields of powder-in-tube-processed MgB_2/Fe tape conductors. Appl. Phys. Lett. **84**(18), 3669-3671 (2004). doi:10.1063/1.1738947

105. Chen, S.K., Lockman, Z., Wei, M., Glowacki, B.A., MacManus-Driscoll, J.L.: Improved current densities in MgB_2 by liquid-assisted sintering. Appl. Phys. Lett. **86**(24) (2005). doi:10.1063/1.1947374

106. Wu, Y.F., Lu, Y.F., Li, J.S., Chen, S.K., Yan, G., Pu, M.H., Li, C.S., Zhang, P.X.: The microstructures and superconducting properties of MgB_2 bulks prepared by a high-energy milling method. Physica C **467**(1-2), 38-42 (2007). doi:10.1016/j.physc.2007.08.010

107. Senkowicz, B.J., Polyanskii, A., Mungall, R.J., Zhu, Y., Giencke, J.E., Voyles, P.M., Eom, C.B., Hellstrom, E.E., Larbalestier, D.C.: Understanding the route to high critical current density in mechanically alloyed Mg($B_{1-x}C_x)_2$. Supercond. Sci. Technol. **20**(7), 650-657 (2007). doi:10.1088/0953-2048/20/7/011

108. Xu, X., Kim, J.H., Yeoh, W.K., Zhang, Y., Dou, S.X.: Improved Jc of MgB_2 superconductor by ball milling using different media. Supercond. Sci. Technol. **19**(11), L47-L50 (2006). doi:10.1088/0953-2048/19/11/l01

109. Prikhna, T.A., Gawalek, W., Savchuk, Y.M., Moshchil, V.E., Sergienko, N.V., Habisreuther, T., Wendt, M., Hergt, R., Schmidt, C., Dellith, J., Melnikov, V.S., Assmann, A., Litzkendorf, D., Nagorny, P.A.: High-pressure synthesis of MgB_2 with addition of Ti. Physica C **402**(3), 223-233 (2004). doi:10.1016/j.physc.2003.10.021

110. Prikhna, T.A., Gawalek, W., Savchuk, Y.M., Habisreuther, T., Wendt, M., Sergienko, N.V., Moshchil, V.E., Nagorny, P., Schmidt, C., Dellith, J., Dittrich, U., Litzkendorf, D., Melnikov, V.S., Sverdun, V.B.: The inclusions of Mg-B (MgB_{12}?) as potential pinning centres in high-pressure-high-temperature-synthesized or sintered magnesium diboride. Supercond. Sci. Technol. **20**(9), S257-S263 (2007). doi:10.1088/0953-2048/20/9/s21

111. Frederick, N.A., Li, S., Maple, M.B., Nesterenko, V.F., Indrakanti, S.S.: Improved superconducting properties of MgB_2. Physica C **363**(1), 1-5 (2001). doi:10.1016/s0921-4534(01)00948-0

112. Maeda, M., Zhao, Y., Dou, S.X., Nakayama, Y., Kawakami, T., Kobayashi, H., Kubota, Y.: Fabrication of highly dense MgB_2 bulk at ambient pressure. Supercond. Sci. Technol. **21**(3) (2008). doi:10.1088/0953-2048/21/3/032004

113. Giunchi, G., Ripamonti, G., Cavallin, T., Bassani, E.: The reactive liquid Mg infiltration process to produce large superconducting bulk MgB_2 manufacts. Cryogenics **46**(2-3), 237-242 (2006). doi:10.1016/j.cryogenics.2005.11.011

114. Giunchi, G.: High density MgB_2 obtained by reactive liquid Mg infiltration. International Journal of Modern Physics B **17**(4-6), 453-460 (2003). doi:10.1142/s0217979203016091

115. Giunchi, G., Ceresara, S., Ripamonti, G., Di Zenobio, A., Rossi, S., Chiarelli, S., Spadoni, M., Wesche, R., Bruzzone, P.L.: High performance new MgB_2 superconducting hollow wires. Supercond. Sci. Technol. **16**(2), 285-291 (2003). doi:10.1088/0953-2048/16/2/328

116. Hur, J.M., Togano, K., Matsumoto, A., Kumakura, H., Wada, H., Kimura, K.: Fabrication of high-performance MgB_2 wires by an internal Mg diffusion process. Supercond. Sci. Technol. **21**(3) (2008). doi:10.1088/0953-2048/21/3/032001

117. Togano, K., Hur, J.M., Matsumoto, A., Kumakura, H.: Fabrication of seven-core multi-filamentary MgB_2 wires with high critical current density by an internal Mg diffusion process. Supercond. Sci. Technol. **22**(1) (2009). doi:10.1088/0953-2048/22/1/015003

118. Ferrando, V., Orgiani, P., Pogrebnyakov, A.V., Chen, J., Li, Q., Redwing, J.M., Xi, X.X., Giencke, J.E., Eom, C.B., Feng, Q.R., Betts, J.B., Mielke, C.H.: High upper critical field and irreversibility field in MgB_2 coated-conductor fibers. Appl. Phys. Lett. **87**(25) (2005). doi:10.1063/1.2149289

119. Komori, K., Kawagishi, K., Takano, Y., Fujii, H., Arisawa, S., Kumakura, H., Fukutomi, M., Togano, K.: Approach for the fabrication of MgB_2 superconducting tape with large in-field transport critical current density. Appl. Phys. Lett. **81**(6), 1047-1049 (2002). doi:10.1063/1.1495087

120. Abe, H., Nishida, K., Imai, M., Kitazawa, H., Yoshii, K.: Superconducting properties of MgB_2 films electroplated to stainless steel substrates. Appl. Phys. Lett. **85**(25), 6197-6199 (2004). doi:10.1063/1.1839644

121. Auinger, M., Gritzner, G.: Magnesium diboride films on iron substrates. Supercond. Sci. Technol. **21**(1) (2008). doi:10.1088/0953-2048/21/01/015006

122. Chen, L.P., Li, F., Guo, T., Zhuang, C.G., Yao, D., Ding, L.L., Zhang, K.C., Gan, Z.Z., Xiong, G.C., Feng, Q.R.: Deposition of MgB_2 superconducting films on different metal substrates. Chinese Physics Letters **24**(7), 2074-2076 (2007).

123. Zhuang, C.G., Yao, D., Li, F., Zhang, K.C., Feng, Q.R., Gan, Z.Z.: Study of micron-thick MgB_2 films on niobium substrates. Supercond. Sci. Technol. **20**(3), 287-291 (2007). doi:10.1088/0953-2048/20/3/030

124. Kumakura, H., Matsumoto, A., Nakane, T., Kitaguchi, H.: Fabrication and properties of powder-in-tube-processed MgB_2 tape conductors. Physica C **456**(1-2), 196-202 (2007). doi:10.1016/j.physc.2006.12.017

125. Suo, H.L., Beneduce, C., Dhalle, M., Musolino, N., Genoud, J.Y., Flukiger, R.: Large transport critical currents in dense Fe- and Ni-clad MgB_2 superconducting tapes. Appl. Phys. Lett. **79**(19), 3116-3118 (2001). doi:10.1063/1.1415349

126. Kumakura, H., Matsumoto, A., Fujii, H., Togano, K.: High transport critical current density obtained for powder-in-tube-processed MgB_2 tapes and wires using stainless steel and Cu-Ni tubes. Appl. Phys. Lett. **79**(15), 2435-2437 (2001). doi:10.1063/1.1407856

127. Grasso, G., Malagoli, A., Ferdeghini, C., Roncallo, S., Braccini, V., Siri, A.S., Cimberle, M.R.: Large transport critical currents in unsintered MgB_2 superconducting tapes. Appl. Phys. Lett. **79**(2), 230-232 (2001). doi:10.1063/1.1384905

128. Fang, H., Putman, P.T., Padmanabhan, S., Zhou, Y.X., Salama, K.: Transport critical current on Fe-sheathed MgB_2 coils. Supercond. Sci. Technol. **17**(4), 717-720 (2004). doi:10.1088/0953-2048/17/4/028

129. Glowacki, B.A., Majoros, M., Vickers, M., Evetts, J.E., Shi, Y., McDougall, I.: Superconductivity of powder-in-tube MgB_2 wires. Supercond. Sci. Technol. **14**(4), 193-199 (2001). doi:10.1088/0953-2048/14/4/304

130. Jun, B.H., Kim, Y.J., Tan, K.S., Kim, J.H., Xu, X., Dou, S.X., Kim, C.J.: Influence of intermediate annealing on the microstructure of in situ MgB_2/Fe wire. Physica C **468**(15-20), 1825-1828 (2008). doi:10.1016/j.physc.2008.05.152

131. Devadas, K.M., Rahul, S., Thomas, S., Varghese, N., Vinod, K., Syamaprasad, U., Pradhan, S., Chattopadhyay, M.K., Roy, S.B.: Transport properties of sealed MgB_2/Fe/Ni multifilamentary wires heat treated in air. J. Alloy. Compd. **509**(31), 8038-8041 (2011). doi:10.1016/j.jallcom.2011.04.147

132. Wang, Q.Y., Jiao, G.F., Liu, G.Q., Xiong, X.M., Yan, S.C., Zhang, P.X., Sulpice, A., Mossang, E., Feng, Y., Yan, G.: Fabrication and properties of multifilamentary MgB_2 wires by in-situ powder-in-tube process. Physica C **470**(20), 1415-1418 (2010). doi:10.1016/j.physc.2010.05.126

133. Soltanian, S., Wang, X.L., Li, A.H., Collings, E.W., Sumption, M.D., Lee, E., Liu, H.K., Dou, S.X.: Fabrication and critical current density in 16-filament stainless steel/Fe/MgB_2 square wire. Solid State Commun. **124**(1-2), 59-62 (2002). doi:10.1016/s0038-1098(02)00380-0

134. Kovac, P., Melisek, T., Kopera, L., Husek, I., Polak, M., Kulich, M.: Progress in electrical and mechanical properties of rectangular MgB_2 wires. Supercond. Sci. Technol. **22**(7) (2009). doi:10.1088/0953-2048/22/7/075026

135. Kovac, P., Husek, I., Melisek, T., Kulich, M., Kopera, L.: Bending strain tolerance of MgB_2 superconducting wires. Supercond. Sci. Technol. **29**(4) (2016). doi:10.1088/0953-2048/29/4/045002

136. Kovac, P., Husek, I., Melisek, T., Kopera, L., Reissner, M.: Cu stabilized MgB_2 composite wire with an NbTi barrier. Supercond. Sci. Technol. **23**(2) (2010). doi:10.1088/0953-2048/23/2/025014

137. Tomsic, M., Rindfleisch, M., Yue, J.J., McFadden, K., Doll, D., Phillips, J., Sumption, M.D., Bhatia, M., Bohnenstiehl, S., Collings, E.W.: Development of magnesium diboride (MgB_2) wires and magnets using in situ strand fabrication method. Physica C **456**(1-2), 203-208 (2007). doi:10.1016/j.physc.2007.01.009

138. Kovac, P., Husek, I., Melisek, T.: MgB_2 cable made from two-axially rolled wires. Supercond. Sci. Technol. **21**(12) (2008). doi:10.1088/0953-2048/21/12/125003

139. Kang, W.N., Kim, H.J., Choi, E.M., Jung, C.U., Lee, S.L.: MgB_2 superconducting thin films with a transition temperature of 39 kelvin. Science **292**(5521), 1521-1523 (2001). doi:10.1126/science.1060822

140. Kim, H.J., Kang, W.N., Choi, E.M., Kim, M.S., Kim, K.H.P., Lee, S.: High current-carrying capability in c-axis-oriented superconducting MgB_2 thin films. Phys. Rev. Lett. **87**(8) (2001). doi:10.1103/PhysRevLett.87.087002

141. Zeng, X.H., Pogrebnyakov, A.V., Kotcharov, A., Jones, J.E., Xi, X.X., Lysczek, E.M., Redwing, J.M., Xu, S.Y., Lettieri, J., Schlom, D.G., Tian, W., Pan, X.Q., Liu, Z.K.: In situ epitaxial MgB_2 thin films for superconducting electronics. Nat. Mater. **1**(1), 35-38 (2002). doi:10.1038/nmat703

142. Lee, S.: Crystal growth of MgB_2. Physica C **385**(1-2), 31-41 (2003). doi:10.1016/s0921-4534(02)02323-7

143. Karpinski, J., Kazakov, S.M., Jun, J., Angst, M., Puzniak, R., Wisniewski, A., Bordet, P.: Single crystal growth of MgB_2 and thermodynamics of Mg-B-N system at high pressure. Physica C **385**(1-2), 42-48 (2003). doi:10.1016/s0921-4534(02)02308-0

144. Jiang, J., Senkowicz, B.J., Larbalestier, D.C., Hellstrom, E.E.: Influence of boron powder purification on the connectivity of bulk MgB_2. Supercond. Sci. Technol. **19**(8), L33-L36 (2006). doi:10.1088/0953-2048/19/8/l02

145. Collings, E.W., Sumption, M.D., Bhatia, M., Susner, M.A., Bohnenstiehl, S.D.: Prospects for improving the intrinsic and extrinsic properties of magnesium diboride superconducting strands. Supercond. Sci. Technol. **21**(10) (2008). doi:10.1088/0953-2048/21/10/103001

146. Cetner, T., Morawski, A., Gajda, D., Hassler, W., Rindfleisch, M., Tomsic, M., Zaleski, A., Czujko, T., Zuchowska, E., Przyslupski, P.: Hot isostatic pressing of multifilamentary MgB_2 wires in solid state media for large scale application. Supercond. Sci. Technol. **28**(4) (2015). doi:10.1088/0953-2048/28/4/045009

147. Serquis, A., Civale, L., Hammon, D.L., Liao, X.Z., Coulter, J.Y., Zhu, Y.T., Jaime, M., Peterson, D.E., Mueller, F.M., Nesterenko, V.F., Gu, Y.: Hot isostatic pressing of powder in tube MgB_2 wires. Appl. Phys. Lett. **82**(17), 2847-2849 (2003). doi:10.1063/1.1571231

148. Jie, H., Qiu, W.B., Billah, M., Mustapic, M., Patel, D., Ma, Z.Q., Gajda, D., Morawski, A., Cetner, T., Shahabuddin, M., Yanmaz, E., Rindfleisch, M., Kim, J.H., Hossain, M.S.A.: Superior transport Jc obtained in in-situ MgB_2 wires by tailoring the starting materials and using a combined cold high pressure densification and hot isostatic pressure treatment. Scr. Mater. **129**, 79-83 (2017). doi:10.1016/j.scriptamat.2016.09.042

149. Flukiger, R., Hossain, M.S.A., Kulich, M., Senatore, C.: Technical aspects of Cold High Pressure Densification (CHPD) on long lengths of in situ MgB_2 wires with enhanced Jc values. In: Balachandran, U. (ed.) Advances in Cryogenic Engineering, Vol 58, vol. 1435. AIP Conference Proceedings, pp. 353-362. Amer Inst Physics, Melville (2012)

150. Hossain, M.S.A., Senatore, C., Fluekiger, R., Rindfleisch, M.A., Tomsic, M.J., Kim, J.H., Dou, S.X.: The enhanced Jc and B_{irr} of in situ MgB_2 wires and tapes alloyed with $C_4H_6O_5$ (malic acid) after cold high pressure densification. Supercond. Sci. Technol. **22**(9) (2009). doi:10.1088/0953-2048/22/9/095004

151. Vinod, K., Varghese, N., Rahul, S., Devadas, K.M., Thomas, S., Gurusamy, P., Kedia, S., Pradhan, S., Syamaprasad, U.: On the current transfer length and current sharing in short length MgB_2 wires. Supercond. Sci. Technol. **23**(10) (2010). doi:10.1088/0953-2048/23/10/105002

152. Eisterer, M.: Magnetic properties and critical currents of MgB_2. Supercond. Sci. Technol. **20**(12), R47-R73 (2007). doi:10.1088/0953-2048/20/12/r01

153. Matsushita, T., Kiuchi, M., Yamamoto, A., Shimoyama, J.-I., Kishio, K.: Essential factors for the critical current density in superconducting MgB_2: connectivity and flux pinning by grain boundaries. Supercond. Sci. Technol. **21**(1) (2008). doi:10.1088/0953-2048/21/01/015008

154. Bud'ko, S.L., Lapertot, G., Petrovic, C., Cunningham, C.E., Anderson, N., Canfield, P.C.: Boron isotope effect in superconducting MgB_2. Phys. Rev. Lett. **86**(9), 1877-1880 (2001). doi:10.1103/PhysRevLett.86.1877

155. Gurevich, A.: Enhancement of the upper critical field by nonmagnetic impurities in dirty two-gap superconductors. Phys. Rev. B **67**(18) (2003). doi:10.1103/PhysRevB.67.184515

156. Gurevich, A., Patnaik, S., Braccini, V., Kim, K.H., Mielke, C., Song, X., Cooley, L.D., Bu, S.D., Kim, D.M., Choi, J.H., Belenky, L.J., Giencke, J., Lee, M.K., Tian, W., Pan, X.Q., Siri, A., Hellstrom, E.E., Eom, C.B., Larbalestier, D.C.: Very high upper critical fields in MgB_2 produced by selective tuning of impurity scattering. Supercond. Sci. Technol. **17**(2), 278-286 (2004). doi:10.1088/0953-2048/17/2/008

157. Liu, Y., Lan, F., Ma, Z., Chen, N., Li, H., Barua, S., Patel, D., Shahriar, M., Hossain, A., Acar, S., Kim, J.H., Dou, S.X.: Significantly enhanced critical current density in nano-MgB_2 grains rapidly formed at low temperature with homogeneous carbon doping. Supercond. Sci. Technol. **28**(5) (2015). doi:10.1088/0953-2048/28/5/055005

158. Kim, J.H., Dou, S.X., Wang, J.L., Shi, D.Q., Xu, X., Hossain, M.S.A., Yeoh, W.K., Choi, S., Kiyoshi, T.: The effects of sintering temperature on superconductivity in MgB_2/Fe wires. Supercond. Sci. Technol. **20**(5), 448-451 (2007). doi:10.1088/0953-2048/20/5/007

159. Kario, A., Nast, R., Haessler, W., Rodig, C., Mickel, C., Goldacker, W., Holzapfel, B., Schultz, L.: Critical current density enhancement in strongly reactive ex situ MgB_2 bulk and tapes prepared by high energy milling. Supercond. Sci. Technol. **24**(7) (2011). doi:10.1088/0953-2048/24/7/075011

160. Vinod, K., Varghese, N., Kumar, R.G.A., Syamaprasad, U., Roy, S.B.: Influence of Mg particle size on the reactivity and superconducting properties of in situ MgB_2. J. Alloy. Compd. **464**(1-2), 33-37 (2008). doi:10.1016/j.jallcom.2007.10.030

161. Vignolo, M., Romano, G., Martinelli, A., Bernini, C., Siri, A.S.: A Novel Process to Produce Amorphous Nanosized Boron Useful for MgB_2 Synthesis. IEEE Trans. Appl. Supercond. **22**(4) (2012). doi:10.1109/tasc.2012.2190510

162. Pallecchi, I., Ferrando, V., Tarantini, C., Putti, M., Ferdeghini, C., Zhu, Y., Voyles, P.M., Xi, X.X.: Increased in-field critical current density in neutron-irradiated MgB_2 films. Supercond. Sci. Technol. **22**(1) (2009). doi:10.1088/0953-2048/22/1/015023

163. Pallecchi, I., Tarantini, C., Aebersold, H.U., Braccini, V., Fanciulli, C., Ferdeghini, C., Gatti, F., Lehmann, E., Manfrinetti, P., Marre, D., Palenzona, A., Siri, A.S., Vignolo, M., Putti, M.: Enhanced flux pinning in neutron irradiated MgB_2. Phys. Rev. B **71**(21) (2005). doi:10.1103/PhysRevB.71.212507

164. Perkins, G.K., Bugoslavsky, Y., Caplin, A.D., Moore, J., Tate, T.J., Gwilliam, R., Jun, J., Kazakov, S.M., Karpinski, J., Cohen, L.F.: Effects of proton irradiation and ageing on the superconducting properties of single crystalline and polycrystalline MgB_2. Supercond. Sci. Technol. **17**(1), 232-235 (2004). doi:10.1088/0953-2048/17/1/039

165. Bugoslavsky, Y., Cohen, L.F., Perkins, G.K., Polichetti, M., Tate, T.J., Gwilliam, R., Caplin, A.D.: Enhancement of the high-magnetic field critical current density of superconducting MgB_2 by proton irradiation. Nature **411**(6837), 561-563 (2001). doi:10.1038/35079024

166. Wang, Y.-B., Xue, C., Feng, Q.-R.: The effects of Ti ion-irradiation on critical current and flux pinning in MgB_2 thin film. Acta Physica Sinica **61**(19) (2012). doi:10.7498/aps.61.197401

167. Chikumoto, N., Yamamoto, A., Konczykowski, M., Murakami, M.: Effect of heavy-ion irradiation on the pinning properties of MgB_2. Physica C **388**, 167-168 (2003). doi:10.1016/s0921-4534(02)02709-0

168. Feng, Y., Zhao, Y., Pradhan, A.K., Cheng, C.H., Yau, J.K.F., Zhou, L., Koshizuka, N., Murakami, M.: Enhanced flux pinning in Zr-doped MgB_2 bulk superconductors prepared at ambient pressure. J. Appl. Phys. **92**(5), 2614-2619 (2002). doi:10.1063/1.1496128

169. Zhao, Y., Feng, Y., Cheng, C.H., Zhou, L., Wu, Y., Machi, T., Fudamoto, Y., Koshizuka, N., Murakami, M.: High critical current density of MgB_2 bulk superconductor doped with Ti and sintered at ambient pressure. Appl. Phys. Lett. **79**(8), 1154-1156 (2001). doi:10.1063/1.1396629

170. Yeoh, W.K., Dou, S.: Enhancement of H_{C2} and J_C by carbon-based chemical doping. Physica C **456**(1-2), 170-179 (2007). doi:10.1016/j.physc.2007.01.024

171. Soltanian, S., Horvat, J., Wang, X.L., Munroe, P., Dou, S.: Effect of nano-carbon particle doping on the flux pinning properties of MgB_2 superconductor. Physica C **390**(3), 185-190 (2003). doi:10.1016/s0921-4534(03)00960-2

172. Pogrebnyakov, A.V., Xi, X.X., Redwing, J.M., Vaithyanathan, V., Schlom, D.G., Soukiassian, A., Mi, S.B., Jia, C.L., Giencke, J.E., Eom, C.B., Chen, J., Hu, Y.F., Cui, Y., Li, Q.: Properties of MgB_2 thin films with carbon doping. Appl. Phys. Lett. **85**(11), 2017-2019 (2004). doi:10.1063/1.1782258

173. Cheng, C.H., Yang, Y., Munroe, P., Zhao, Y.: Comparison between nano-diamond and carbon nanotube doping effects on critical current density and flux pinning in MgB_2. Supercond. Sci. Technol. **20**(3), 296-301 (2007). doi:10.1088/0953-2048/20/3/032

174. Serrano, G., Serquis, A., Dou, S.X., Soltanian, S., Civale, L., Maiorov, B., Holesinger, T.G., Balakirev, F., Jaime, M.: SiC and carbon nanotube distinctive effects on the superconducting properties of bulk MgB_2. J. Appl. Phys. **103**(2) (2008). doi:10.1063/1.2832463

175. Yeoh, W.K., Horvat, J., Dou, S.X., Munroe, P.: Effect of carbon nanotube size on superconductivity properties of MgB_2. IEEE Trans. Appl. Supercond. **15**(2), 3284-3287 (2005). doi:10.1109/tasc.2005.848853

176. Pan, X.F., Zhao, Y., Feng, Y., Yang, Y., Cheng, C.H.: Effects of graphite doping on critical current density and microstructure of MgB_2 bulks by an improved Mg-diffusion method. Physica C **468**(15-20), 1169-1173 (2008). doi:10.1016/j.physc.2008.05.025

177. Herrmann, M., Haessler, W., Rodig, C., Gruner, W., Holzapfel, B., Schultz, L.: Touching the properties of NbTi by carbon doped tapes with mechanically alloyed MgB_2. Appl. Phys. Lett. **91**(8) (2007). doi:10.1063/1.2773942

178. Ma, Y.W., Zhang, X.P., Nishijima, G., Watanabe, K., Awaji, S., Bai, X.D.: Significantly enhanced critical current densities in MgB_2 tapes made by a scaleable nanocarbon addition route. Appl. Phys. Lett. **88**(7) (2006). doi:10.1063/1.2173635

179. Dou, S.X., Soltanian, S., Horvat, J., Wang, X.L., Zhou, S.H., Ionescu, M., Liu, H.K., Munroe, P., Tomsic, M.: Enhancement of the critical current density and flux pinning of MgB_2 superconductor by nanoparticle SiC doping. Appl. Phys. Lett. **81**(18), 3419-3421 (2002). doi:10.1063/1.1517398

180. Dou, S.X., Pan, A.V., Zhou, S., Ionescu, M., Wang, X.L., Horvat, J., Liu, H.K., Munroe, P.R.: Superconductivity, critical current density, and flux pinning in MgB_2-$x(SiC)_{x/2}$ superconductor after SiC nanoparticle doping. J. Appl. Phys. **94**(3), 1850-1856 (2003). doi:10.1063/1.1586467

181. Dou, S.X., Pan, A.V., Zhou, S., Ionescu, M., Liu, H.K., Munroe, P.R.: Substitution-induced pinning in MgB_2 superconductor doped with SiC nano-particles. Supercond. Sci. Technol. **15**(11), 1587-1591 (2002). doi:10.1088/0953-2048/15/11/317

182. Sumption, M.D., Bhatia, M., Rindfleisch, M., Tomsic, M., Soltanian, S., Dou, S.X., Collings, E.W.: Large upper critical field and irreversibility field in MgB_2 wires with SiC additions. Appl. Phys. Lett. **86**(9) (2005). doi:10.1063/1.1872210

183. Matsumoto, A., Kumakura, H., Kitaguchi, H., Senkowicz, B.J., Jewell, M.C., Hellstrom, E.E., Zhu, Y., Voyles, P.M., Larbalestier, D.C.: Evaluation of connectivity, flux pinning, and upper critical field contributions to the critical current density of bulk pure and SiC-alloyed MgB_2. Appl. Phys. Lett. **89**(13) (2006). doi:10.1063/1.2357027

184. Zhou, S., Pan, A.V., Wexler, D., Dou, S.X.: Sugar coating of boron powder for efficient carbon doping of MgB_2 with enhanced current-carrying performance. Advanced Materials **19**(10), 1373-+ (2007). doi:10.1002/adma.200601659

185. Gao, Z., Ma, Y., Zhang, X., Wang, D., Yu, Z., Watanabe, K., Yang, H., Wen, H.: Strongly enhanced critical current density in MgB_2/Fe tapes by stearic acid and stearate doping. Supercond. Sci. Technol. **20**(5), 485-489 (2007). doi:10.1088/0953-2048/20/5/013

186. Bohnenstiehl, S.D., Susner, M.A., Yang, Y., Collings, E.W., Sumption, M.D., Rindfleisch, M.A., Boone, R.: Carbon doping of MgB_2 by toluene and malic-acid-in-toluene. Physica C **471**(3-4), 108-111 (2011). doi:10.1016/j.physc.2010.12.005

187. Yamada, H., Hirakawa, M., Kumakura, H., Kitaguchi, H.: Effect of aromatic hydrocarbon addition on in situ powder-in-tube processed MgB_2 tapes. Supercond. Sci. Technol. **19**(2), 175-177 (2006). doi:10.1088/0953-2048/19/2/004

188. Wang, D., Zhang, X., Gao, Z., Wang, L., Ma, Y., Awaji, S., Nishijima, G., Watanabe, K., Mossang, E.: Effect of processing temperature on the superconducting properties of acetone doped MgB_2 tapes. Physica C **469**(1), 23-26 (2009). doi:10.1016/j.physc.2008.10.005

189. Jiang, C.H., Dou, S.X., Cheng, Z.X., Wang, X.L.: Light carbon doping by oxygen-free paraffin wax to enhance the current density of MgB_2 in the entire field regime. Supercond. Sci. Technol. **21**(6) (2008). doi:10.1088/0953-2048/21/6/065017

190. Vinod, K., Varghese, N., Roy, S.B., Syamaprasad, U.: Significant enhancement of the in-field critical current density of the MgB_2 superconductor through codoping of nano-TiC with nano-SiC. Supercond. Sci. Technol. **22**(5) (2009). doi:10.1088/0953-2048/22/5/055009

191. Vinod, K., Varghese, N., Sundaresan, A., Syamaprasad, U.: Highly enhanced in-field critical current density of MgB_2 superconductor by combined addition of burned rice husk and nano Ho_2O_3. Solid State Sci. **12**(4), 610-616 (2010). doi:10.1016/j.solidstatesciences.2010.01.012

192. Varghese, N., Vinod, K., Chattopadhyay, M.K., Roy, S.B., Syamaprasad, U.: Effect of combined addition of nano-SiC and nano-Ho_2O_3 on the in-field critical current density of MgB_2 superconductor. J. Appl. Phys. **107**(1) (2010). doi:10.1063/1.3275504

193. Iwasa, Y., Larbalestier, D.C., Okada, M., Penco, R., Sumption, M.D., Xi, X.X.: A round table discussion on MgB_2 toward a wide market or a niche production? A summary. IEEE Trans. Appl. Supercond. **16**(2), 1457-1464 (2006). doi:10.1109/tasc.2006.873235

194. Iwasa, Y., Bascunan, J., Hahn, S., Park, D.K.: Solid-Cryogen Cooling Technique for Superconducting Magnets of NMR and MRI. In: Kes, P.H., Rogalla, H. (eds.) Superconductivity Centennial Conference 2011, vol. 36. Physics Procedia, pp. 1348-1353. Elsevier Science Bv, Amsterdam (2012)

195. Stautner, W., Xu, M., Mine, S., Amm, K.: Hydrogen Cooling Options for MgB_2-based Superconducting Systems. In: Weisend, J.G., Breon, S., Demko, J., DiPirro, M., Fesmire, J., Kittel, P., Klebaner, A., Marquardt, J., Nellis, G., Peterson, T., Pfotenhauer, J., Yuan, S., Zagarola, M., Zeller, A. (eds.) Advances in Cryogenic Engineering, vol. 1573. AIP Conference Proceedings, pp. 82-90. (2014)

196. Yao, W.J., Bascunan, J., Hahn, S.Y., Iwasa, Y.: MgB_2 Coils for MRI Applications. IEEE Trans. Appl. Supercond. **20**(3), 756-759 (2010). doi:10.1109/tasc.2010.2044035

197. Ling, J.Y., Voccio, J., Kim, Y., Hahn, S., Bascunan, J., Park, D.K., Iwasa, Y.: Monofilament MgB_2 Wire for a Whole-Body MRI Magnet: Superconducting Joints and Test Coils. IEEE Trans. Appl. Supercond. **23**(3) (2013). doi:10.1109/tasc.2012.2234183

198. Hascicek, Y.S., Akin, Y., Baldwin, T.W., Rindfleisch, M.M., Yue, J., Sumption, M.D., Tomsic, M.: A MgB_2 12.5 kVA superconductor transformer. Supercond. Sci. Technol. **22**(6) (2009). doi:10.1088/0953-2048/22/6/065002

199. Kajikawa, K., Uchida, Y., Nakamura, T., Kobayashi, H., Wakuda, T., Tanaka, K.: Development of Stator Windings for Fully Superconducting Motor With MgB_2 Wires. IEEE Trans. Appl. Supercond. **23**(3) (2013). doi:10.1109/tasc.2013.2240033

200. Collings, E.W., Kawabata, S., Bhatia, M., Tomsic, M., Sumption, M.D.: Magnesium diboride superconducting strand for accelerator and light source applications. IEEE Trans. Appl. Supercond. **16**(2), 1445-1448 (2006). doi:10.1109/tasc.2006.870779

201. Atomura, N., Takahashi, T., Amata, H., Iwasaki, T., Son, K., Miyagi, D., Tsuda, M., Hamajima, T., Shintomi, T., Makida, Y., Takao, T., Munakata, K., Kajiwara, M.: Conceptual design of MgB_2 coil for the 100 MJ SMES of advanced superconducting power conditioning system (ASPCS). In: Enpuku, K., Izumi, T. (eds.) Advances in Superconductivity Xxiv, vol. 27. Physics Procedia, pp. 400-403. (2012)

202. Tomsic, M., Rindfleisch, M., Yue, J.J., McFadden, K., Phillips, J., Sumption, M.D., Bhatia, M., Bohnenstiehl, S., Collings, E.W.: Overview of MgB_2 superconductor applications. International Journal of Applied Ceramic Technology **4**(3), 250-259 (2007). doi:10.1111/j.1744-7402.2007.02138.x

Chapter 2

Preparation and characterisation of MgB_2

In this work, MgB_2 was prepared in bulk and wire (mono and multifilamentary) forms and various structural and superconducting characterisations were performed. This chapter details the preparation techniques adopted and describes the characterisations done.

2.1 Preparation techniques

In the present study MgB_2 was prepared in bulk and wire forms. The *In-situ* method was adopted for the preparation. Mg powder from 'Good Fellow' (-325 mesh, 99.8%) and amorphous B powder from Merck (-325 mesh, 99 %) were the starting materials. [Details of nano dopants, added to enhance the in-field properties and of sheath materials used are given in the relevant sections]. The amount of Mg and B were selected so that the atomic ratio, Mg:B = 1:2 (MgB_2 stoichiometry). The stoichiometric calculations of Mg and B powders are given below.

$$\text{Stoichiometric weight of Mg} = \frac{\text{Molecular weight of Mg}}{\text{No. atoms in Mg molecule}} \times \text{stoichiometry of Mg}$$
$$= \left(\frac{24.305}{1} \times 1\right) \text{grams}$$
$$= 24.305 \text{ grams}$$

$$\text{Stoichiometric weight of B} = \frac{\text{Molecular weight of B}}{\text{No. atoms in B molecule}} \times \text{stoichiometry of B}$$
$$= \left(\frac{10.811}{1} \times 2\right) \text{grams}$$
$$= 21.622 \text{ grams}$$

$$\left.\begin{matrix}\text{Amount of Mg required} \\ \text{to prepare X gram } MgB_2\end{matrix}\right\} = \frac{\text{Stoichiometric weight of Mg}}{\text{Stoichiometric weight of Mg + Stoichiometric weight of B}} \times X$$
$$= \left(\frac{24.305}{45.927} \times X\right) \text{grams}$$

$$\left.\begin{matrix}\text{Amount of B required} \\ \text{to prepare X gram } MgB_2\end{matrix}\right\} = \frac{\text{Stoichiometric weight of B}}{\text{Stoichiometric weight of Mg + Stoichiometric weight of B}} \times X$$
$$= \left(\frac{21.622}{45.927} \times X\right) \text{grams}$$

Stoichiometrically weighed Mg and B powders were homogeneously mixed and ground thoroughly using an agate mortar and pestle in air.

2.1.1 MgB_2 in bulk form

Powder In Sealed Tube (PIST) method was used for the preparation of bulk samples [1]. SS tubes of OD/ID = 10/8 mm were used as the sheath material. One end of the tube was pressed using a hydraulic press and precursor powder was filled in it and mechanically compacted. After filling the powder the other end was also press sealed and the powder filled middle portion was also flattened by applying a pressure of about 1 GPa to obtain a dense bar shaped sample. The ends were further welded electrically to ensure avoidance of both oxidation of Mg and Mg vapour loss during heat treatment. A heat treatment temperature of 800 ^{o}C-900 ^{o}C for two hours was usually used for bulk samples. Samples were heat treated in a programmable muffle furnace with 'Eurotherm (model number 2404)' temperature controller. Samples were furnace cooled to room temperature after heat treatment. To recover the superconductor, sheath was carefully ground and removed using an electric grinder. The recovered MgB_2 bulk superconductor was powdered/fractured/shaped for various structural and superconducting characterisations. Figure (2.1) schematically details PIST method.

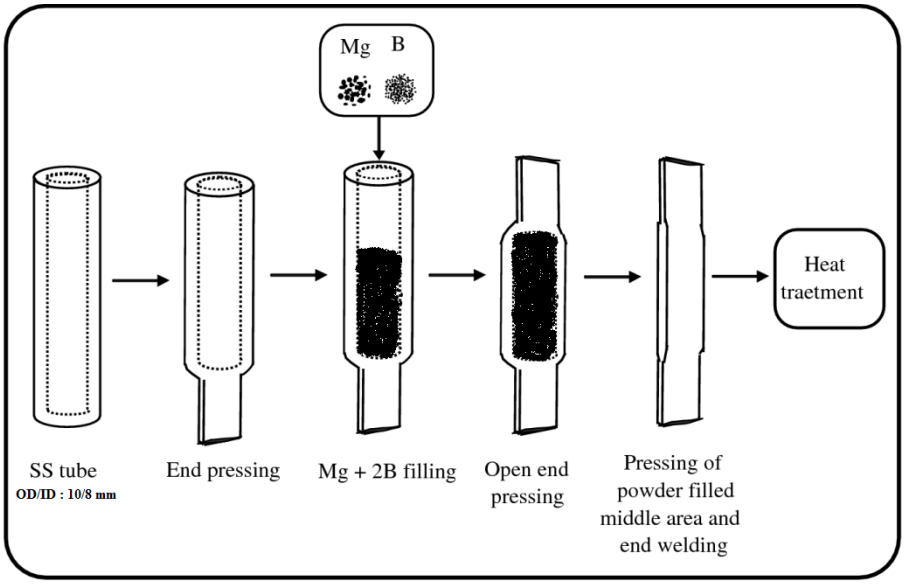

Fig (2.1) Schematic representation of PIST method.

2.1.2 MgB_2 in wire form

In this work Powder In Tube (PIT) method was adopted to make MgB_2 wires [2, 3]. Homogeneously mixed Mg and B powder was filled in a metal tubes (Fe, Ni, Nb, SS and monel

were used in the present study) of suitable dimensions (OD/ID = 6/4 or 5/3 mm were mainly used) and mechanically compacted. Ends of the tubes were plugged and sealed using Cu studs. The powder filled tube was rolled down through a set of grooves in a groove roller to the desired length and diameter. Figure (2.2) shows the groove rolling machine. The Cu filled area was cut and removed and both ends were sealed using a capping technique [2]. For this ends of the conductors were inserted into suitable iron tubes of short length and mechanically fixed with the tube using a hydraulic press. The ends of the iron tubes were welded electrically and samples were heat treated. Heat treatment temperatures from 600 ^{O}C to 850 ^{O}C and heat treatment durations from 15 minutes to 5 hours were used for wire samples. As in the case of bulk samples, a muffle furnace with Eurotherm temperature controller was used for heat treating wire samples and these were then furnace cooled to room temperature.

Fig (2.2) (a) Groove rolling machine, (b) Wire rolling in progress.

For preparing multifilamentary wires, Wire In Tube (WIT) method was adopted. In this method, unreacted monofilamentary wires were cut and bundled along with OFHC copper wires (thermal stabilisers) of suitable diameters in a second metal tube and rolled down to desired length and diameter. Heat treatment is similar to that of monofilamentary wires [2]. Figure (2.3 a) shows an Fe sheathed monofilamentary wire and (2.3 b) shows the cross sectional view of a multifilamentary wire, with Fe barrier, Cu stabilisers and Ni outer sheath. Figure (2.4) schematically represents PIT/WIT method. For various superconducting characterisations, short wire samples were cut from the middle of the heat treated wires and for structural characterisations, the superconductor core was retrieved by mechanically peeling off the sheath. Figure (2.5) is a flowchart representing the preparation of MgB_2 in bulk and mono and multifilamentary wire forms.

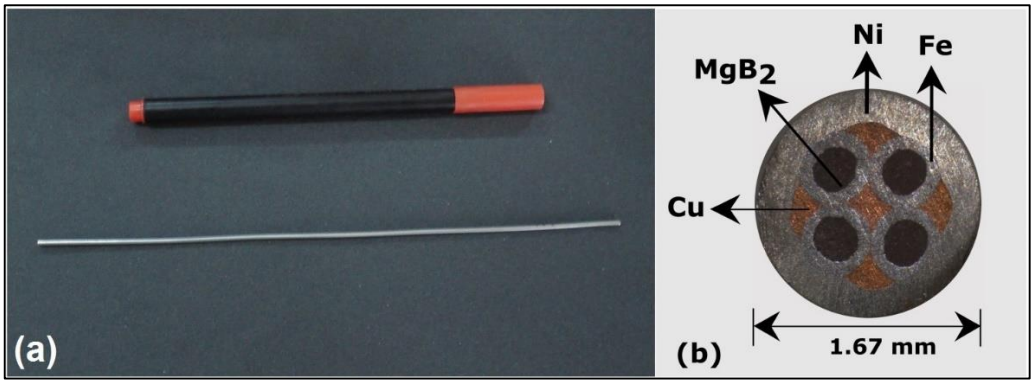

Fig (2.3) (a) Fe sheathed MgB_2 wire, (b) Cross section of multifilamentary wire.

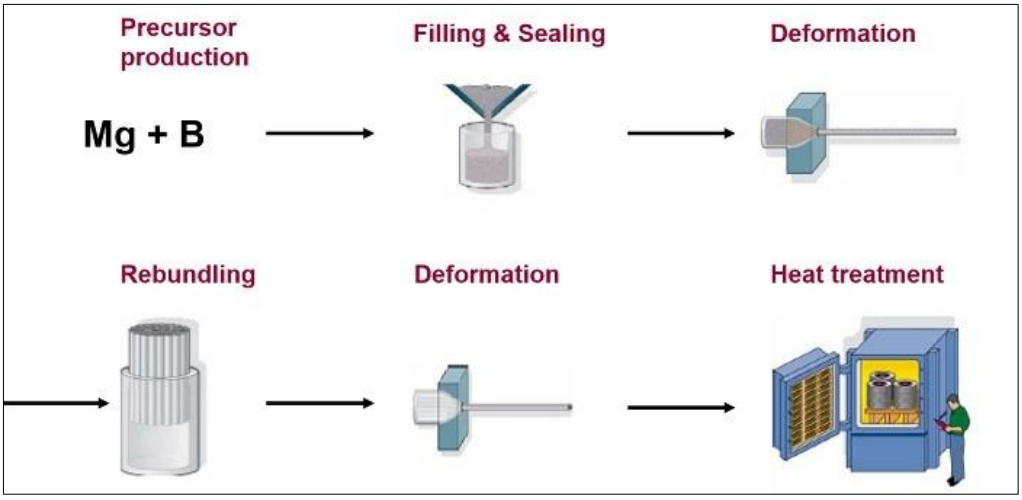

Fig (2.4) PIT/WIT wire fabrication technique.

2.2 Structural characterisation

2.2.1 Powder X-ray diffraction analysis

X-ray diffraction (XRD) is an analytical technique used for phase identification and information regarding unit cell dimensions of crystalline materials. An X-ray tube, a sample holder and a detector are the basic components of an X-ray diffractometer. X-rays are generated in a cathode ray tube. These X-rays are filtered to produce a monochromatic radiation, collimated to concentrate and directed onto the sample. When conditions satisfy Bragg's law ($2d\sin\theta = n\lambda$), constructive interference of the radiation from successive planes occurs. Here λ is the wavelength of X-ray, θ is the diffraction angle and *d* is the interplanar spacing and n is a positive integer. The detector collects the diffracted rays and processes and converts it into a count rate. The sample is scanned through a range of 2θ angles to cover all

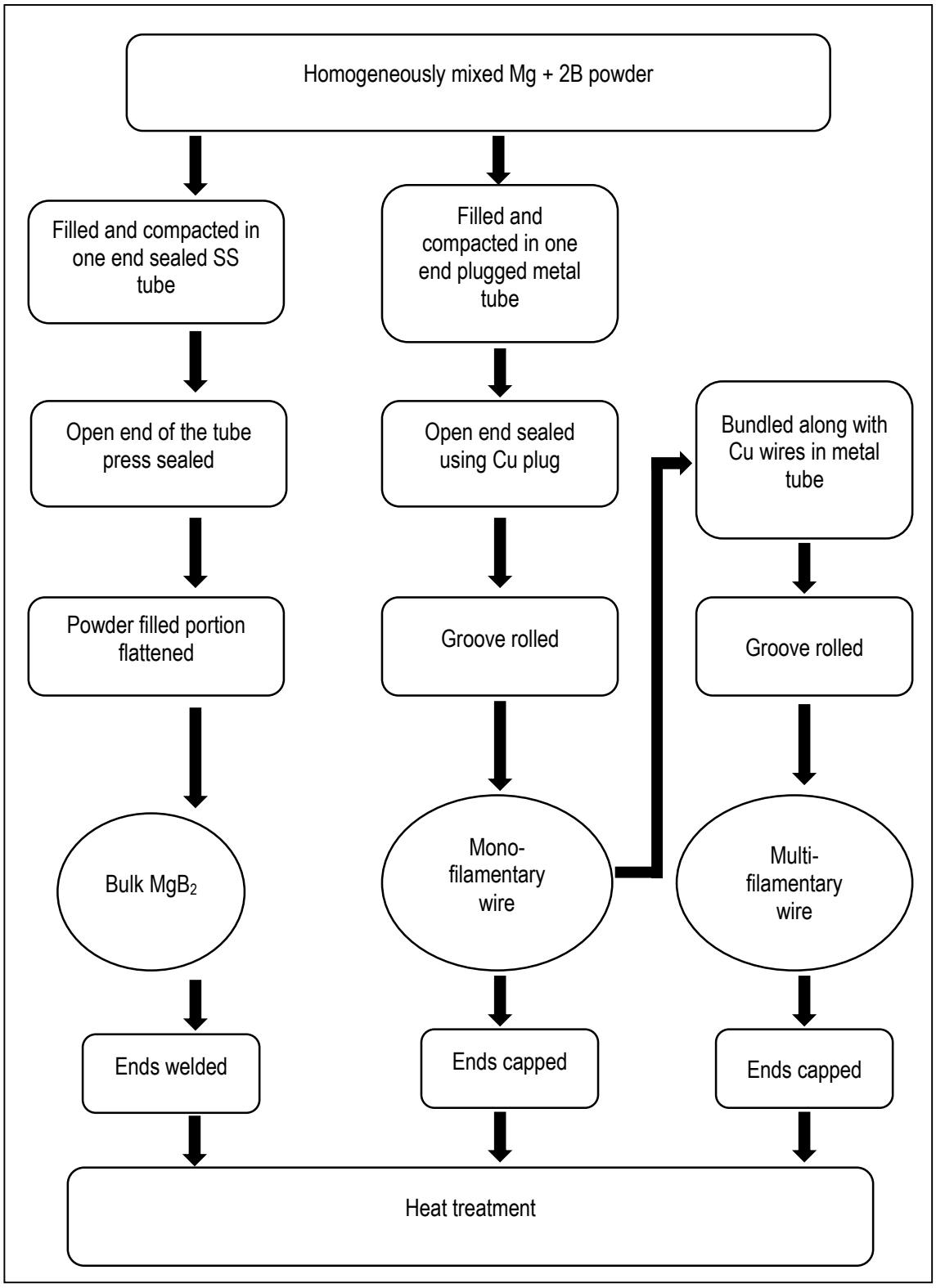

Fig (2.5) Flowchart for preparation of MgB_2 superconductor.

possible diffraction directions. Each crystalline material has a unique set of *d* spacings and the conversion of diffraction peaks to *d* spacing allows the identification of the material. This is done by comparing the *d* values with standard reference patterns [4, 5].

In the present study XRD patterns of samples were taken using Panalytical X'pert Pro (model number PW 3040/60) X-ray diffractometer with Cu Kα radiation (λ = 1.540566 Å) employing a proprietary detector - X'celerator and a monochromator at the diffracted beam side. The machine has θ-θ Bragg-Brentano geometry and its operation and data acquisition are fully automated. The superconducting core was retrieved from bulk and wire samples and finely powdered. The powder was filled in a standard sample holder or spread on top of a zero background holder (when the quantity of the powder was low) to record the XRD patterns. In this work, XRD patterns were recorded at room temperature and appropriate slits were used to restrict the X-ray beam to the sample area. For general scans, X-ray tube voltage and current were 40 KV and 30 mA. The samples were scanned from 20^{o} to 85^{o} 2θ values with a step size of ~ 0.02^{o}. The average scan takes about 20 minutes while slow scans were performed in special cases. XRD patterns were analysed for phase identification using X'Pert Highscore Plus software loaded with ICDD-PDF-2 database. Semi-quantitative phase analyses were done using the relation,

$$Vol.\%\ of\ phase\ X = \frac{\Sigma\ peak\ intensities\ of\ phase\ X}{\Sigma\ peak\ intensities\ of\ all\ phases} \qquad (2.1).$$

The *d* values of peaks were used for lattice parameter calculation. MgB_2 has hexagonal crystal structure and it belongs to the space group p6/mmm. The lattice parameters and *d* values are connected by the relation,

$$\frac{1}{d^2} = \frac{4(h^2+hk+k^2)}{3a^2} + \frac{l^2}{c^2} \qquad (2.2).$$

Substituting the *d* and (*hkl*) values of selected peaks, 'a' and 'c' lattice parameters are calculated. The full width at half maximum (FWHM) of XRD peaks depend on crystallite size and lattice strain. FWHM of selected peaks were used for calculating lattice strain using Williamson-Hall plots.

2.2.2 Microstructural analysis

Optical microscopy: In the present study an optical microscope was mainly used for examining the cross sectional features like geometry, size, orientation and homogeneity of filaments in wire samples. The presence of any reaction layer between sheath and superconducting core

could be detected using an optical microscope. A stereo microscope (Leica, model EZ4 HD) with a maximum magnification of 30× and an inbuilt 3 megapixel camera was used for these purposes. Proprietary software (Leica LAS EZ) interfaced the camera to a computer which enabled recording of images and various measurements like area and length of the samples. Accurate measurements of the cross sectional area of the superconducting core and whole sample are needed for estimating the critical current density and engineering current density respectively. For optical microscopy, small samples (1-2 cm) were cut from long conductors, polished and placed under the microscope in suitable holders.

Scanning electron microscopy: The scanning electron microscope (SEM) uses a focussed beam of high energy electrons to derive information about external morphology, crystalline structure and chemical composition of samples. In SEM, electron-sample interactions produce a variety of signals including secondary electrons, back scattered electrons, diffracted back scattered electrons, photons, visible light and heat. Secondary electrons and back scattered electrons are used for creating images. Secondary electrons are useful for showing morphology and topography of samples and back scattered electrons are useful for illustrating contrasts in multiphase samples. SEM is a non-destructive analysis and the same samples can be analysed repeatedly. Areas ranging from approximately 1 cm to 5 microns could be imaged using a conventional SEM. Magnifications from 20× to 30,000× and spatial resolution from 50 to 100 nm are possible. Essential components of an SEM are electron source (Gun), electron lenses, sample stage, detectors and data output devices [6, 7].

The wavelength of visible light limits the resolution of an optical microscope and therefore finer details like grain size, orientation, characteristics of grain boundaries, porosity in the matrix etc. could not be studied using an optical microscope. The higher resolution, magnification and greater depth of focus of an SEM come in handy in such situations. In the present study a JEOL JSM 5600 LV scanning electron microscope was used in Secondary Electron Imaging (SEI) mode. Fractured bulk samples, as well as polished cross sections of wire samples, were mounted on a metal base using adhesive carbon tape. No gold coating was used for MgB_2 samples because of its fairly good conductivity even in normal state.

Transmission electron microscopy: A Transmission Electron Microscope (TEM) is similar to a light microscope but instead of light it uses electrons. The much lower wavelength of electrons makes it possible to get a resolution a thousand times better than with a light microscope. TEM facilitates to see objects to the order of a few angstrom. In TEM, electromagnetic lenses focus electrons to a very thin beam. The electron beam passes through the material we want to study.

Depending on the density of the material some electrons are scattered and lost from the beam. The unscattered electrons hit a fluorescent screen at the bottom of the microscope and form a 'shadow image' of the sample. Depending on the density of different parts of the sample they will be displayed in varied darkness [8, 9].

TEM offers even higher magnification and resolution than SEM. In this work TEM analysis was used for information regarding inter and intra grain features and sub-micron and nano sized inclusions in them. The instrument used was HRTEM FEI-Tecnai G^2 30S- Twin 300 KV. For TEM analysis MgB_2 superconductor was finely powdered and sonicated in acetone to remove agglomeration. Immediately after sonication, the solution was dropped on carbon and polymeric film coated copper grids and kept for 24 hours to evaporate the solvent before analysis.

2.3 Superconducting characterisation

To assess the quality of the samples, superconducting parameters like, critical temperature (T_C), self-field critical current density (J_C), in-field critical current density ($J_C(H)$) and irreversibility field (H_{irr}) were estimated using both transport and magnetic measurements. Wire samples were used for transport measurements and bulk samples for magnetic measurements. A closed cycle cryocooler, integrated with a cryostat was mainly used for self-field transport measurements. It is a two stage Gifford-McMahan cooler manufactured by Sumitomo Heavy Industries Ltd. Compressor unit model is CSW-71D and cold head model, SRDK-408. Figure (2.6) shows the schematic diagram of the cryocooler integrated cryostat. Temperature as low as 7 K can be achieved at the second stage by operating the system for about 1 h. Avoidance of a liquid cryogen makes the operation of a cryocooler easy and less costly.

For in-field transport measurements, a liquid helium based 8T magnet system manufactured by American Magnetics Inc. (AMI, model A8030-3) was employed. Figure (2.7) shows the schematic diagram and photograph of the magnet system. The superconducting magnet, variable temperature insert (VTI) with helium vapour cooled current leads and liquid helium dewar are seen in the photograph. The magnet is immersed in LHe and the sample is cooled using He vapour. Since this is a liquid He based system, its operation is more complicated than the cryocooler. The high cost and scarcity of LHe are some other issues to be taken care of. Magnetic measurements were done using a Vibrating Sample Magnetometer (VSM) based Physical Property Measurement System (PPMS) [PPMS DynaCool, Quantum

Design, USA] at NIIST. Some samples were measured at RRCAT Indore and JNCASR Bengaluru.

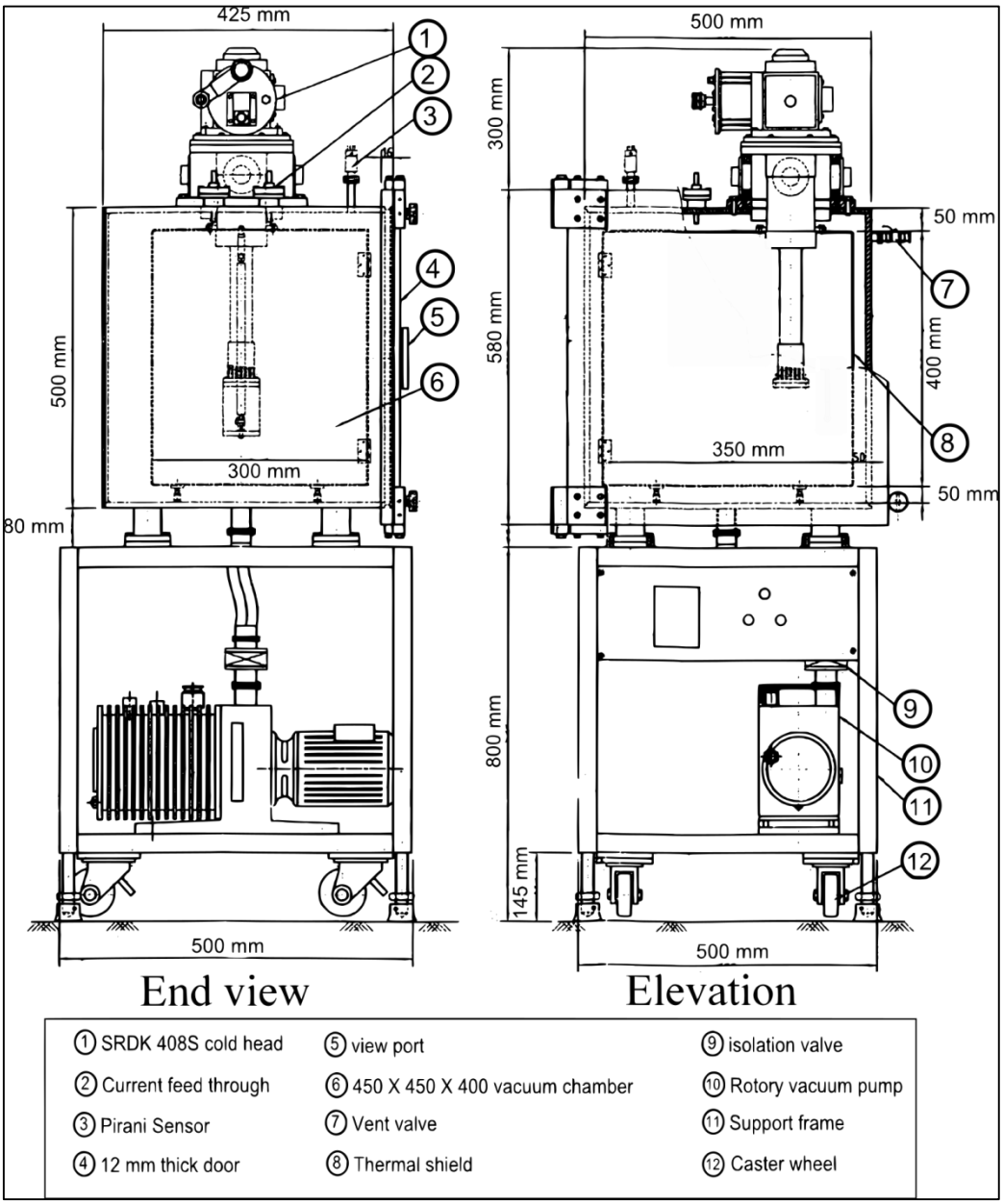

Fig (2.6) Cryocooler integrated cryostat.

2.3.1 Transport Measurements

For self-field transport measurements, short wire samples of ~ 6 cm length were properly anchored to the second stage of the cryocooler using a homemade sample holder. Temperatures of the sample at the first and second stages of the cryocooler were monitored and

controlled using Lakeshore (L332/L340) temperature controllers. Silicon diode based temperature sensors (Lakeshore DT-670A-SD) were installed near the sample and at both stages of the cryocooler. A heater coil was installed at the second stage of the cryocooler and

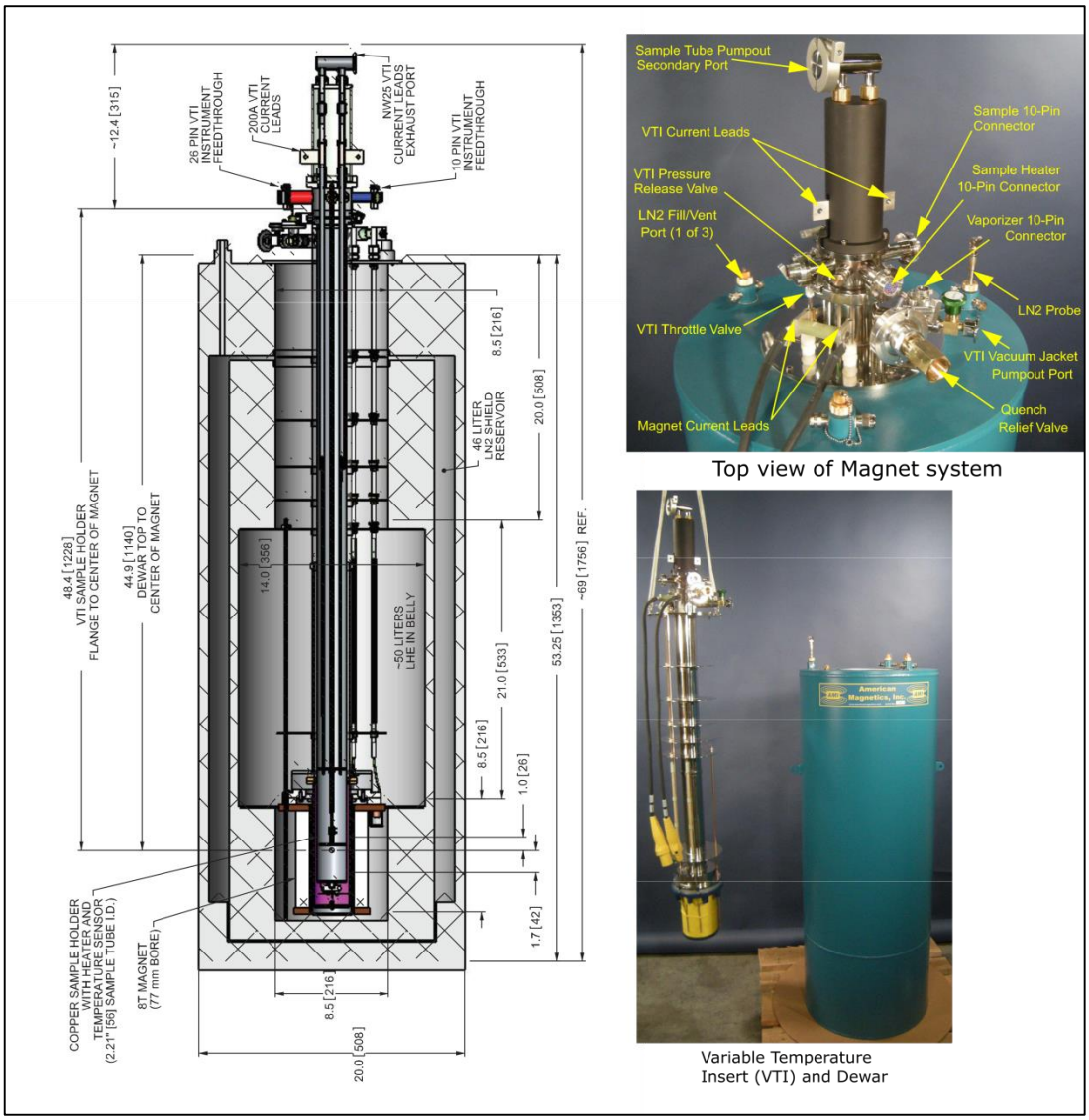

Fig (2.7) 8T magnet system.

connected to the temperature controller. For transport measurements, four probe resistivity method was used. High quality, insulated copper wires were used as the current and voltage leads. These leads were directly soldered to the outer sheath of the sample using ortho phosphoric acid as flux after cleaning the surface.

R-T measurement: Resistance versus temperature plots were recorded to determine the T_C of the samples. A constant current of 10 mA is passed through the sample (using Keithley 6220 current source) and the voltage developed across the sample is measured using a nanovoltmeter

(Keithley 2182A). This is repeated at regular intervals. The temperature of the sample is also recorded simultaneously. Sample is slowly cooled from room temperature. The temperature at which the resistance falls sharply is taken as the T_C. The difference in temperatures corresponding to 90 % and 10 % of the normal state resistance ($T_{C90} - T_{C10}$) is defined as the transition width, ΔT_C.

I-V measurement: To determine critical current density, current versus voltage plots were recorded. For self-field J_C estimation, measurement was done using the cryocooler integrated cryostat. First temperature of the sample is fixed at a desirable value below T_C. A current is passed through the sample for a short duration and the voltage developed across the sample is measured using a nanovoltmeter (Keithley 2182A). Current is gradually ramped up and the corresponding voltages are recorded. The current which produces a voltage of 1μV/cm across the sample is taken as the critical current, I_C. J_C is calculated by dividing I_C by the cross sectional area of the superconductor. For I-V measurements constant current sources (APLAB 9711P, 30 V and 100 A/ Sorensen –DHP 5 1000 M1M9D, 5 V and 1000 A) with ratings from 100 A to 1000 A were used.

In-field transport measurements were done in the AMI magnet system. It has a 75 mm bore and provisions to do four probe resistivity measurements of wire samples. A sample of length ~ 2 cm is rigidly anchored between the high current leads (these are superconductor leads embedded in thick copper bars) of the system and inserted into the uniform magnet field zone through the top of the dewar such that the wire sample is oriented perpendicular to the axial field of the magnet. Maximum field achievable in this system is 8T. Mainly I-V characteristics of wire samples are done in the magnet system. First, the field is set to the desired value and then I-V plots are recorded in the same way as with the cryocooler based system. By adjusting the helium vapour flow to the sample and by a heater in the vicinity of the sample, temperature of the sample could be varied. Cernox sensors (Lakeshore CX-1030-BG) are used in the magnet system for monitoring the temperature. All the R-T and I-V measurements are automated with self-coded programs in 'LabVIEW'. The electronic instruments are interfaced to the PC through GPIB cables. A schematic representation of transport measurement of MgB_2 wire sample is shown in figure (2.8).

2.3.2 Magnetic measurements

For magnetic measurements, bulk MgB_2 samples were shaped into parallelepipeds of size: 3 × 3 × 1.5 mm or 2.5 × 2.5 × 1.5 mm and the magnetisation in the sample was recorded

by varying the temperature (M-T) and by varying the applied field (M-H). M-T plots were recorded in zero field cooling condition at 100 Oe. Transition temperature and transition width were determined from M-T plots. The temperature at which magnetisation begins to fall is taken as T_C and the difference in temperatures corresponding to 90 % and 10 % of the maximum

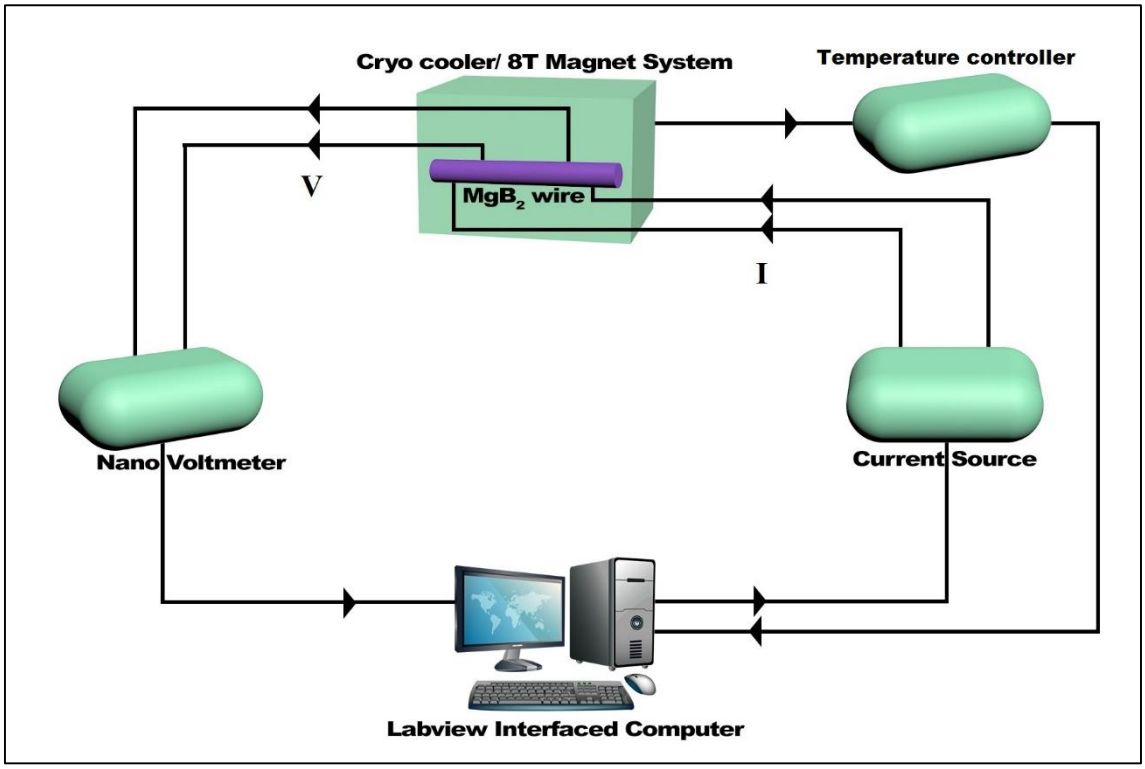

Fig (2.8) Transport measurement of MgB_2 wire sample.

shielding signal is taken as ΔT_C. From M-H plot, critical current density of the sample is estimated using Bean critical state model [10]

$$J_c(H) = \frac{20 \times \Delta M}{a\left(1 - \frac{a}{3b}\right)} \qquad (2.3)$$

where ΔM (in emu/cm^3) is the width of the M-H loop, a and b (in cm) are dimensions (a < b) perpendicular to the field for a parallelepiped shaped sample. M-H hysteresis loops were measured at 5 K (for some samples at 15 K also) from 0-8 T. Irreversibility field, H_{irr} of the sample is estimated as the field at which J_C falls below 100 A/cm^2.

Reference

1. Varghese, N., Vinod, K., Rao, A., Kuo, Y.K., Syamaprasad, U.: Enhanced superconducting properties of bulk MgB_2 prepared by in situ Powder-In-Sealed-Tube method. J. Alloy. Compd. **470**(1-2), 63-66 (2009). doi:10.1016/j.jallcom.2008.03.056

2. Devadas, K.M., Rahul, S., Thomas, S., Varghese, N., Vinod, K., Syamaprasad, U., Pradhan, S., Chattopadhyay, M.K., Roy, S.B.: Transport properties of sealed MgB_2/Fe/Ni multifilamentary wires heat treated in air. J. Alloy. Compd. **509**(31), 8038-8041 (2011). doi:10.1016/j.jallcom.2011.04.147

3. Vinod, K., Varghese, N., Rahul, S., Syamaprasad, U.: Preparation of in situ MgB_2/Fe superconducting tapes with highly densified core by hot pressing of electrically self-heated PIT wires. Mater. Sci. Eng. B-Adv. Funct. Solid-State Mater. **164**(2), 131-134 (2009). doi:10.1016/j.mseb.2009.08.008

4. Pecharsky, V.K., Zavalij, P.Y.: Fundamentals of powder diffraction and structural characterization of materials. Springer, New York (2009)

5. Giacovazzo, C.: Fundamentals of crystallography. Oxford Univ. Press, Oxford [u.a.] (2002)

6. Echlin, P.: Handbook of sample preparation for scanning electron microscopy and x-ray microanalysis. Springer Science+Business Media, New York (2010)

7. Reimer, L.: Scanning electron microscopy : physics of image formation and microanalysis. Springer, Berlin; New York (1998).

8. Williams, D.B., Carter, C.B.: Transmission Electron Microscopy : A Textbook for Materials Science.Springer, New York (2009).

9. De Graef, M.: Introduction to conventional transmission electron microscopy. Cambridge Univ. Pr., Cambridge (2003)

10. Bean, C.P.: Magnetization of Hard Superconductors. Phys. Rev. Lett. **8**(6), 250-253 (1962). doi:10.1103/PhysRevLett.8.250

Chapter 3

Improving the in-field critical current density of MgB_2 in bulk form through chemical doping

Magnesium diboride had been known and commercially available since the 1950s [1] and the discovery of superconductivity at 39 K in it came as a surprise [2], since intermetallic compounds had been explored for superconductivity for a long time. MgB_2 is a promising superconductor with a simple crystal structure, low anisotropy, large coherence length, 'weak – link' free grain boundaries [3] and two superconducting gaps, a phenomenon never before seen experimentally [4]. As far as critical temperature (T_C) is concerned MgB_2 holds a clear edge over any of the low temperature superconductors (LTS) and is suitable for operation in 20–30 K. Long multifilamentary wires of MgB_2 with good current carrying capabilities have been successfully prepared by Powder In Tube (PIT) technique by several groups [5-8]; but still MgB_2 is a long way from replacing Nb based superconductors in commercial superconducting magnets. Further developments are needed to deploy MgB_2 in high magnetic field applications where classical superconductors are playing a key role for decades.

The main disadvantage of MgB_2 is its drastically decreasing critical current density (J_C) in an applied magnetic field due to the inherent weak flux pinning. Most of the research in MgB_2 is concentrated on improving the in-field critical current density, $J_C(H)$. In-field critical current density depends on pinning force, '$F_p = J_C$ B' that prevents the movement of flux vortices. By introducing defects in the superconductor matrix pinning force can be improved. These defects should be homogeneously distributed in the matrix with its size comparable to the coherence length and spacing matching that of the vortex. Of the various methods tried so far chemical doping is the most effective method to improve flux pinning in MgB_2 [9-17]. Depending on the nature of the dopants, chemical doping may cause substitution at Mg and/or B sites, by a third atom. Another possibility is the inclusion of nano particles, either a reacted secondary phase or the additive itself, in the superconductor matrix. Thus doping modifies the crystalline and microstructural properties of the superconductor and introduces additional pinning centers in the form of lattice defects. This improves the upper critical field (H_{C2}) and irreversibility field (H_{irr}) of MgB_2 and hence enhances the in-field J_C. The variety of dopants tried so far include nano and submicron particles of metallic elements, carbon in its various

forms, carbides, silicides, nitrides, borides, oxides, hydrocarbons etc. [9, 12, 13, 18-33]. Dou *et al* classified dopants used with MgB_2 into four categories and the best dopants are those which cause carbon substitution at boron sites and form some reacted secondary phases in the MgB_2 matrix [9]. Among this category nano SiC is well accepted as one of the best dopants which form nano size Mg_2Si particles within the MgB_2 grains and enable C substitution at B sites. Unlike other dopants, it does not affect the T_C appreciably and enhances H_{C2} and $J_C(H)$. SiC added to the (Mg + B) system dissociates and reacts with Mg to form Mg_2Si and causes considerable C substitution at B sites at relatively lower temperatures (600 – 700 ^{O}C) [12, 28-30].

In the present chapter, results of chemical doping to improve the in-field critical current density of MgB_2 are presented. In the first section of this chapter effects of nano diamond (n D) and nano SiO_2 (n SiO_2) on the structural and superconducting properties of MgB_2 are discussed [17]. A novel technique to tackle the agglomeration of Mg_2Si dopant in MgB_2 is discussed in the second section [34].

3.1 Combined addition of nano diamond and nano SiO_2, an effective method to improve the in–field critical current density of MgB_2 superconductor

This work is motivated by the success of SiC and some alternative sources of Si and C, like burned rice husk in improving the superconducting properties of MgB_2 [12, 28-32]. In this work we compare the mono as well as codoping effects of nano SiO_2 and nano diamond on the structural and superconducting properties of MgB_2. Here diamond is used as the C source and SiO_2 is used for incorporating secondary phases like Mg_2Si in the MgB_2 lattice. Such a combination is selected because C substitution at B sites and nano particle inclusions in the superconductor matrix always used to give better superconducting properties [9, 33].

3.1.1 Preparation and characterisation

The samples, $MgB_{2-y}C_y$ + x wt % of nano SiO_2 (where x = 0, 5 and y = 0, 0.1, 0.2), were prepared by *in-situ* Powder In Sealed Tube (PIST) method, using Mg (-325 mesh, 99.8 %), amorphous B (-325 mesh, 99 %), nano diamond (< 10 nm, 95 +%) and nano SiO_2 (10 nm, 99.5 %) as starting powders. These compositions were chosen based on our initial studies. Stoichiometric weights of the powders were homogeneously mixed and ground thoroughly using an agate mortar and pestle and packed in stainless steel tubes of OD/ID = 10/8 mm. Both

ends of the tubes were press-sealed using a hydraulic press followed by electrical welding. This end sealing avoids both oxidation of Mg and Mg vapour loss during heat treatment. The powder filled middle area of the sample was also pressed to get a dense core. The samples were then heat treated in air at 800 ^{O}C for 2 hours in a muffle furnace at a ramp rate of 2 ^{O}C per minute and furnace cooled. The sample details and sample names are given in table (3.1).

The structural and phase analysis of the samples were performed using an X-ray diffractometer (Panalytical X'pert Pro) with Cu K_{α} radiation employing a high resolution detector namely, X' Celerator and a monochromator at the diffracted beam side. Phase identification was done using X' Pert Highscore Plus software in support with ICDD-PDF-2 database. A scanning electron microscope (SEM – JEOL JSM 5600 LV) and a high resolution transmission electron microscope (HRTEM FEI – Tecnai G^2 30 S – Twin 300 kV) were used for examining the microstructure. DC magnetization measurements were carried using a vibrating sample magnetometer in a physical property measuring system (PPMS, Quantum Design, USA) on rectangular shaped samples of size $3 \times 3 \times 1.5$ mm.

3.1.2 Results and Discussion

As evident from the powder XRD patterns of the samples shown in figure (3.1), MgB_2 is the main phase in all samples. Apart from MgB_2, Mg and MgO are the other phases commonly present in all samples. Peak intensities of these phases vary significantly depending

Table 3.1 Semi-quantitative phase analysis of different phases and strain in undoped and doped samples

Sample Name	x	y	Volume % of				Strain (%)
			MgB_2	Mg	Mg_2Si	MgO	
MBSD 00	0	0	95.3	3.0	0	1.7	0.78
MBSD 50	5	0	84.9	0.9	10.9	3.3	0.51
MBSD 01	0	0.1	89.0	8.7	0	2.3	1.45
MBSD 02	0	0.2	80.6	16.8	0	2.6	1.37
MBSD 51	5	0.1	82.5	0.9	13.4	3.2	1.19
MBSD 52	5	0.2	78.7	1.1	16.0	4.2	1.15

on the nature and quantity of dopants present in the samples. Samples added with SiO_2 show the presence of Mg_2Si. No peaks of SiO_2 or any other secondary phases are observed in the samples. A semi-quantitative phase analysis of different phases formed is done using the relation,

$$Vol.\%\ of\ phase\ X = \frac{\Sigma\ peak\ intensities\ of\ phase\ X}{\Sigma\ peak\ intensities\ of\ all\ phases}$$

and are tabulated in table (3.1). As expected the undoped sample has the highest MgB_2 volume fraction and it decreases as the doping level increases. SiO_2 doped samples show a higher volume percentage of MgO compared to the undoped one. The entrapped air in the precursor and the added SiO_2 act as the oxygen sources in these samples.

From the XRD patterns it is observed that (100) and (110) peaks of doped samples are slightly shifted towards higher angles and it indicates a decrease in in-plane lattice constant 'a'. But the (002) peaks maintained the same positions in both doped and undoped samples. These observations were confirmed by the calculation of 'a' and 'c' lattice parameters and are shown

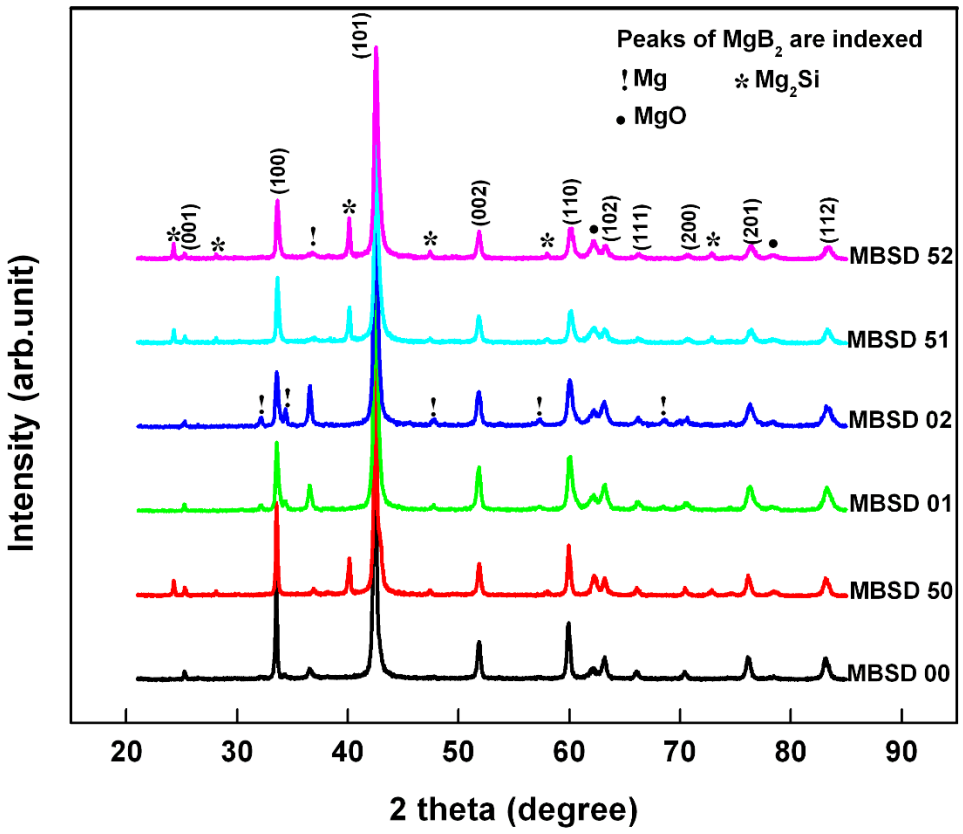

Fig (3.1) Powder XRD patterns of pure, n D and n SiO_2 doped samples.

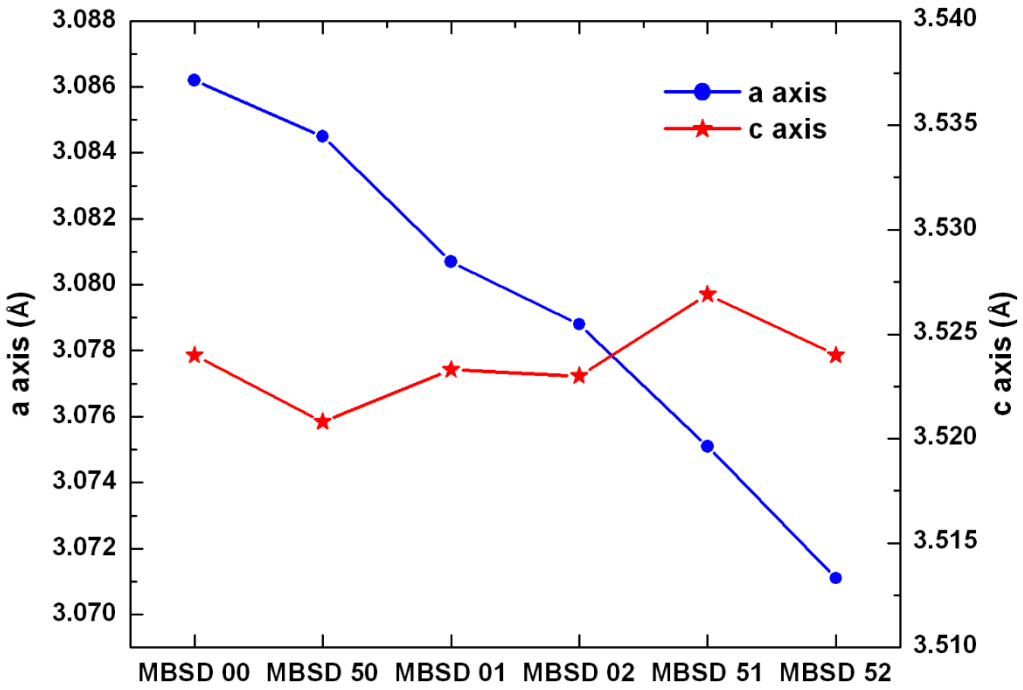

Fig (3.2) Variation in lattice parameters caused by n D and n SiO_2 doping.

in figure (3.2). The SiO_2 doped sample shows a slight decrease in 'a' value compared to the undoped one, whereas the diamond doped samples exhibit significant reduction. The codoped samples show still lower 'a' values and the sample MBSD 52 shows the lowest. The slight decrease in 'a' in mono SiO_2 added sample is due to lattice distortions caused by the inclusion of reacted nano particles (Mg_2Si) in the MgB_2 matrix and in diamond added samples the decrease in 'a' value is mainly due to C substitution at B sites. When carbon is added to MgB_2 system having a hexagonal structure with B atoms forming a graphite like honeycomb network and Mg atoms occupying the pores of these hexagons, C atoms replace some of the B atoms [35, 36]. This leads to the contraction of in-plane lattice since the covalent radius of C is lower than that of B.

The Full Width at Half Maximum (FWHM) of selected peaks are shown in figure (3.3). There is no significant variation in FWHM values of (002) peaks due to doping whereas (100) and (110) peaks show consistent variation. The SiO_2 addition slightly reduces the FWHM values but diamond causes considerable broadening of (hk0) peaks and the sample MBSD 02 shows the maximum peak broadening. Due to the opposing effects of SiO_2 and diamond, the codoped samples show slightly reduced FWHM values compared to the corresponding diamond doped samples. Broadening of peaks points to reduced crystallite size and increased

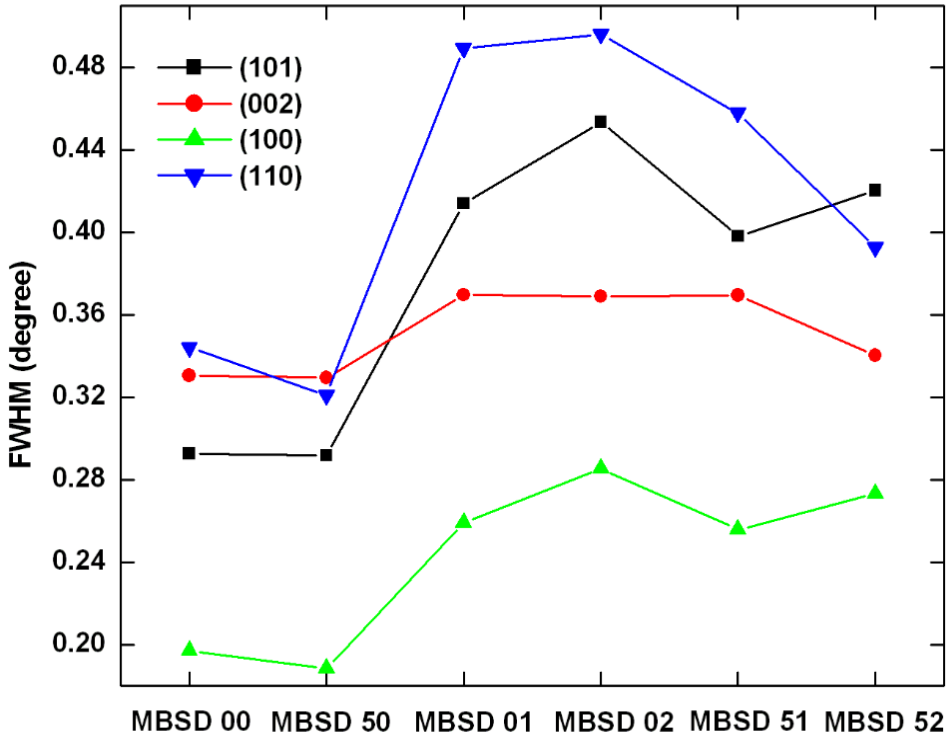

Fig (3.3) FWHM of selected peaks of the samples.

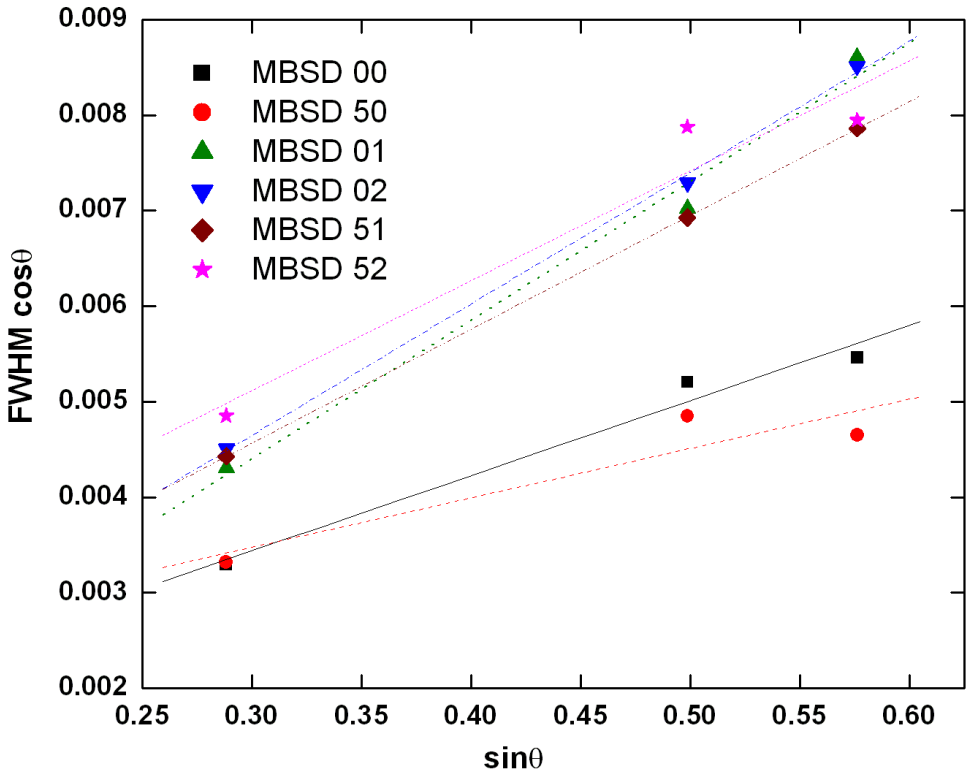

Fig (3.4) Williamson-Hall plots of (hk0) peaks.

lattice strain. Again the carbon substitution at boron sites and nano particle inclusions are responsible for this. Figure (3.4) shows the Williamson – Hall plots of the (hk0) peaks, wherein the slopes of the plots represent the lattice strain and the values are tabulated in table (3.1). All the doped samples, except solo SiO_2 added one, show higher strain values compared to the pure sample.

From the analysis of powder XRD patterns of the samples it is clear that addition of SiO_2 and diamond to MgB_2 system causes distinct changes to the crystalline properties of undoped sample. So it will be interesting to have a look into the microstructure of doped and undoped samples. SEM images of the fractured surfaces of the samples are shown in figure (3.5). The pure (MBSD 00) and solo SiO_2 (MBSD 50) added samples show identical microstructures with randomly oriented but well defined hexagonal grains. The solo diamond doped samples (MBSD 01 and MBSD 02) exhibit a unique microstructure, with partially molten hexagonal grains. The effect is more visible in the diamond rich sample. In the codoped samples (MBSD 51 and MBSD 52) the grains are too small and tightly packed and therefore they are not individually distinguishable under the same magnification used for other samples. The smaller grain size will increase the density of grain boundaries in these samples which will improve flux pinning and thus J_C at higher fields. Figure (3.6) shows the TEM image of sample MBSD 51, in which nanometer sized intragrain inclusions are clearly visible, with small clusters of these nano particles at some regions. The size of these nano particles is of the order of coherence length of cooper pairs in MgB_2 and hence they can act as strong flux pinners.

Now moving on to the superconducting properties, figure (3.7) shows the Zero Field Cooled (ZFC) magnetization curves for the samples at 100 Oe. T_C and ΔT_C (defined as the difference in temperatures corresponding to 10 % and 90 % of the maximum shielding signal) are tabulated in table (3.2). The pure sample has the highest T_C of 38.4 K which comes down slightly to 38.2 K with SiO_2 addition. This is due to the inclusion of secondary phases in the MgB_2 matrix. Diamond doped samples show still lower T_C (36.8 K for MBSD 01 and 36.3 K for MBSD 02) values. C substitution at B sites reduces the hole concentration and causes changes in the phonon modes. The reduced density of states and weakened electron - phonon coupling are the reasons for T_C reduction in C doped samples [37]. The codoped samples MBSD 51 and MBSD 52 show T_C of 36.3 K and 35.6 K respectively. Diamond doped samples show a ΔT_C in the range 2.3 - 2.4 K and it is 1.0 K for undoped and solo SiO_2 doped samples. The results show that carbon substitution has a stronger effect on T_C and ΔT_C than the secondary phases present in the superconductor matrix.

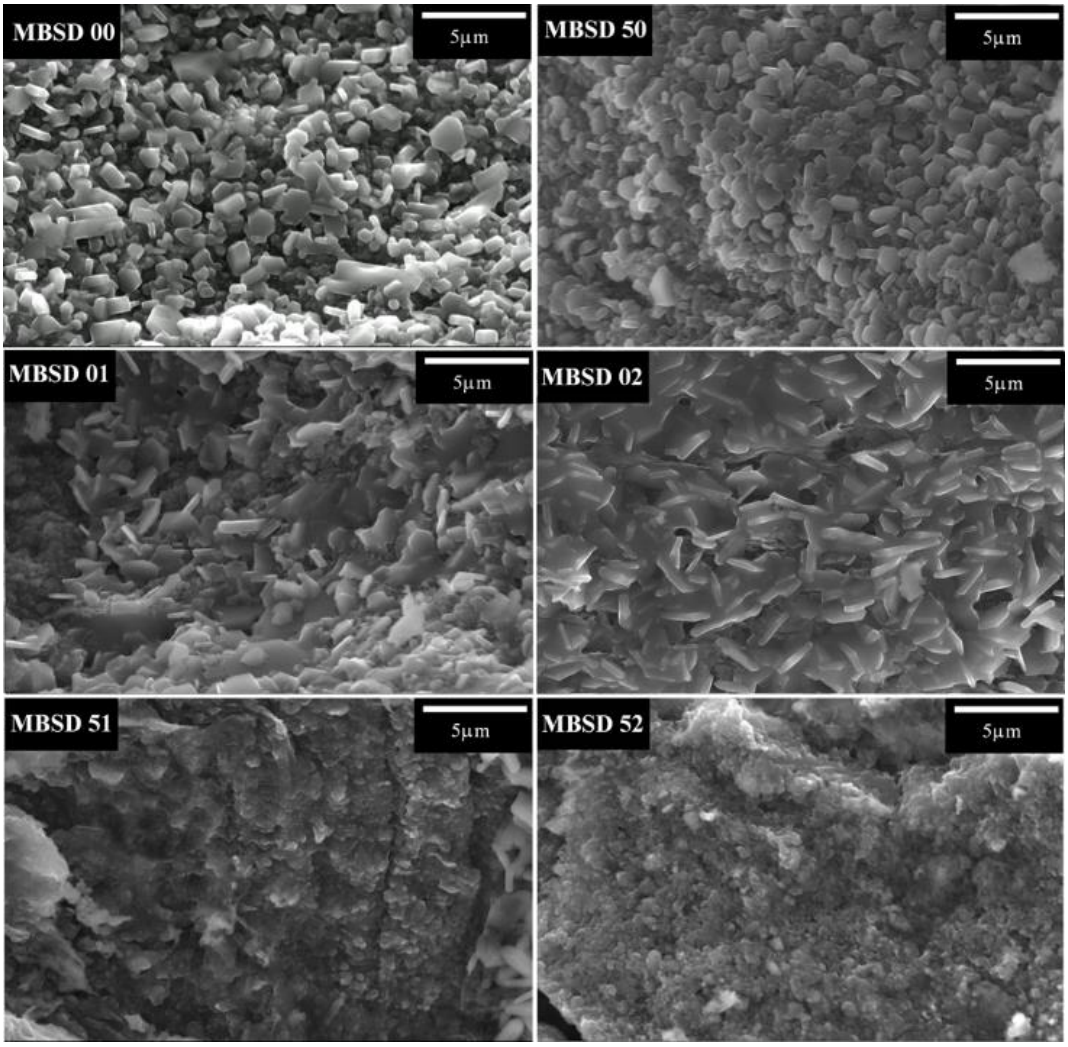

Fig (3.5) SEM images of the fractured surfaces of pure and doped samples.

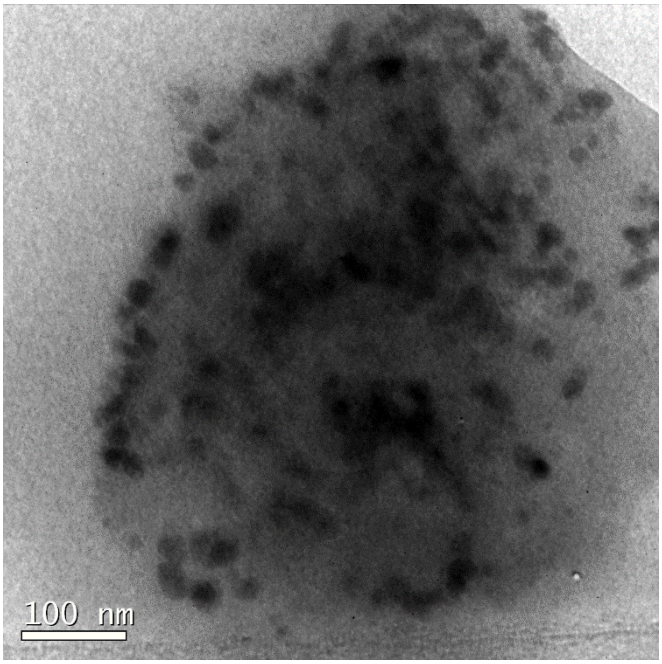

Fig (3.6) TEM image of the sample MBSD 51.

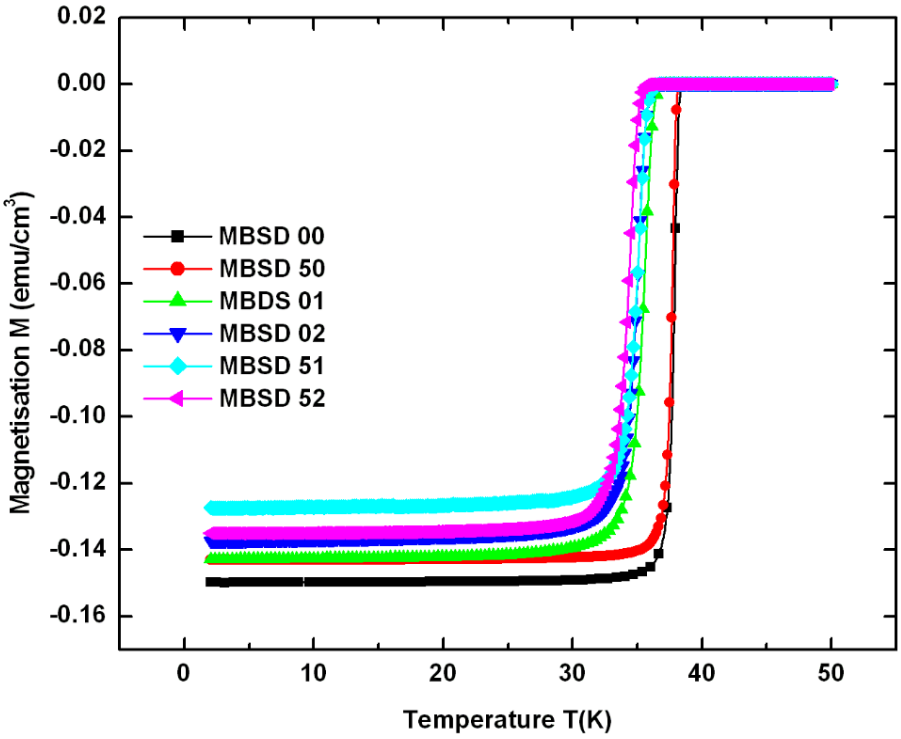

Fig (3.7) ZFC M-T plots of all samples taken at 100 Oe.

Table 3.2 Superconducting properties of pure and doped samples

Sample	T_C (K)	ΔT_C (K)	J_C at 5 K (× 10^3 A/cm^2)		H_{irr} (T)	
			3 T	8 T	5 K	15 K
MBSD 00	38.4	1.0	40.8	0.2	8.4	6.0
MBSD 50	38.2	1.0	64.1	0.9	10.4	7.1
MBSD 01	36.8	2.4	33.3	1.3	11.6	6.6
MBSD 02	36.3	2.4	27.5	1.6	12.5	6.7
MBSD 51	36.3	2.3	28.1	2.1	13.6	7.6
MBSD 52	35.6	2.4	20.9	1.7	13.1	7.5

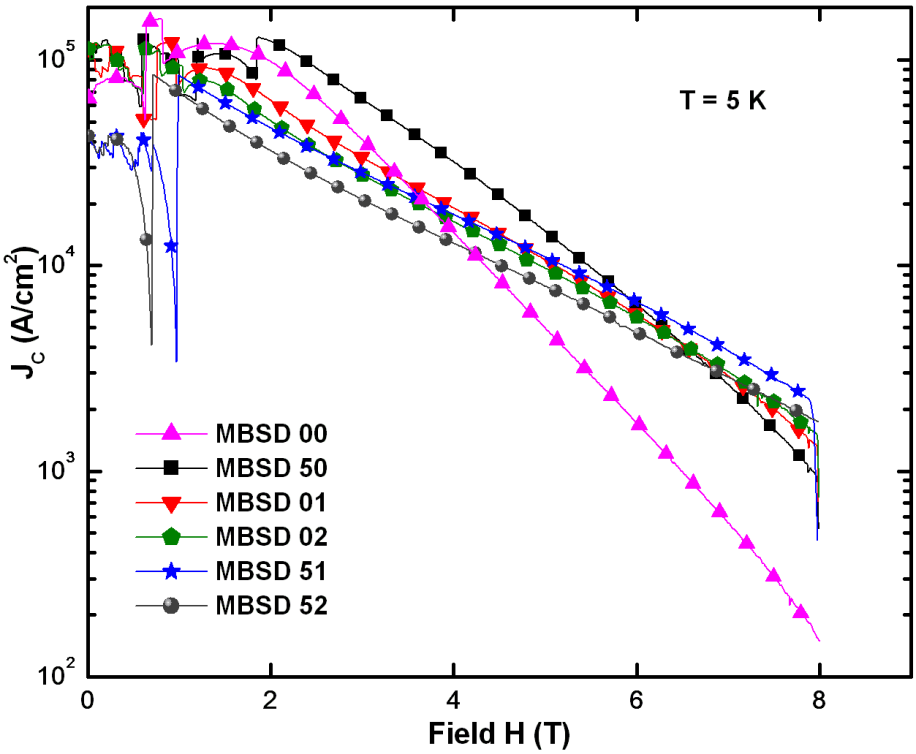

Fig (3.8) Variation in J_C of undoped and doped samples with applied magnetic field.

The field dependence of J_C at 5 K calculated from isothermal magnetic hysteresis loops is shown in figure (3.8). Thermo magnetic flux jumps distort the shape of the curves at lower fields. The origin of flux jumps in MgB_2 has been discussed in detail by Romero-Salazar *et al* [38, 39]. $J_C(H)$ calculation is done based on Bean critical state model using the formula $J_c(H) = \frac{20 \times \Delta M}{a\left(1 - \frac{a}{3b}\right)}$ where ΔM (in emu/cm^3) is the width of the M-H loop, 'a' and 'b' (in cm) are dimensions (a < b) perpendicular to the field for a parallelepiped shaped sample [40]. At lower fields estimation of J_C is not accurate due to flux jumps but the general trend is that the undoped and the SiO_2 doped samples perform better in this region with the latter showing a slightly better J_C than the former. As the field increases J_C of the pure sample drops drastically compared to the doped samples. The codoped samples and the diamond doped samples perform consistently better throughout the entire field of study, with the sample MBSD 51 showing the best J_C of 2.17 × 10^3 A/cm^2 at 5 K and 8 T. Among the diamond doped samples MBSD 02 has the best J_C of 1.65 × 10^3 A/cm^2. The critical current density of the samples at 5 K and selected fields are listed in table (3.2). When the temperature is increased to 15 K the trend remains the

same, with the SiO_2 added sample and the undoped sample giving the best results in low fields and the codoped samples performing well in high field regions (figure 3.9).

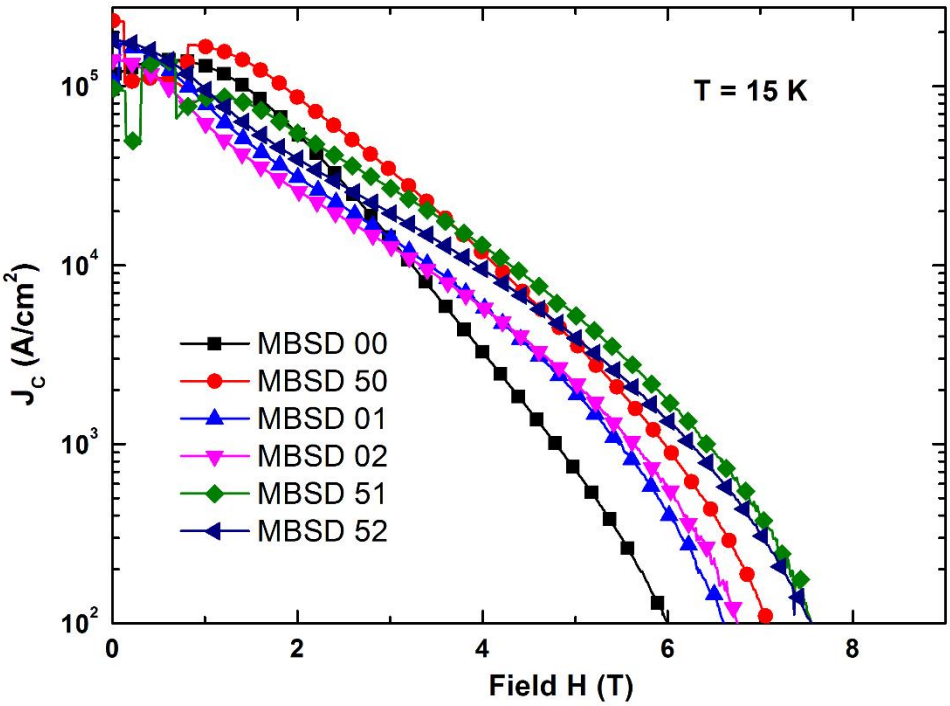

Fig (3.9) J_C vs. H plots of the samples at 15 K.

The reason for the improved J_C performance of doped samples at higher fields is their enhanced flux pinning capabilities due to the lattice defects caused by C substitution at B sites and the nano particle inclusions of reacted secondary phases, both of which act as strong flux pinners. The irreversibility fields (H_{irr}) of the samples are determined by linearly extrapolating the high field segments of the Kramer curves and are tabulated in table (3.2). The doped samples show better H_{irr} values with the codoped sample MBSD 51 topping the list with 13.6 T at 5 K.

3.1.3 Conclusion

The effects of mono, as well as codoping of nano SiO_2 and nano diamond on the structural and superconducting properties of MgB_2, were studied. Both dopants imparted significant modifications in the crystalline and microstructural properties of undoped sample. The in-plane lattice constant ‘a’ and FWHM of (hk0) peaks showed systematic variations with the level of doping. The ‘a’ values showed a significant reduction for mono diamond doped

and codoped samples. Similarly (hk0) peaks showed noticeable broadening, especially for diamond added samples. These structural variations are due to the C substitution at B sites and lattice distortions caused by the inclusions of nano particles of reacted secondary phases in the MgB_2 matrix. The SEM and TEM images of the samples supported these conclusions. The T_C was slightly reduced by the diamond addition due to the reduced crystallinity. J_C of the pure sample dropped rapidly in applied magnetic fields but the performance of doped samples was consistently better in the high field regions. At higher fields the best codoped sample showed a J_C of 2.17×10^3 A/cm^2 (5 K, 8 T) which is more than one order higher than that of the undoped sample. The increased flux pinning capability provided by different kinds of pinning centers due to the different additives is responsible for the enhanced in-field J_C of the doped samples.

3.2 Tackling the agglomeration of Mg_2Si dopant in MgB_2 superconductor using cast Mg-Si alloy

A major issue which limits the benefits of chemical doping is the agglomeration of added nano particles. Usually, the dopant is mixed with Mg and B powders in an agate mortar and pestle or by ball milling and it is very difficult to ensure their homogeneous distribution in the matrix. This work presents a novel technique to resolve the agglomeration issue by using 'Mg-Si' cast alloy as one of our starting powders instead of Mg for the preparation of doped MgB_2 superconductor. Undoped and SiC doped MgB_2 samples were also prepared by the usual method for comparison.

3.2.1 Preparation and characterisation

Magnesium ingot (99.8 %) and silicon crystals (99.99 %) were used to prepare Mg-Si alloy. Mg + Si (6 wt %) mixture was melted at 740 ^{O}C for 20 minutes in a low carbon steel crucible using a resistance heated furnace under protective flux atmosphere. The mixture was stirred well and the melt was poured into a preheated (350 ^{O}C) rectangular steel mould to prepare Mg-Si alloy casting. This method ensures a uniform distribution of Mg_2Si particles in the Mg matrix since at the processing temperature Si will react with Mg to form Mg_2Si phase. Our starting Mg-Si powder was prepared by grinding and sieving the cast ingot. Mg-Si alloy (-325 mesh) and amorphous B (-325 mesh, 99 %) were stoichiometrically weighed to prepare doped MgB_2. Nano carbon (< 50 nm, 99+ %) was added in different weight percentage to the mix. Table (3.3) details the composition of the samples and sample codes. PIST technique was

followed for the preparation of bulk samples. For the preparation of undoped and SiC doped samples Mg powder (-325 mesh, 99.8 %) was used. The powders were mixed and ground thoroughly using an agate mortar and pestle and packed in stainless steel tubes of OD/ID = 10/8 mm. The ends of the tubes were press sealed using a hydraulic press and welded. The powder filled middle area was also pressed to densify the core. Samples were heat treated at 850 ^{O}C for 2 hours in a muffle furnace at a ramp rate of 2 ^{O}C/minute and furnace cooled. The phase and structural analyses of the samples were done using an X-ray diffractometer (Panalytical) with Cu K_{α} radiation employing an X' Celerator and a monochromator at the diffracted beam side. X' Pert Highscore Plus software in support with ICDD-PDF-2 data base was used for phase identification. A scanning electron microscope and a high resolution transmission electron microscope were employed for examining the microstructure. DC magnetisation measurements of the samples were done in a vibrating sample magnetometer in a physical property measuring system (PPMS, Quantum Design) on rectangular shaped samples of size 2.5 × 2.5 × 1.5 mm.

3.2.2 Results and discussion

XRD pattern of the home made Mg-Si alloy powder (figure 3.10) shows peaks of Mg and Mg_2Si. A semi-quantitative phase analysis of the alloy is done and it shows that nearly 86 vol. % of the casting is Mg and the remaining is Mg_2Si. No peak of Si or any other impurity phase is observed. Powder XRD patterns of the MgB_2 samples (both pure and those containing Si and n C) are shown in figure (3.11). MgB_2 is the main phase in all samples. Minor quantities of MgO are found in samples. Mg_2Si peaks are observed in all samples except the one which was made of pure Mg. A semi-quantitative phase analysis of different phases formed is done and the results are tabulated in table (3.3). In the undoped sample, MSBC 00, more than 99 vol. % constitutes MgB_2 phase. Rest of the samples contain almost 90 vol. % MgB_2 and the remaining volume is Mg_2Si. A small quantity, nearly 1 % of the total volume is MgO in samples MSBC 00, MSBC 61 and MSBC 62. Mg_2Si phase in the samples is expected to be uniformly distributed in the matrix because of the special preparation technique used here and will act as effective flux pinners.

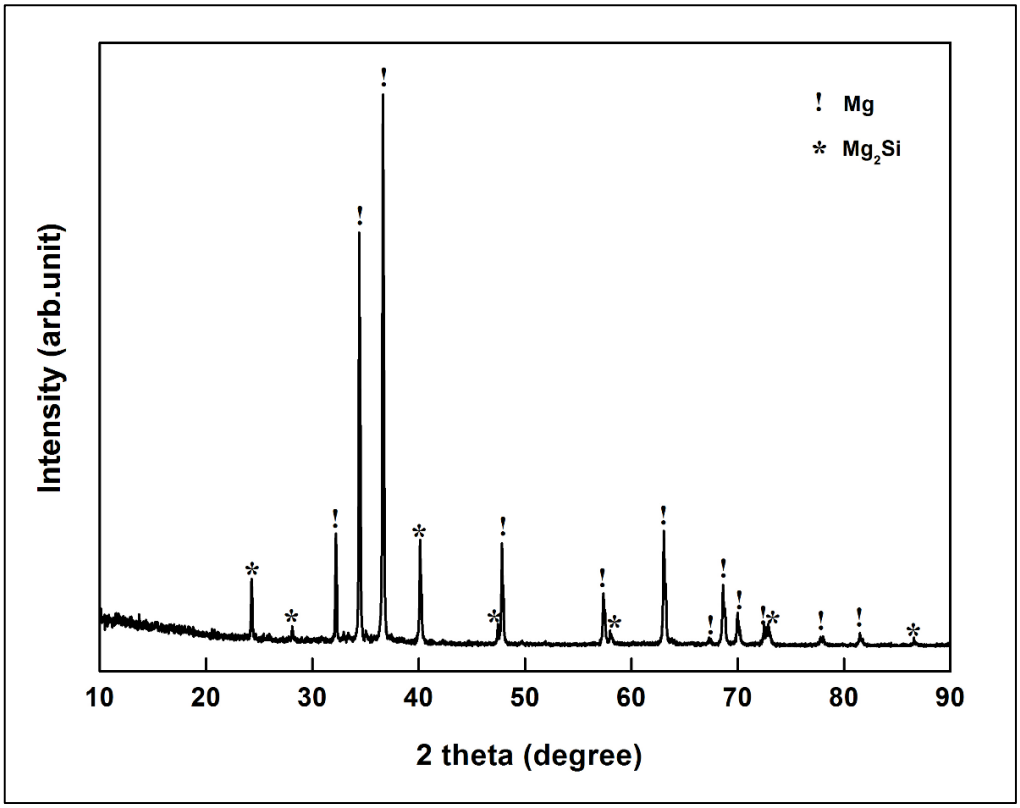

Fig (3.10) Powder XRD pattern of Mg-Si alloy prepared by casting.

Table 3.3 Sample composition, semi-quantitative phase analysis and strain in undoped and doped samples

Sample name	Initial Weight % of		Volume % of			Strain (%)
	Si	C	MgB_2	Mg_2Si	MgO	
MSBC 00	0	0	99.3	-	0.7	0.43
MSBC 60	6	0	89.7	9.0	1.3	0.88
MSBC 61	6	1	91.5	7.5	1.0	0.94
MSBC 62	6	2	93.1	6.6	0.3	0.88
MSBC 63	6	3	91.0	8.8	0.2	1.68
MSBC 64	6	4	88.4	11.4	0.2	1.33

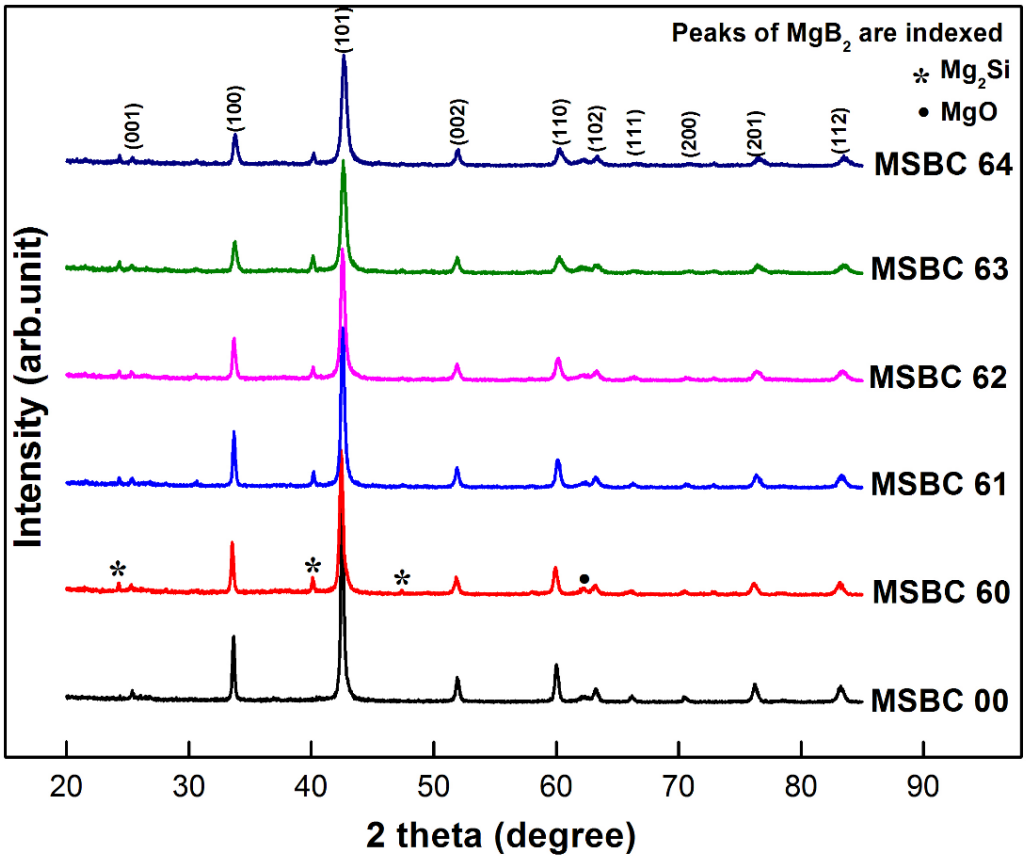

Fig (3.11) XRD patterns of undoped and doped MgB_2 samples.

The lattice parameters were calculated from the XRD patterns and their variation with respect to doping level is shown in figure (3.12). The in-plane lattice constant ‘a’ shows a consistent decrease with increase in doping while ‘c’ does not show any significant variation. Compared to the pure sample MSBC 00, the sample MSBC 60 shows only a slight decrease in ‘a’ and this is due to the lattice distortions caused by the presence of Mg_2Si phase. While it is a known fact that carbon will result in a significant reduction in ‘a’ due to its substitution of some of the B atoms. Since the covalent radius of C is lower than that of B, its substitution results in a contraction of in-plane lattice [35, 36]. All the C doped samples show significant reduction in ‘a’. Variation in FWHM of selected peaks is shown in figure (3.13). The peaks corresponding to (100), (101) and (110) planes show consistent increase in FWHM with increase in doping level while (002) peaks do not show much variation. Peak broadening points to reduced crystallite size and an increase in lattice strain.

Reduction in grain size with doping was confirmed by the examination of SEM images and is discussed later. Slopes of the Williamson-Hall plots of (hk0) peaks (figure 3.14) give

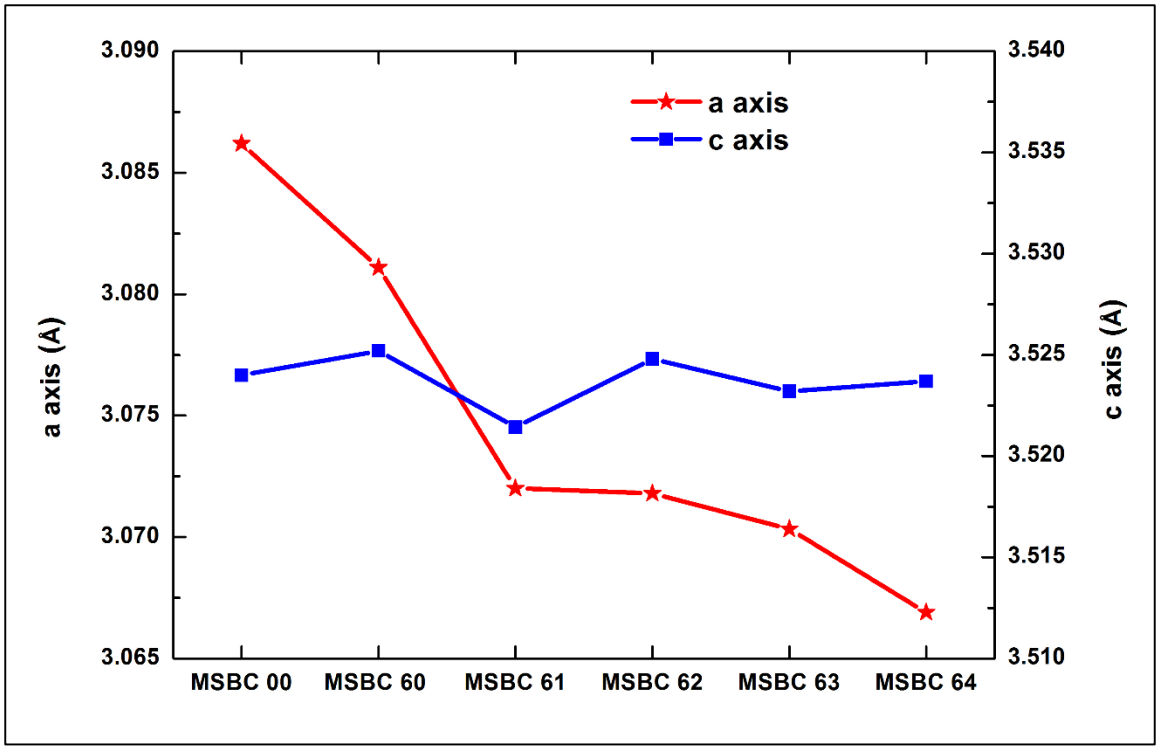

Fig (3.12) Variation in lattice parameters 'a' and 'c' with doping.

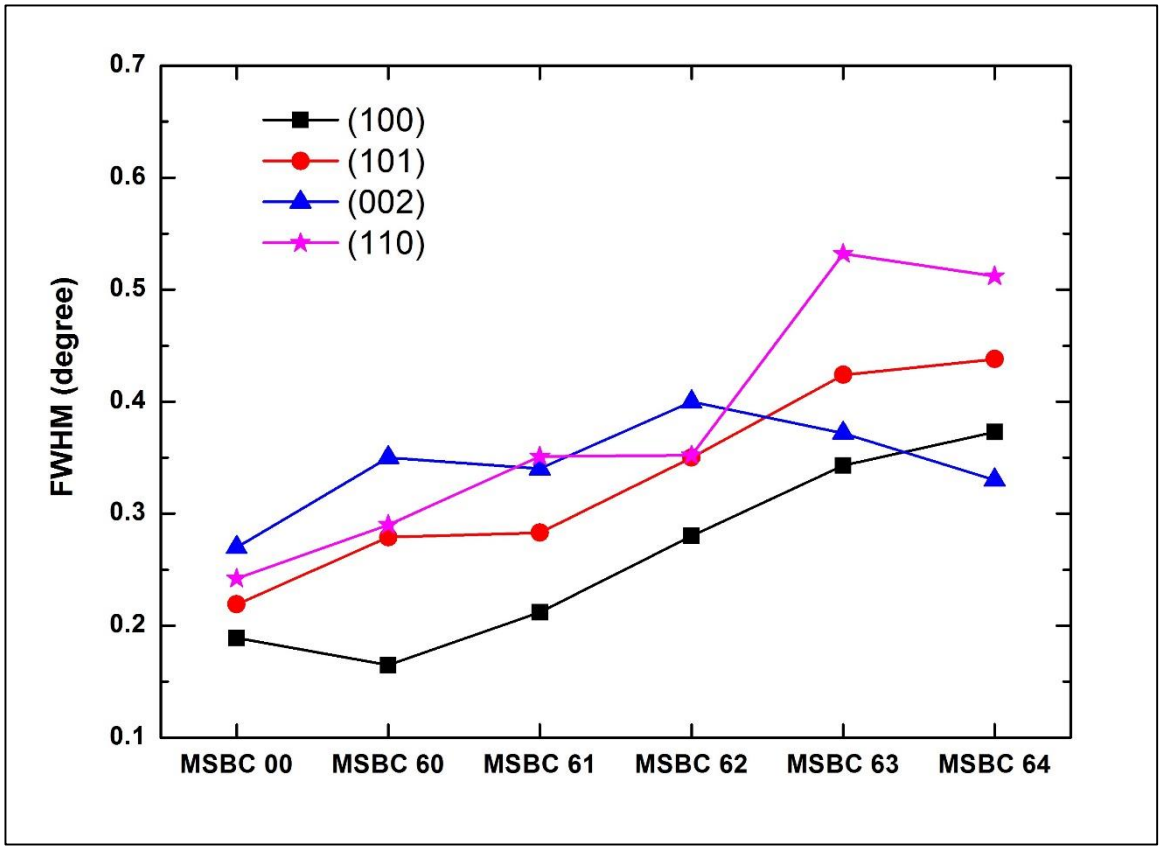

Fig (3.13) FWHM of selected peaks of the samples.

the lattice strain values and are tabulated in table (3.3). All the doped samples show higher strain values compared to the pure sample. SEM images of the fractured surfaces of the samples are shown in figure (3.15). The undoped sample has a microstructure with randomly oriented but well defined hexagonal grains. All the doped samples show grains with distinctly smaller size and reduced crystallinity. Even though there are some bigger grains scattered in the matrix of some of the doped samples, majority of grains are of smaller size. All the carbon containing samples have randomly oriented, tightly packed smaller grains with improved connectivity. These smaller grains provide more grain boundaries which help to enhance the flux pinning and thus the J_C at higher fields. The uniform distribution of Mg_2Si particles in samples prepared using cast Mg-Si alloy is evident from HRTEM examination. Figure (3.16a) shows TEM image of MSBC 62 (the sample which has shown the best J_C), prepared using cast Mg-Si alloy and figure (3.16b) shows MgB_2 added with 6.7 wt % of nano SiC (~2 wt % of C) which was directly mixed with Mg and B powders. Agglomerates of Mg_2Si particles are seen in figure (3.16b) while they are much more evenly distributed in the former sample (MSBC 62) thus providing flux pinning centres which are better distributed and therefore more effective.

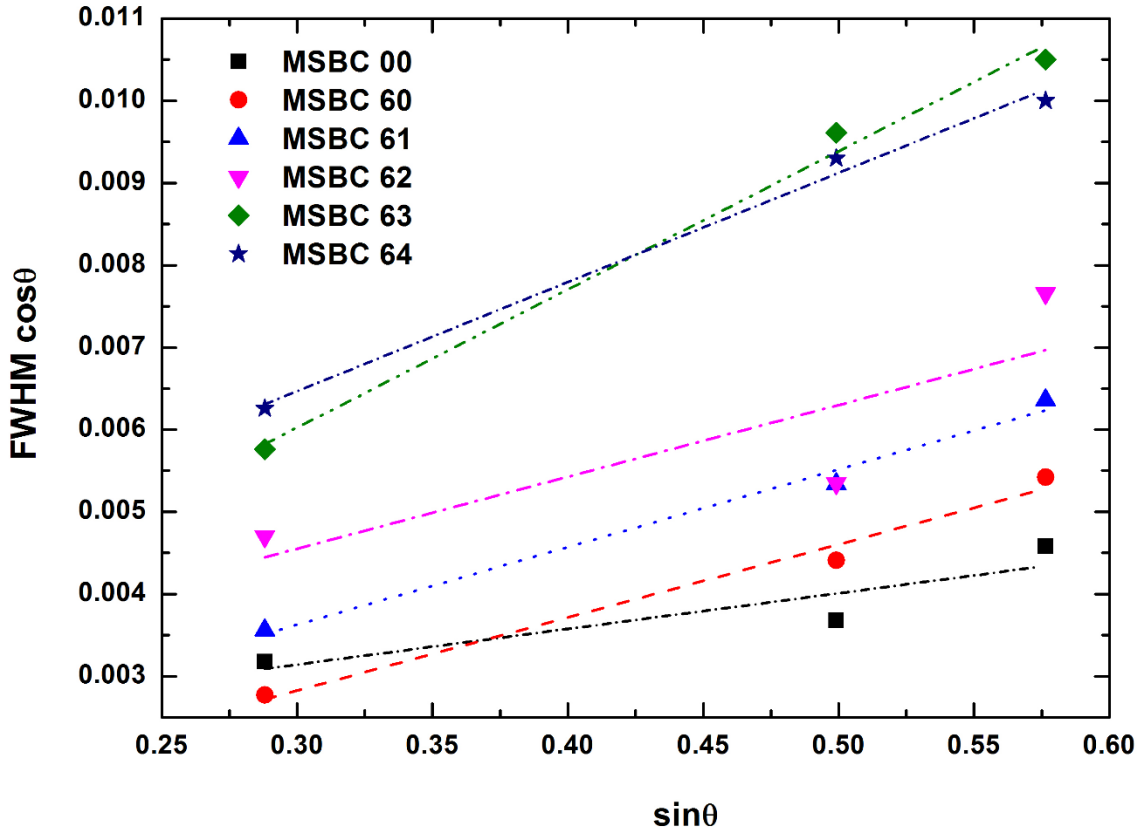

Fig (3.14) Williamson – Hall plots of (hk0) peaks.

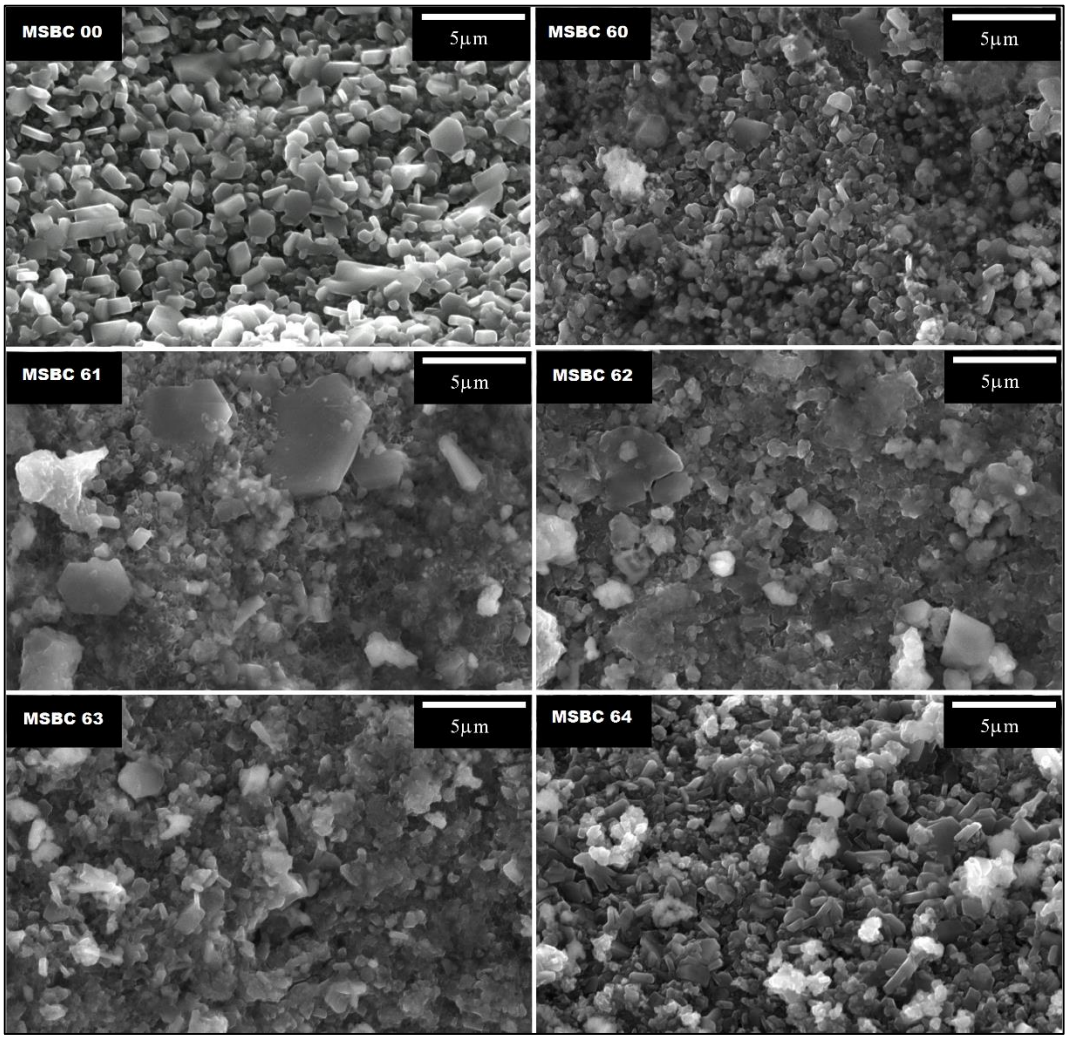

Fig (3.15) SEM images of the fractured surfaces of the samples.

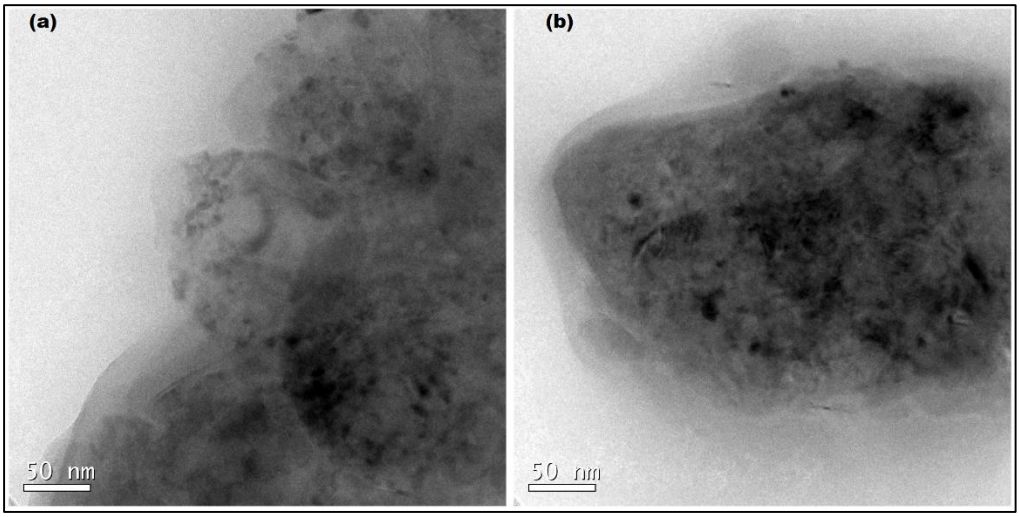

Fig (3.16) TEM images of (a) sample MSBC 62, prepared using cast Mg - Si alloy (b) MgB_2 doped with n SiC, prepared using the normal route.

Examining the superconducting properties, transition temperatures (T_CS) of all samples are determined from Zero Field Cooled (ZFC) magnetization curves taken at 100 Oe. The undoped sample MSBC 00 has the highest T_C of 38.7 K. Sample MSBC 60 which was prepared from Mg-Si alloy has a slightly lower T_C of 38.5 K. Carbon addition reduces the T_C further; with increasing C content T_C decreased from 37.2 K (MSBC 61) to 36.5 K (MSBC 64). When carbon substitutes boron atoms a reduction in hole concentration happens. The reduced density of states and weakened electron-phonon coupling result in a decrease in T_C [37]. The strain caused by the inclusion of Mg_2Si phase also plays a part in reducing T_C. Transition temperatures of all samples are tabulated in table (3.4) and the normalized magnetization vs. temperature plot is shown in figure (3.17).

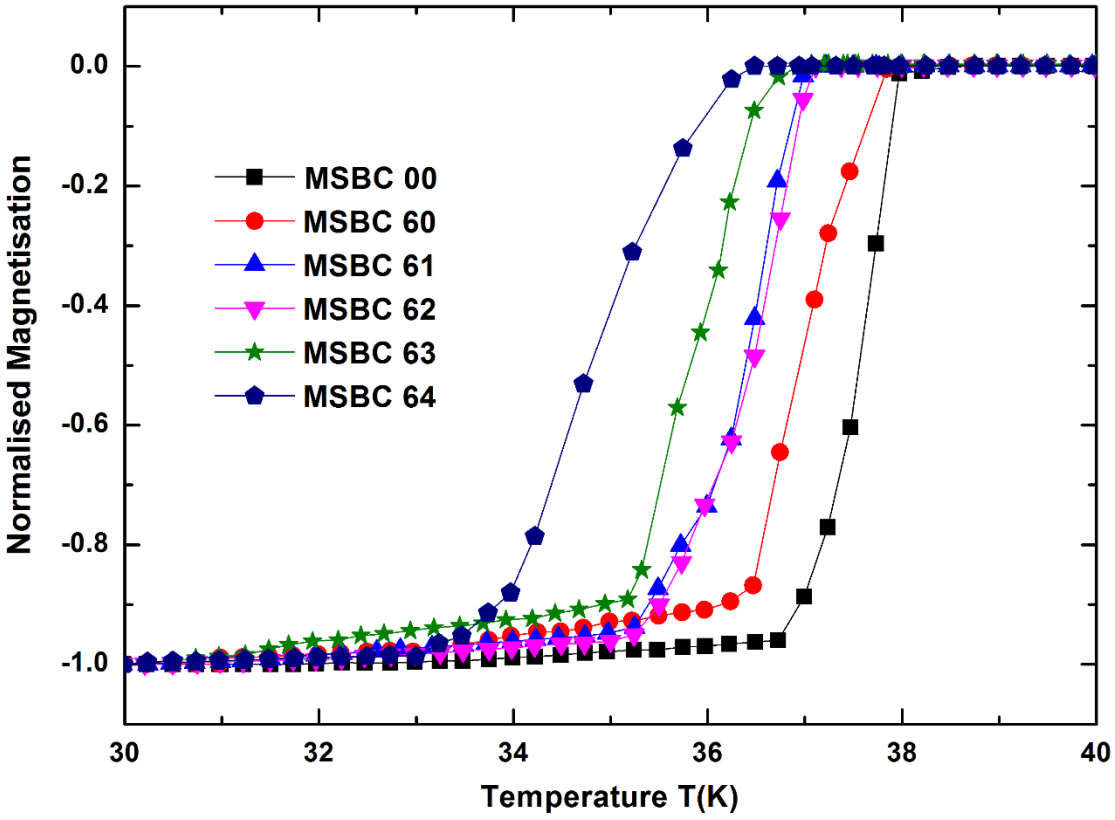

Fig (3.17) ZFC normalized magnetization vs. temperature plots at 100 Oe.

Field dependent critical current density, $J_C(H)$ of the samples is calculated from isothermal magnetic hysteresis loops and is shown in figure (3.18). Bean critical state model is used for the calculation of $J_C(H)$. The $J_C(H)$ plots show that at lower fields thermomagnetic flux jumps distort the shape of the curves and the determination of J_C is not accurate [38, 39].

Table 3.4 Transition temperature, in-field critical current density and irreversibility field of samples

Sample name	T_C (K)	J_C at 5 K ($\times 10^4$ A/cm^2)		H_{irr} (T) at 5 K
		3 T	8 T	
MSBC 00	38.7	20.7	0.06	8.6
MSBC 60	38.5	8.4	0.11	9.9
MSBC 61	37.2	16.1	0.88	15.1
MSBC 62	37.1	21.0	1.55	16.3
MSBC 63	36.9	4.0	0.18	11.4
MSBC 64	36.5	3.8	0.05	8.8

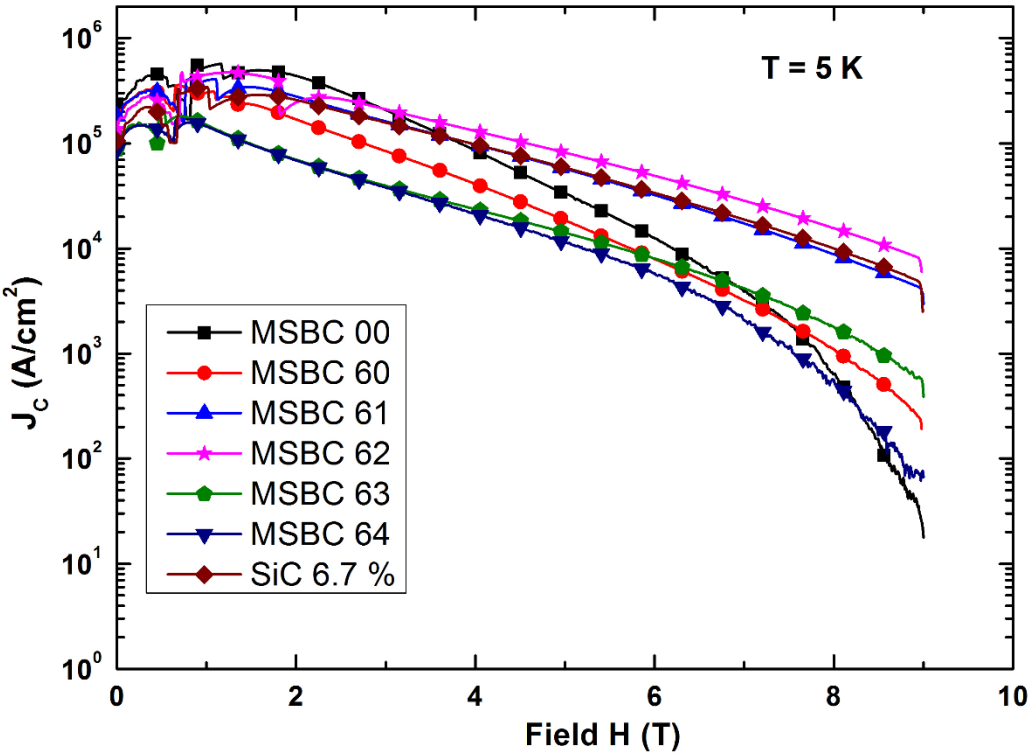

Fig (3.18) Variation in critical current density of the samples with applied magnetic field at 5 K.

Unsurprisingly at lower fields, up to around 3 T pure MgB_2 sample shows the highest J_C. Better phase purity and homogeneity are required to obtain better J_C at lower fields. Samples MSBC

61 and MSBC 62 perform consistently well throughout the entire field range studied. The J_C of the pure sample drops drastically as the field increased and at 9 T its performance is the worst among all the samples studied as we can see from figure (3.18). The $J_C(H)$ plot of the sample MSBC 60, which contains uniformly distributed Mg_2Si particles and no carbon, lies in the middle of lightly doped (MSBC 61 and MSBC 62) and heavily doped (MSBC 63 and MSBC 64) carbon containing samples [at around 6 T MSBC 60 is overtaken by MSBC 63]. Critical current density is an order higher for MSBC 60 compared to the pure sample, MSBC 00 at 5 K and 9 T. The best samples are MSBC 61 and MSBC 62 which give J_Cs of 0.88×10^4 A/cm^2 and 1.55×10^4 A/cm^2 at 5 K and 8 T, which are more than an order higher than the pure sample. The critical current densities of all samples at 5 K and 8 T are tabulated in table (3.4).

In order to compare the effects of dopant addition through Mg-Si cast alloy and normal techniques (direct addition of SiC), a sample added with 6.7 wt % of nano SiC and ground thoroughly using an agate mortar and pestle is prepared. Mg powder (-325 mesh, 99.8 %), amorphous B powder (-325 mesh, 99 %) and nano SiC (< 100 nm, 99.5 %) are used for the preparation. The $J_C(H)$ plot of this 6.7 wt % n SiC doped sample is also included in figure (3.18) for reference. While this sample shows good J_C values in the entire field range, its J_C of 1.0×10^4 A/cm^2 at 5 K and 8 T is lower than the J_C of sample MSBC 62. Mg_2Si particles which are uniformly distributed in the superconductor matrix because of the special preparation technique adopted in this work and lattice defects caused by C substitution at B sites act as good flux pinners. The enhanced flux pinning capabilities of the doped samples result in their superior performance at higher fields. The irreversibility fields (H_{irr}), determined by linearly extrapolating the high-field segments of the Kramer curves are tabulated in table (3.4). The doped samples show much improved H_{irr} values compared to the pure sample. Samples MSBC 00, MSBC 60, MSBC 61 and MSBC 62 show H_{irr} values of 8.6 T, 9.9 T, 15.1 T and 16.3 T respectively at 5 K.

In this study, the agglomeration of Mg_2Si particles in the MgB_2 matrix was minimised by using powdered Mg-Si cast alloy instead of Mg and nano SiC as the starting materials. In addition nano carbon was added to the Mg-Si + B mix and ground using a mortar and pestle. No matter how much care we take, mixing in a mortar-pestle or ball milling will not give the same homogeneity of the dopants as in the case of melting and casting. Nevertheless, a drawback of this study is that we do not know the level of homogeneity of C as it was added

to Mg-Si + B mix by solid state mixing. If one can ensure uniform distribution of C likewise we did with Mg_2Si by some novel processing technique, the results could be improved further.

3.2.3 Conclusion

This work is an attempt to address the agglomeration issue associated with chemical doping of Mg_2Si in MgB_2 superconductor. Mg-6% Si alloy with uniformly distributed Mg_2Si in it was prepared by casting technique and the powdered alloy was used as the starting powder for subsequent preparation of Mg_2Si doped MgB_2. Nano carbon in various weight percentages was added to the mix. The dopants caused systematic variations in the structural and superconducting properties of the MgB_2 samples. XRD patterns showed the presence of Mg_2Si in the Si containing samples. The addition of C caused a systematic reduction in 'a' lattice parameter indicating its substitution of some of the B atoms. FWHM of (hk0) peaks increased with doping concentration which indicated a reduction in crystallite size and an increase in lattice strain. SEM images of doped samples confirmed that they consisted of smaller grains compared to the pure sample. HRTEM analysis showed that the doped Mg_2Si particles are more homogeneously distributed within the MgB_2 grains in the samples prepared using cast Mg-Si alloy as compared to the normally doped one. Doping did not greatly reduce the transition temperature of the samples, with the most heavily doped sample MSBC 64 exhibiting a T_C of 36.5 K. In-field critical current density was significantly improved by C and Si doping. Solo Mg_2Si doped sample has a J_C which is an order higher than pure sample at 5 K and 9 T. Best results were obtained for the codoped samples, with the sample MSBC 62 having a J_C of 1.55×10^4 A/cm^2 at 5 K and 8 T which is better than the J_C of the sample prepared by normal route. The key to improving $J_C(H)$ is the more uniform distribution of pinning centres which was aided by the preparation technique followed in this work.

3.3 Summary

This chapter discusses in detail the approaches to improve the in-field critical current density of MgB_2 bulk samples through chemical doping. MgB_2 bulk samples added with nano SiO_2 and/or nano diamond were prepared by PIST method and the effects of addition on structural and superconducting properties were studied. X-ray diffraction analysis revealed that the addition caused systematic reduction in 'a' lattice parameter due to the substitution of C atoms at B sites and lattice distortion caused by reacted intragrain nano particles of Mg_2Si as evinced by transmission electron microscope image. Scanning electron microscopy images

showed distinct microstructural variations with SiO_2/diamond addition. It was evident from DC magnetization measurements that the in-field critical current density of doped samples did not fall drastically like the undoped sample. Among the doped samples the $J_C(H)$ of co-doped samples were significantly higher and the best co-doped sample yielded a J_C (2.1×10^3 A/cm^2), an order of magnitude more than the undoped one at 5 K and 8 T.

Realising that the full potential of chemical doping was not attained due to an issue which was not addressed before, agglomeration of nano dopants in the superconductor matrix, a novel technique was developed to tackle the agglomeration of Mg_2Si dopant in MgB_2. Mg-Si alloy which has uniformly distributed Mg_2Si particles in it was prepared by casting technique. The alloy was used as the Mg source for the preparation of MgB_2 samples doped with various weight percentage of nano carbon. XRD patterns showed peaks of Mg_2Si in all Si containing samples. SEM images showed a microstructure with distinctly smaller grains and

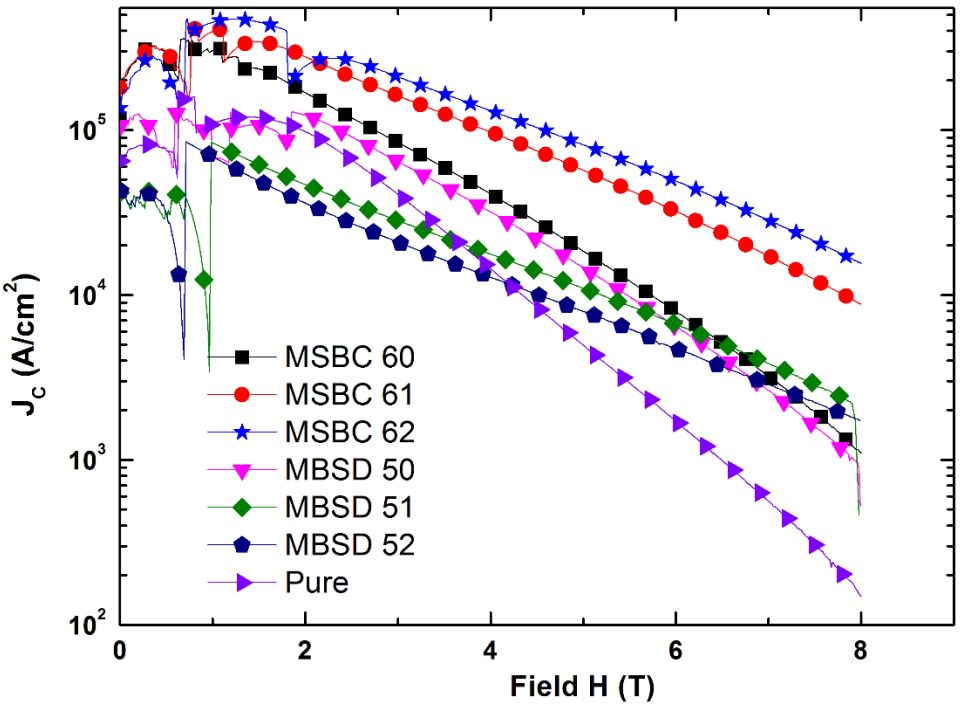

Fig (3.19) Comparison of the critical current density improvement through doping.

reduced crystallinity in doped samples. HRTEM analysis confirmed that the method led to better distribution of Mg_2Si particles within the MgB_2 grains as compared to the normally prepared sample. It was found that doping has not severely affected the transition temperature of the samples and at the same time enhanced the in-field critical current density. The new technique bettered the 'best' J_C attained through codoping of n D and n SiO_2 by about an order.

Figure (3.19) compares the J_Cs of the two works discussed in this chapter. And it is clear from the figure that, Mg-Si approach is much more effective than the usual 'mortar-pestle' or 'ball milling' approach used for adding nano dopants with 'Mg + B' powder.

Reference

1. Jones, M.E., Marsh, R.E.: The Preparation and Structure of Magnesium Boride, MgB_2. Journal of the American Chemical Society **76**(5), 1434-1436 (1954). doi:10.1021/ja01634a089

2. Nagamatsu, J., Nakagawa, N., Muranaka, T., Zenitani, Y., Akimitsu, J.: Superconductivity at 39 K in magnesium diboride. Nature **410**(6824), 63-64 (2001). doi:10.1038/35065039

3. Larbalestier, D.C., Cooley, L.D., Rikel, M.O., Polyanskii, A.A., Jiang, J., Patnaik, S., Cai, X.Y., Feldmann, D.M., Gurevich, A., Squitieri, A.A., Naus, M.T., Eom, C.B., Hellstrom, E.E., Cava, R.J., Regan, K.A., Rogado, N., Hayward, M.A., He, T., Slusky, J.S., Khalifah, P., Inumaru, K., Haas, M.: Strongly linked current flow in polycrystalline forms of the superconductor MgB_2. Nature **410**(6825), 186-189 (2001). doi:10.1038/35065559

4. Souma, S., Machida, Y., Sato, T., Takahashi, T., Matsui, H., Wang, S.C., Ding, H., Kaminski, A., Campuzano, J.C., Sasaki, S., Kadowaki, K.: The origin of multiple superconducting gaps in MgB_2. Nature **423**(6935), 65-67 (2003). doi:10.1038/nature01619

5. Kumakura, H., Matsumoto, A., Nakane, T., Kitaguchi, H.: Fabrication and properties of powder-in-tube-processed MgB_2 tape conductors. Physica C **456**(1-2), 196-202 (2007). doi:10.1016/j.physc.2006.12.017

6. Yamada, H., Igarashi, M., Nemoto, Y., Yamada, Y., Tachikawa, K., Kitaguchi, H., Matsumoto, A., Kumakura, H.: Improvement of the critical current properties of in situ powder-in-tube-processed MgB_2 tapes by hot pressing. Supercond. Sci. Technol. **23**(4) (2010). doi:10.1088/0953-2048/23/4/045030

7. Li, G.Z., Yang, Y., Susner, M.A., Sumption, M.D., Collings, E.W.: Critical current densities and n-values of MgB_2 strands over a wide range of temperatures and fields. Supercond. Sci. Technol. **25**(2) (2012). doi:10.1088/0953-2048/25/2/025001

8. Kovac, P., Birajdar, B., Husek, I., Holubek, T., Eibl, O.: Stabilized in situ rectangular MgB_2 wires: the effect of B purity and sheath materials. Supercond. Sci. Technol. **21**(4) (2008). doi:10.1088/0953-2048/21/4/045011

9. Yeoh, W.K., Dou, S.: Enhancement of H_{c2} and Jc by carbon-based chemical doping. Physica C **456**(1-2), 170-179 (2007). doi:10.1016/j.physc.2007.01.024

10. Kim, J.H., Heo, Y.U., Matsumoto, A., Kumakura, H., Rindfleisch, M., Tomsic, M., Dou, S.X.: Comparative study of mono- and multi-filament MgB_2 wires with different boron powders and malic acid addition. Supercond. Sci. Technol. **23**(7) (2010). doi:10.1088/0953-2048/23/7/075014

11. Hossain, M.S.A., Senatore, C., Flukiger, R., Rindfleisch, M.A., Tomsic, M.J., Kim, J.H., Dou, S.X.: The enhanced Jc and B-irr of in situ MgB_2 wires and tapes alloyed with C4H6O5 (malic acid) after cold high pressure densification. Supercond. Sci. Technol. **22**(9) (2009). doi:10.1088/0953-2048/22/9/095004

12. Dou, S.X., Shcherbakova, O., Yoeh, W.K., Kim, J.H., Soltanian, S., Wang, X.L., Senatore, C., Flukiger, R., Dhalle, M., Husnjak, O., Babic, E.: Mechanism of enhancement in electromagnetic properties of MgB_2 by nano SiC doping. Phys. Rev. Lett. **98**(9) (2007). doi:10.1103/PhysRevLett.98.097002

13. Varghese, N., Vinod, K., Syamaprasad, U., Roy, S.B.: Doping effect of nano-SiC on structural and superconducting properties of MgB_2 bulks prepared by PIST method in air. J. Alloy. Compd. **484**(1-2), 734-738 (2009). doi:10.1016/j.jallcom.2009.05.028

14. Wong, D.C.K., Yeoh, W.K., De Silva, K.S.B., Kondyurin, A., Bao, P., Li, W.X., Xu, X., Peleckis, G., Dou, S.X., Ringer, S.P., Zheng, R.K.: Microscopic unravelling of nano-carbon doping in MgB_2 superconductors fabricated by diffusion method. J. Alloy. Compd. **644**, 900-905 (2015). doi:10.1016/j.jallcom.2015.05.082

15. Varghese, N., Vinod, K., Rahul, S., Anees, P., Devadas, K.M., Thomas, S., Shipra, Sundaresan, A., Roy, S.B., Syamaprasad, U.: Effect of Carbon Substitution on the Superconducting Properties of Nanocarbon-, Nanodiamond- and Nano-SiC-Doped MgB_2. J. Am. Ceram. Soc. **94**(4), 1133-1137 (2011). doi:10.1111/j.1551-2916.2010.04163.x

16. Thomas, S., Rahul, S., Devadas, K.M., Varghese, N., Sundaresan, A., Syamaprasad, U.: Co-addition of nano-carbon and nano-silica: An effective method for improving the in-field properties of magnesium diboride superconductor. Mater. Chem. Phys. **148**(1-2), 190-194 (2014). doi:10.1016/j.matchemphys.2014.07.030

17. Rahul, S., Varghese, N., Vinod, K., Devadas, K.M., Thomas, S., Anees, P., Chattopadhyay, M.K., Roy, S.B., Syamaprasad, U.: Combined addition of nano diamond and nano SiO_2, an effective method to improve the in-field critical current density of MgB_2 superconductor. Mater. Res. Bull. **46**(11), 2036-2040 (2011). doi:10.1016/j.materresbull.2011.07.005

18. Collings, E.W., Sumption, M.D., Bhatia, M., Susner, M.A., Bohnenstiehl, S.D.: Prospects for improving the intrinsic and extrinsic properties of magnesium diboride superconducting strands. Supercond. Sci. Technol. **21**(10) (2008). doi:10.1088/0953-2048/21/10/103001

19. Giunchi, G., Perini, E., Orecchia, C., Ripamonti, G., Bassani, E., Carcano, G., DeMarzi, G., Viola, R., Turtu, S.: Analysis of Various Dopants on the MgB_2 Superconducting Properties. IEEE Trans. Appl. Supercond. **19**(3), 2802-2806 (2009). doi:10.1109/tasc.2009.2017955

20. Mudgel, M., Chandra, L.S.S., Ganesan, V., Bhalla, G.L., Kishan, H., Awana, V.P.S.: Enhanced critical parameters of nanocarbon doped MgB_2 superconductor. J. Appl. Phys. **106**(3) (2009). doi:10.1063/1.3186048

21. Ojha, N., Malik, V.K., Singla, R., Bernhard, C., Varma, G.D.: The effect of carbon and rare earth oxide co-doping on the structural and superconducting properties of MgB_2. Supercond. Sci. Technol. **23**(4) (2010). doi:10.1088/0953-2048/23/4/045005

22. Vajpayee, A., Awana, V.P.S., Bhalla, G.L., Bhobe, P.A., Nigam, A.K., Kishan, H.: Superconducting properties of adipic-acid-doped bulk MgB_2 superconductor. Supercond. Sci. Technol. **22**(1) (2009). doi:10.1088/0953-2048/22/1/015016

23. Zeng, R., Lu, L., Dou, S.X.: Significant enhancement of the superconducting properties of MgB_2 by polyvinyl alcohol additives. Supercond. Sci. Technol. **21**(8) (2008). doi:10.1088/0953-2048/21/8/085003

24. Vajpayee, A., Awana, V.P.S., Kishan, H., Narlikar, A.V., Bhalla, G.L., Wang, X.L.: High field performance of nanodiamond doped MgB_2 superconductor. J. Appl. Phys. **103**(7) (2008). doi:10.1063/1.2831778

25. Cheng, C.H., Yang, Y., Munroe, P., Zhao, Y.: Comparison between nano-diamond and carbon nanotube doping effects on critical current density and flux pinning in MgB_2. Supercond. Sci. Technol. **20**(3), 296-301 (2007). doi:10.1088/0953-2048/20/3/032

26. Lim, J.H., Lee, C.M., Park, J.H., Kim, W., Joo, J., Jung, S.B., Lee, Y.H., Kim, C.J.: Fabrication and Characterization of the MgB_2 Bulk Superconductors Doped by Carbon Nanotubes. IEEE Trans. Appl. Supercond. **19**(3), 2767-2770 (2009). doi:10.1109/tasc.2009.2018150

27. Pan, X.F., Zhao, Y., Feng, Y., Yang, Y., Cheng, C.H.: Effects of graphite doping on critical current density and microstructure of MgB_2 bulks by an improved Mg-diffusion method. Physica C **468**(15-20), 1169-1173 (2008). doi:10.1016/j.physc.2008.05.025

28. Dou, S.X., Soltanian, S., Horvat, J., Wang, X.L., Zhou, S.H., Ionescu, M., Liu, H.K., Munroe, P., Tomsic, M.: Enhancement of the critical current density and flux pinning of MgB_2 superconductor by nanoparticle SIC doping. Appl. Phys. Lett. **81**(18), 3419-3421 (2002). doi:10.1063/1.1517398

29. Varghese, N., Vinod, K., Chattopadhyay, M.K., Roy, S.B., Syamaprasad, U.: Effect of combined addition of nano-SiC and nano-Ho_2O_3 on the in-field critical current density of MgB_2 superconductor. J. Appl. Phys. **107**(1) (2010). doi:10.1063/1.3275504

30. Vinod, K., Varghese, N., Roy, S.B., Syamaprasad, U.: Significant enhancement of the in-field critical current density of the MgB_2 superconductor through codoping of nano-TiC with nano-SiC. Supercond. Sci. Technol. **22**(5) (2009). doi:10.1088/0953-2048/22/5/055009

31. Varghese, N., Vinod, K., Shipra, Sundaresan, A., Syamaprasad, U.: Burned Rice Husk: An Effective Additive for Enhancing the Electromagnetic Properties of MgB_2 Superconductor. J. Am. Ceram. Soc. **93**(3), 732-736 (2010). doi:10.1111/j.1551-2916.2009.03438.x

32. Vinod, K., Varghese, N., Sundaresan, A., Syamaprasad, U.: Highly enhanced in-field critical current density of MgB_2 superconductor by combined addition of burned rice husk and nano Ho_2O_3. Solid State Sci. **12**(4), 610-616 (2010). doi:10.1016/j.solidstatesciences.2010.01.012

33. Dou, S.X., Soltanian, S., Yeoh, W.K., Zhang, Y.: Effect of nano-particle doping on the upper critical field and flux pinning in MgB_2. IEEE Trans. Appl. Supercond. **15**(2), 3219-3222 (2005). doi:10.1109/tasc.2005.848799

34. Rahul, S., Thomas, S., Devadas, K.M., Varghese, N., Paulose, A.P., Varma, M.R., Syamaprasad, U.: Tackling the agglomeration of Mg_2Si dopant in MgB_2 superconductor using cast Mg-Si alloy. Materials Research Bulletin. doi:10.1016/j.materresbull.2017.05.022

35. Cheng, Z.H., Shen, B.G., Zhang, J., Zhang, S.Y., Zhao, T.Y., Zhao, H.W.: Superconductivity of $Mg(B_{1-x}C_x)_2$ ternary compounds. J. Appl. Phys. **91**(10), 7125-7127 (2002). doi:10.1063/1.1456422

36. Kazakov, S.M., Puzniak, R., Rogacki, K., Mironov, A.V., Zhigadlo, N.D., Jun, J., Soltmann, C., Batlogg, B., Karpinski, J.: Carbon substitution in MgB_2 single crystals: Structural and superconducting properties. Phys. Rev. B **71**(2) (2005). doi:10.1103/PhysRevB.71.024533

37. Kortus, J., Dolgov, O.V., Kremer, R.K., Golubov, A.A.: Band filling and interband scattering effects in MgB_2: Carbon versus aluminum doping. Phys. Rev. Lett. **94**(2) (2005). doi:10.1103/PhysRevLett.94.027002

38. Romero-Salazar, C., Morales, F., Escudero, R., Duran, A., Hernandez-Flores, O.A.: Flux jumps in hot-isostatic-pressed bulk MgB_2 superconductors: Experiment and theory. Phys. Rev. B **76**(10) (2007). doi:10.1103/PhysRevB.76.104521

39. Duran, A., Verdin, E., Galvan, D.H., Romero-Salazar, C., Morales, F., Adem, E., Rickards, J., Maple, M.B., Escudero, R.: Magnetic instability in irradiated MgB_2 dense samples. J. Appl. Phys. **104**(9) (2008). doi:10.1063/1.3008027

40. Bean, C.P.: Magnetization of Hard Superconductors. Phys. Rev. Lett. **8**(6), 250-253 (1962). doi:10.1103/PhysRevLett.8.250

Chapter 4

Optimising the processing parameters for the development of MgB_2 superconducting wires

One of the most promising applications of a superconductor is to develop magnets. All practically useful superconductors have been tried for magnet development. Even after half a century of discovery, the classical superconductors, NbTi (T_C = 9.2 K) and Nb_3Sn (T_C = 18.3 K) are still the most preferred materials for superconducting magnets [1-6] and these are operated in a liquid helium environment. Helium is available in nature only in poor quantity and already not sufficient for various scientific and industrial applications. The price of helium is on the rise all the time. Also, helium loss during transportation is significant and it is not very easy to handle liquid helium based cooling systems. MgB_2 offers a solution to this, because of its high transition temperature (T_C) it can be operated using a cryocooler or solid nitrogen or a combination of these two. Due to its high heat capacity, the idea of using SN_2 together with a cryocooler, as the cooling source is gaining momentum. SN_2, on its own, is capable of maintaining the operating temperature for a certain time, thus not necessitating the continuous operation of the cryocooler [7, 8]. Modern day cryocoolers are very reliable and practically offer maintenance free operation. With new technologies, the production costs of cryocoolers are coming down. Due to its high T_C, MgB_2 can be operated in the 20-30 K temperature range. A 20 K cryocooler is much cheaper and lighter than a 4 K cryocooler, making the MgB_2-cryocooler combination more attractive than an LTS-cryocooler combination.

For practical applications, it is necessary to develop the superconductor into long flexible conductors with high in-field critical current density and thermo-magnetic stability. Among the various methods, the Powder In Tube (PIT) technique [9] has been accepted as the most suitable one for making good quality MgB_2 wires. This technique is very simple, inexpensive and easily scalable. This chapter details the development of MgB_2 wires in mono and multifilamentary geometry and their characterization under cryogen free condition. Effects of heat treatment temperature and duration on the structural and superconducting properties of undoped monofilamentary wires are discussed in the first section of this chapter. In MgB_2 conductors, sheath materials play an important role. A comparison of commonly used sheath materials regarding their reactivity with the precursor powder, influence on superconducting

properties, strain tolerance, mechanical workability, cost etc. are presented in the second section.

4.1 Effects of heat treatment temperature and duration on the structural and superconducting properties of MgB_2 PIT wires.

In PIT processing of MgB_2 conductors, either a pre-reacted powder (*ex-situ*) or a stoichiometric mixture of Mg and B powders (*in-situ*) is packed into a metal tube and rolled/drawn to desired geometry. *Ex-situ* method gives wires with dense and homogeneous core with practically no impurities. Since the powder is already reacted, sinterability is poor and high sintering temperatures are required. Doping of impurities is also difficult in *ex-situ* method, whereas the *in-situ* method provides a lot of opportunities to develop MgB_2 wires/tapes with superior qualities [10-14]. In *in-situ* method because of the huge difference in the melting points of Mg (650 ^{O}C) and B (2030 ^{O}C), depending on the processing temperature there is scope for solid-solid, solid-liquid and solid-gas interactions. This, in turn, has a vital influence on the phase transformation, microstructure, density and porosity of the MgB_2 superconductor. Phase purity, microstructure, density and porosity are important in transport current properties. Therefore to optimize the processing temperature is crucial to get the best transport critical current density. The present work is an investigation on the effects of processing temperature and duration on structural and superconducting properties of MgB_2/Fe wires.

4.1.1 Preparation and characterisation

Stoichiometrically weighed Mg and B powders were mixed thoroughly using an agate mortar and pestle. The powder was filled in Fe tubes of outside diameter (OD) 6 mm, inside diameter (ID) 4 mm and mechanically compacted. Brass studs were used to plug the ends of the tubes. The composite tubes were groove rolled down to wires of diameter 1.55 mm. Ends of the tubes were sealed using a capping technique [15] and heat treated in air at 600, 650,700, 750, 800 and 850 ^{O}C for 2 hours using a muffle furnace with a ramp rate of 2 ^{O}C/minute and furnace cooled. Sample codes and corresponding heat treatment temperatures are given in table (4.1). The phase analysis of the samples was done using an X-ray diffractometer with Cu Kα radiation. Samples for the powder XRD analysis were recovered from the wires by mechanically peeling of the Fe sheath. Microstructural analysis was performed using a scanning electron microscope. Superconducting properties such as critical temperature (T_C) and

critical current (I_C) were measured using a closed cycle cryocooler interfaced cryostat by DC four probe resistive method. Critical current density (J_C) was obtained by dividing I_C with the cross sectional area of the superconducting core of the wire.

4.1.2 Results and discussion

Figure (4.1) shows the XRD patterns of the samples heat treated at different temperatures. The sample heat treated at 600 ^{O}C shows peaks of MgB_2 and Mg in almost equal intensities. This indicates that the reaction between Mg and B has only started at this temperature. All the other samples have MgB_2 as the main phase with Mg peaks gradually disappearing at higher heat treatment temperatures. A semi-quantitative phase analysis is done from the peak intensities of the samples and tabulated in table (4.1). At 600 ^{O}C reaction is only at the halfway stage and about 47 volume % MgB_2 is present in this sample. At 650 ^{O}C, about 82 % is MgB_2 and it reaches 98 % at 850 ^{O}C. The unreacted Mg has steadily decreased with increasing heat treatment temperature. All samples show the presence of minor quantities of MgO. MgO was formed from the entrapped air in the reaction mixture. The absence of B rich phases [e.g. MgB_4, MgB_{12} etc.] indicates that there is no Mg evaporation loss at our heat treatment conditions.

Table 4.1 Semi-quantitative phase analysis and strain in samples heat treated at different temperatures

Sample name	Heat treatment temperature (^{O}C) / 2 hr	Volume % of			Strain (%)
		MgB_2	Mg	MgO	
S 600	600	47.2	51.8	1.0	-
S 650	650	82.4	16.4	1.2	1.21
S 700	700	90.4	8.3	1.3	0.94
S 750	750	95.2	3.2	1.6	0.51
S 800	800	97.3	1.0	1.7	0.49
S 850	850	97.8	0.3	1.9	0.48

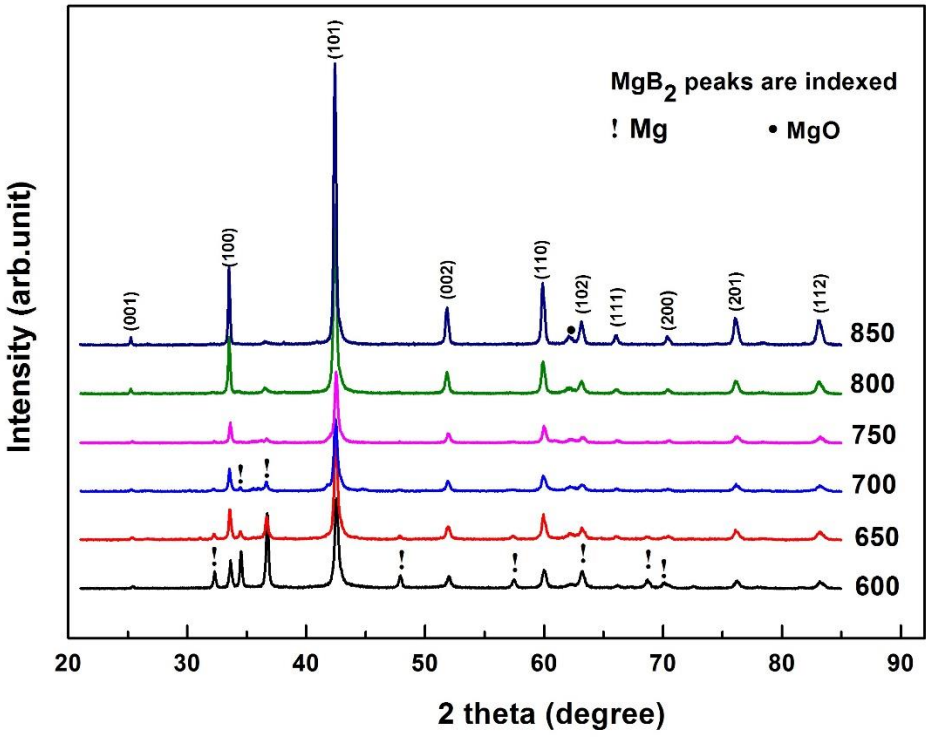

Fig (4.1) XRD patterns of samples heat treated at different temperatures.

Figure (4.2) shows the variation of Full Width at Half Maximum (FWHM) of MgB_2 peaks with sintering temperature. FWHM of all peaks decreases systematically with increasing sintering temperature, indicating improvement in grain size and crystallinity. As indicated by the XRD patterns, higher heat treatment temperatures aid the formation of MgB_2 and reduce the amount of unreacted Mg and B in the matrix. Higher heat treatment temperatures are conducive for the formation of larger grains. Lattice strain values are calculated from Williamson-Hall plots (figure 4.3) of (hk0) peaks. Strain decreases as the heat treatment temperature increases. This indicates that with the increase in heat treatment temperature, crystallinity has improved and defects in the lattice have decreased. The depression of crystallinity for samples sintered at lower temperatures originates from defects in the crystal lattice caused by intragranular precipitates like unreacted Mg and B.

Figure (4.4) shows the resistance vs temperature (R-T) plots of the samples heat treated at different temperatures. All samples show good superconducting transition. The sample heat treated at 600 ^{O}C shows the lowest T_C of 36.8 K because of the low concentration of MgB_2 in it. All other samples show T_C values above 38.5 K, with T_C slightly increasing with heat treatment temperature. Formation of higher volume fraction MgB_2, reduction of unreacted Mg

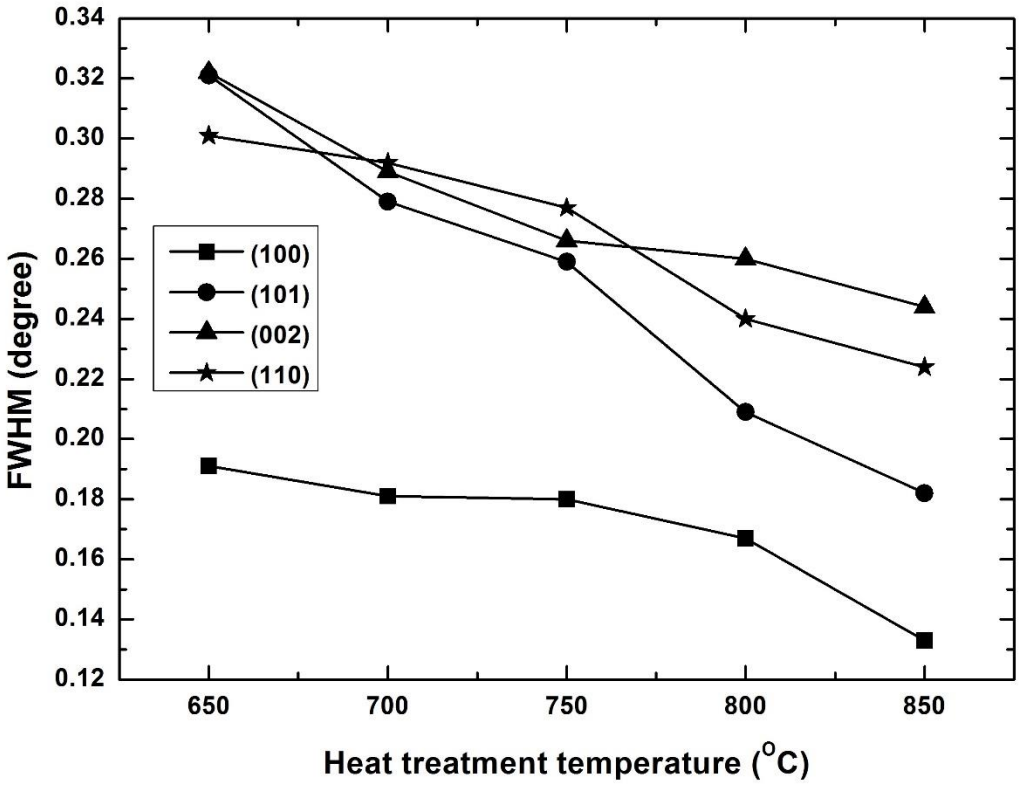

Fig (4.2) Variation in FWHM of MgB_2 peaks with heat treatment temperature.

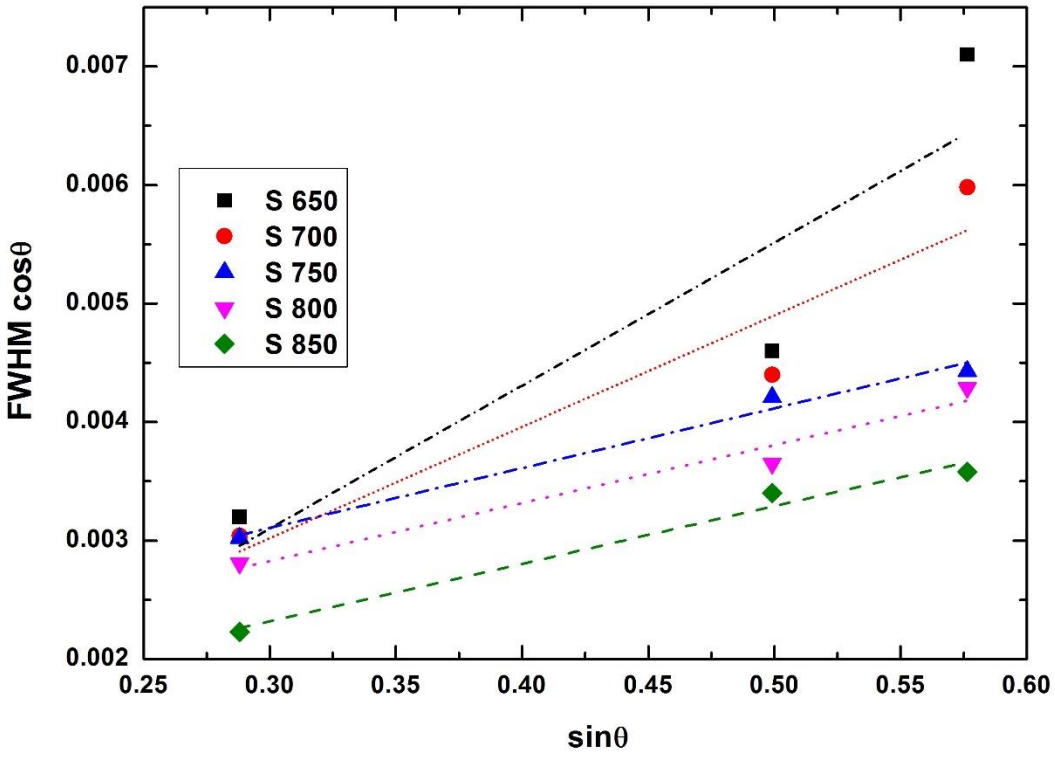

Fig (4.3) Williamson-Hall plots of (hk0) peaks.

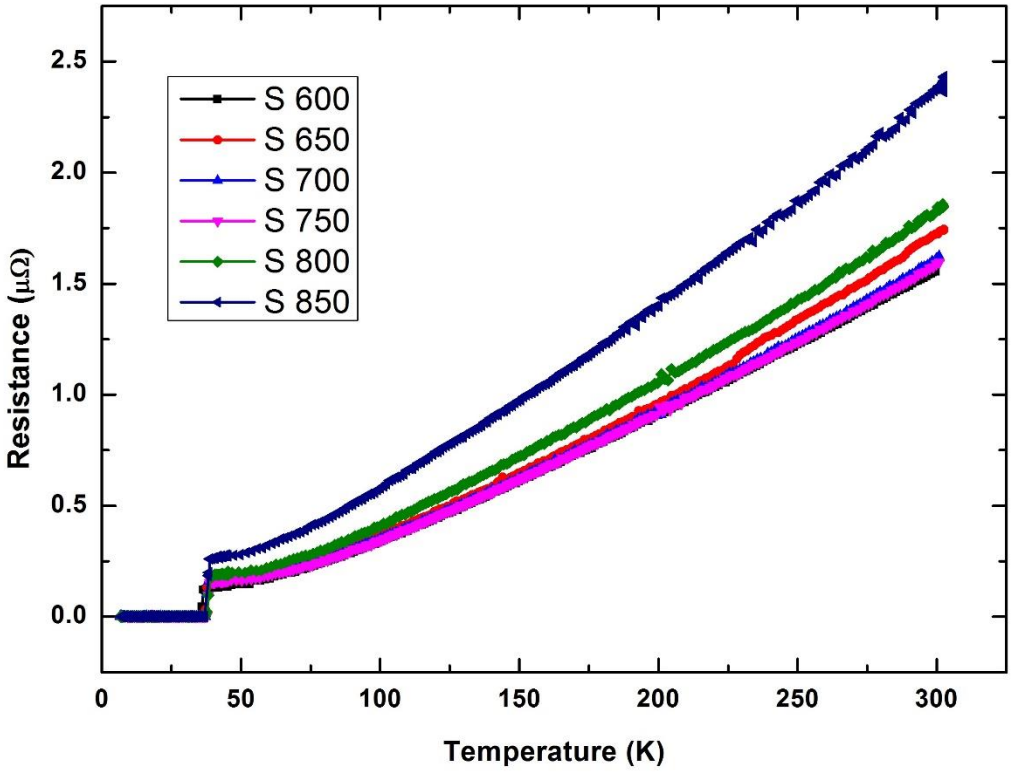

Fig (4.4) R-T plots of samples heat treated at different temperatures.

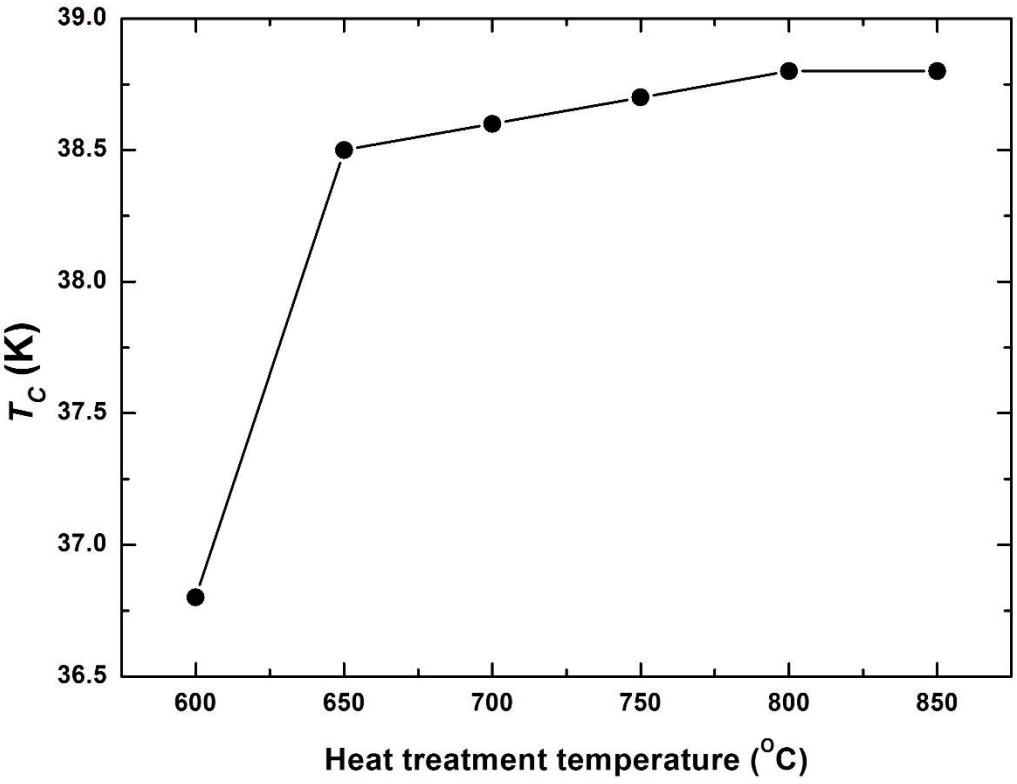

Fig (4.5) Variation in T_C of the samples with heat treatment temperature.

and B, better crystallinity and fewer defects help to improve the T_C of the samples with increase in heat treatment temperature. The variation in T_C of the samples with temperature is shown in figure (4.5). The Current vs Voltage (I-V) plots of the samples measured at 32.5 K and self-field is shown in figure (4.6). The sample S 600 shows the lowest I_C of 12 A, which corresponds to a J_C of 0.35×10^4 A/cm^2. MgB_2 formation has just initiated in this sample, so its low J_C was expected. The best J_C value is shown by the sample S 650 (2.51×10^4 A/cm^2), after that J_C decreases steadily with increasing heat treatment temperature. Figure (4.7) shows the variation of I_C and J_C with heat treatment temperature. XRD analysis of sample S 650 shows that unreacted Mg is present in this sample. It has about 83 vol % MgB_2 and 17 vol % Mg. Still, its I_C and J_C values are better than the samples heat treated at higher temperatures which have more MgB_2 in their core. This is surprising because samples with higher MgB_2 volume fraction and larger grains are expected to perform better in self-field condition. In order to understand the reason behind this reversal in performance, we examined the SEM images of the cross sections of the samples. Figure (4.8) shows the SEM images of the samples heat treated at 600, 650,

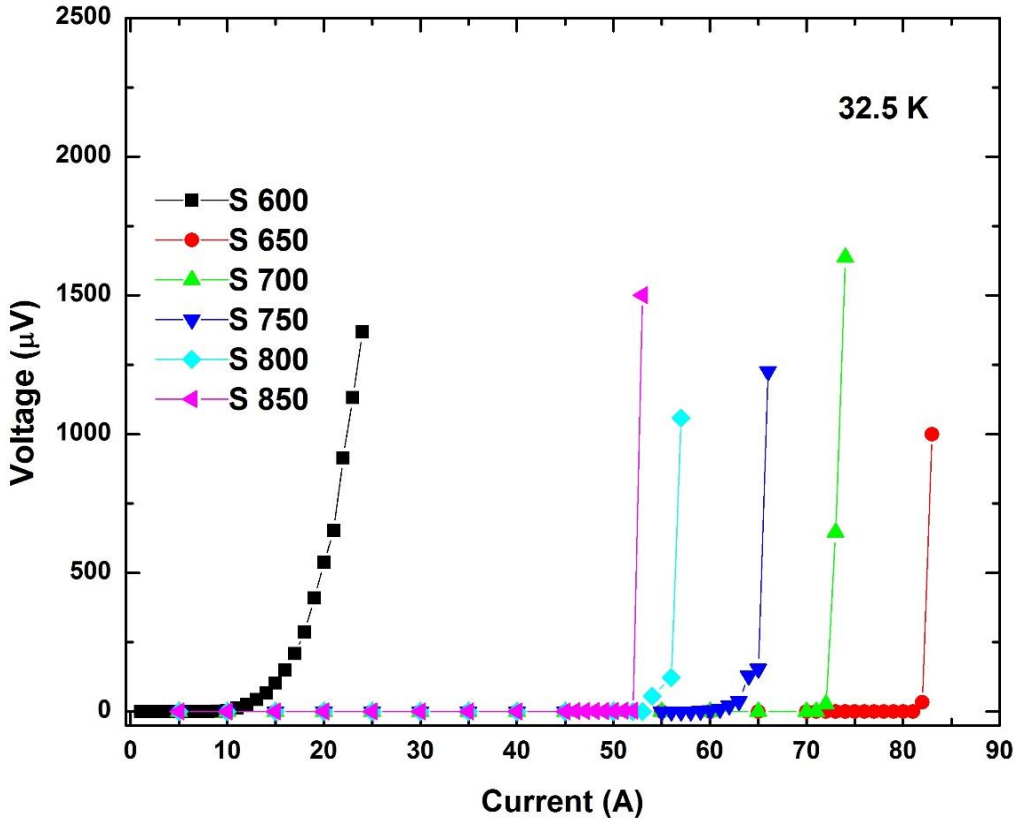

Fig (4.6) I-V plots of all samples at 32.5 K.

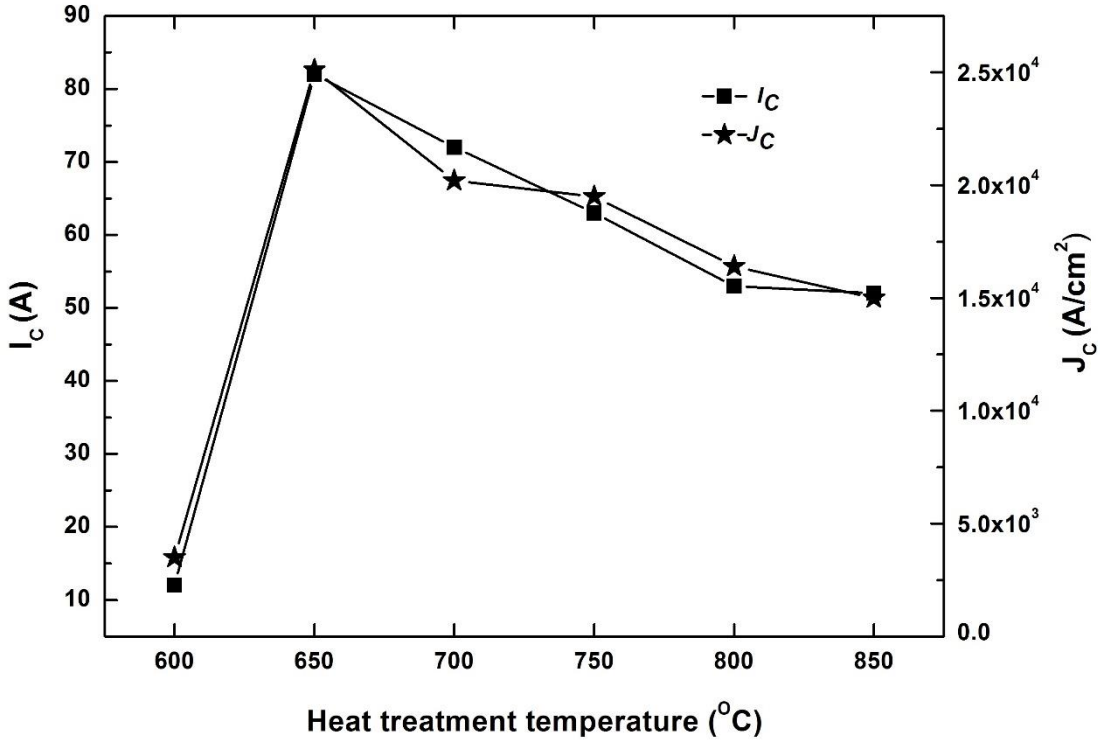

Fig (4.7) Variation in I_C and J_C with heat treatment temperature. Data taken at 32.5 K and self-field.

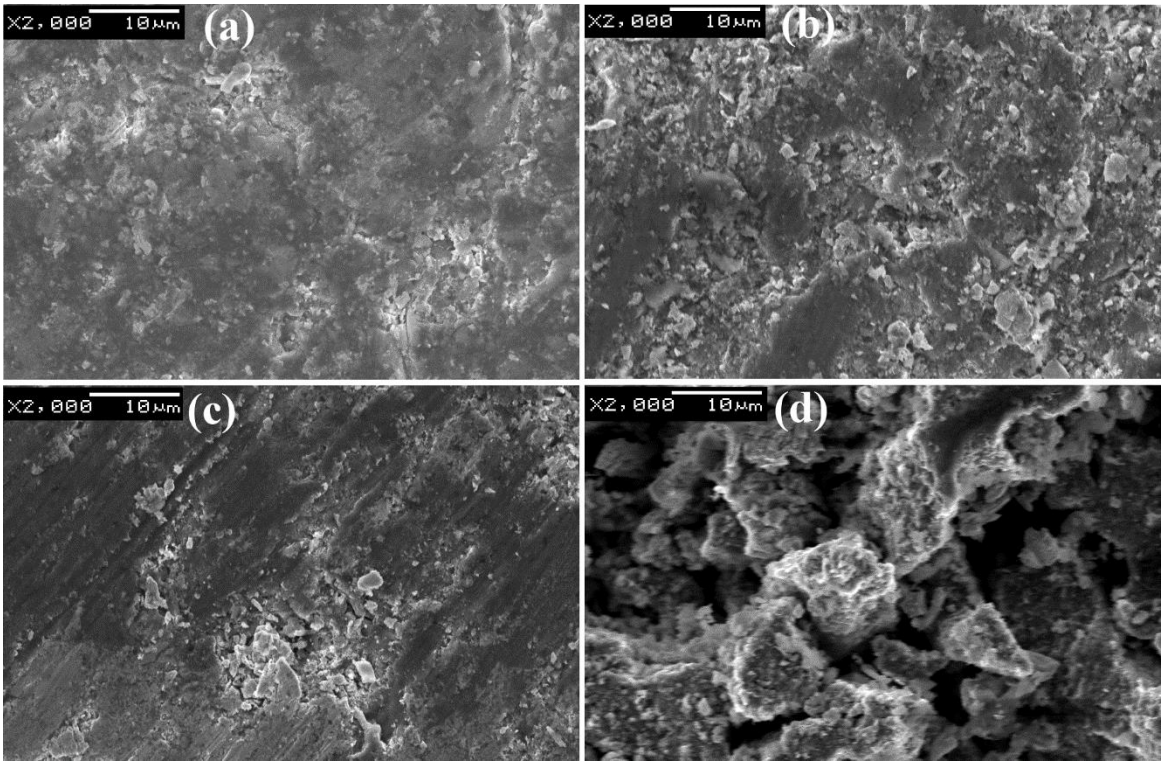

Fig (4.8) SEM images of the superconducting core of the samples heat treated at (a) 600 (b) 650 (c) 700 and (d) 800 ^{O}C.

700 and 800 ^{O}C. The samples heat treated at 700 ^{O}C and above show voids in the superconductor core which is very clear in S 800. The presence of such voids will affect the transport current flow through the sample. When Mg and B react to form MgB_2, there is a volume shrinkage, i.e. $V_{Mg} + V_{2B} > V_{MgB2}$. From the XRD patterns (figure 4.1), it is seen that there are some unreacted Mg and B in samples heat treated at lower temperatures and MgB_2 formation nears completion at higher temperatures. As the MgB_2 phase formed increases at higher temperatures, the density of pores also increases [16, 17] as displayed in figure 4.8(d). Our results show that these pores are adversely affecting the transport current flow. The importance of core density of MgB_2 superconductor is provided by the excellent results achieved by Internal Mg Diffusion [18-21] and Cold High Pressure Densification [22-24] techniques. Samples prepared using such techniques have better core density, achieving a density close to the theoretical density of MgB_2. The unreacted Mg at lower heat treatment temperatures may have played a favourable role in increasing J_C as well. Some reports suggest that Mg can improve the grain connectivity and thus the J_C in MgB_2 [25, 26].

Having found that 650 ^{O}C is the optimum heat treatment temperature for our samples, we studied the effects of processing duration on I_C performance. Samples were heat treated for different durations, from 15 minutes to 5 hours, at 650 ^{O}C. The I-V characteristics of the samples are shown in figure (4.9). It is found that the difference in I_C values of all samples are

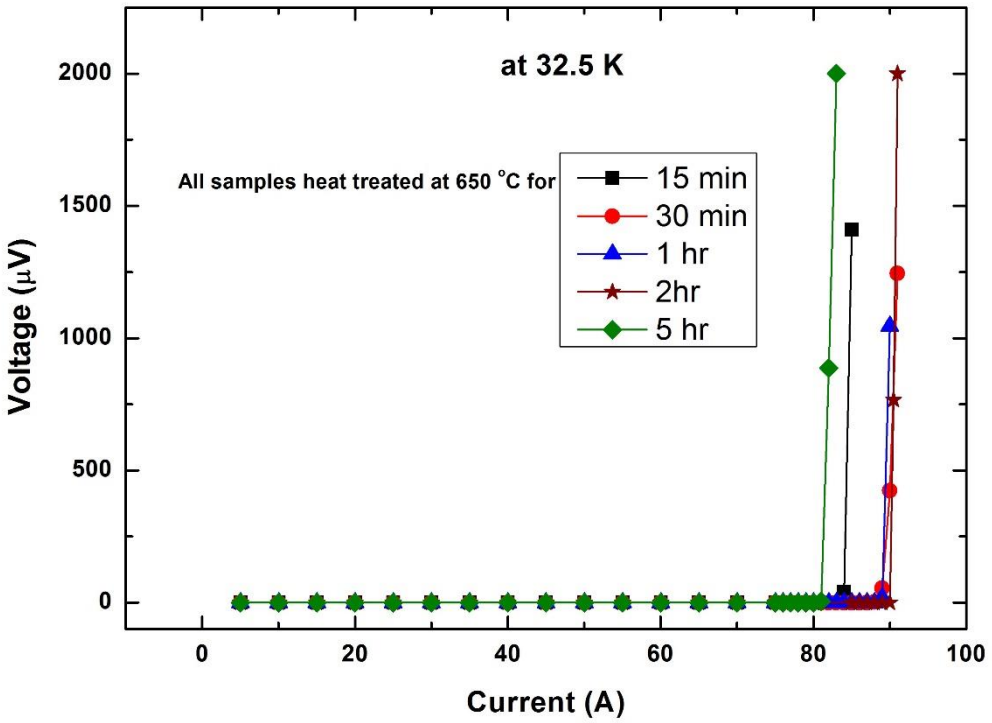

Fig (4.9) I-V plots of samples heat treated for different durations at 650 ^{O}C.

covered within a range of 10 A. At a heat treatment temperature of 650 ^{O}C, the duration has not changed the J_C considerably. Even a 15 minute heat treatment is giving good critical current value (84 A). A lowering trend in I_C is seen in the sample heat treated for 5 hour (81 A). Very long heat treatment durations may lead to formation pores in the core similar to heat treatment

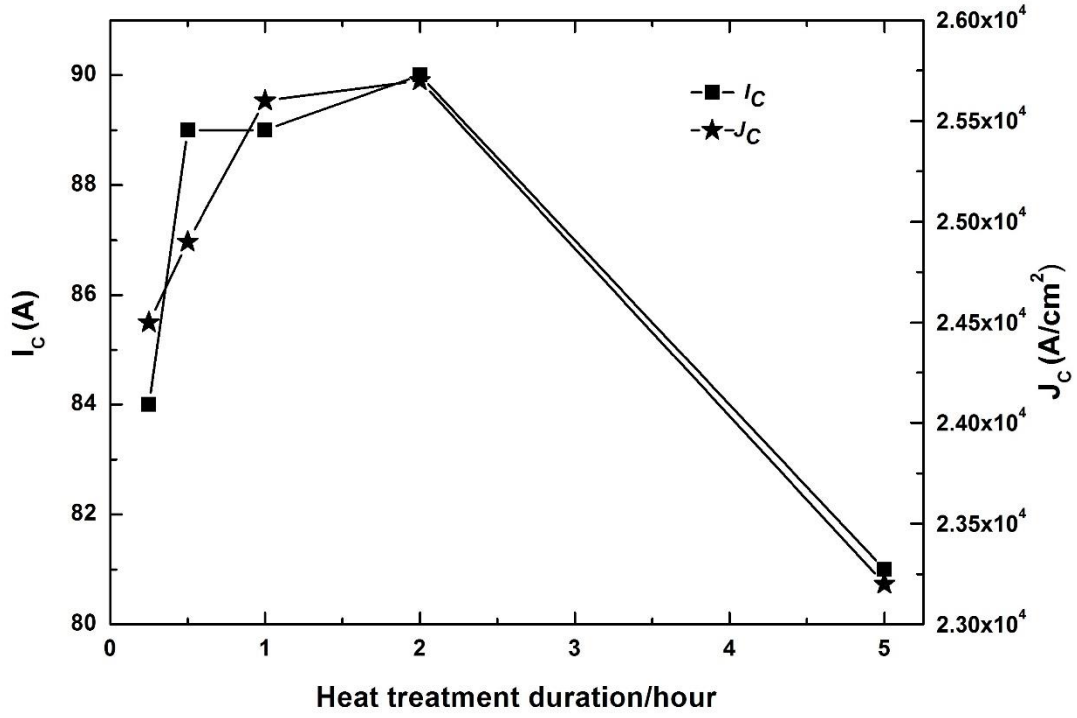

Fig (4.10) Variation in I_C and J_C for different heat treatment durations. Data taken at 32.5 K and self-field.

at higher temperatures and obstruct the transport current flow. Figure (4.10) shows the variation in I_C and J_C with heat treatment duration.

4.1.3 Conclusion

The effects of processing temperature and duration on structural and superconducting properties of MgB_2/Fe wires were studied. Monofilamentary wires in Fe sheath, prepared using PIT technique were heat treated at different temperatures from 600-850 ^{O}C for 2 hours. XRD patterns confirmed that the formation of MgB_2 started at 600 ^{O}C itself but MgB_2 was a minor phase at this temperature. XRD patterns of samples heat treated at 650 ^{O}C and above have MgB_2 as the main phase with its volume fraction increasing with temperature. FWHM of MgB_2 peaks decreased with increasing processing temperature, indicating the growth of grains with temperature. Higher temperatures ensure better crystallinity and fewer defects in the matrix.

The decrease of lattice strain with the increase in heat treatment temperature confirmed this conclusion. Again the T_C values of samples showed a steady increase with temperature. Thus all the analyses pointed to better phase purity, grain connectivity and fewer defects at higher heat treatment temperatures. The behavior of J_C values showed a reverse trend, the sample S 650 showed the best J_C, with J_C slightly decreasing as the heat treatment temperature increased. The reason for depression in J_C at higher temperatures was the increase in the density of pores with heat treatment temperature. These pores seriously limited the transport current flow through the core. SEM images of the samples confirmed this conclusion with large pores visible in the samples heat treated at higher temperatures. At 650 ^{O}C the heat treatment duration didn't appear to have too much of an influence on the I_C performance of the samples. A duration of 1 to 2 hours is adequate to achieve the best result.

4.2 Superconducting and Bending Strain Properties of MgB_2 PIT Wires with Fe, Ni, SS, Nb and Monel Sheaths

In '*in-situ*' PIT method a stoichiometric mixture of Mg and B, both in powder form is filled in a suitable metal tube and rolled, extruded or drawn into desired size and shape and then heat treated. Heat treatment is usually done at 600–850 ^{O}C. The metal tube or the sheath material used with MgB_2 should have certain essential properties. It should not form reacted phases with Mg/B/MgB_2 at the reaction temperature which will deteriorate the superconducting properties. The sheath material should provide adequate mechanical support to the superconducting core and should be ductile enough to make long conductors. In the undesirable event of a quench, the sheath material used should be suitable to transfer the heat generated to the protective dumps associated with the magnet. Reports on influence of certain sheath materials on the behaviour of MgB_2 PIT wires are available in the literature [27-37]. Although these works provided valuable information, arriving at an outright favourite for sheath material would not be straight forward. Since these works differed in wire configuration, precursor powder used, heat treatment temperature, measurement conditions etc. a direct comparison was not possible. The present work focuses on a comparative study on the performance of MgB_2 PIT wires prepared using five commonly used sheath metals namely, Fe, Ni, SS, Nb and monel. MgB_2 wires in mono and multifilamentary geometry with the above sheath materials were

prepared and their structural and superconducting properties as well as bend-strain tolerance of J_C, mechanical workability, scalability etc. were compared.

4.2.1 Preparation and characterisation

PIT method was used to prepare monofilamentary wires, where the ends of the rolled and cut wires were sealed by a simple capping technique [15]. Stoichiometrically weighed Mg powder (-325 mesh, 99.8% purity) and amorphous B powder (-325 mesh 99% purity) were mixed thoroughly in an agate mortar and pestle. The mixture was filled in seamless metal (Fe, Ni, SS, Nb and monel) tubes of length 5 cm, outside diameter (OD) 6 mm and inside diameter (ID) 4 mm and mechanically compacted. Brass studs were used to plug the ends of the tubes. The composite tubes were groove rolled down to wires of diameter 1.55 mm. For studying the bending strain tolerance, multifilamentary wires were prepared by Wire In Tube (WIT) method. Four monofilamentary wires of diameter 2.1 mm were bundled along with five Cu wires (OFHC, 0.75 mm diameter) in another tube of OD/ID = 8/6 mm. In each case the outer sheath used was the same as used for monofilamentary wires. The multifilamentary wires were rolled down to 1.60 mm diameter. To impart desired bending strain, samples were bent carefully into circular arcs of different radius of curvatures with the help of specially made cylindrical mandrels. After sealing the ends, samples were heat treated in air using a muffle furnace at 650 ^{O}C for two hours with a ramp rate of 2 ^{O}C/minute and furnace cooled [Nb sheathed wire samples were heat treated in high purity Ar atmosphere because of the high oxygen affinity of Nb]. Phase analysis of the samples was done using an X-ray diffractometer. For phase identification of the samples, X'pert Highscore Plus Software supported by the ICDD-PDF-2 database was employed. Microstructural examination of the samples was carried out using a scanning electron microscope. The 'R–T' measurements of monofilamentary wires and self-field 'I-V' measurements of multifilamentary wires at 30 K were carried out in a closed cycle cryocooler integrated cryostat by DC four-probe resistive method. The in-field transport critical current [$I_C(H)$] from 3 to 8 T at 4.2 K was measured using a 9 T, 75 mm bore liquid helium cooled magnet system (AMI). The critical current was determined using 1μV/cm criterion.

4.2.2 Results and discussion

Analysing the X-Ray Diffraction patterns of the superconductor cores of the monofilamentary wires [figure (4.11)], it is evident that MgB_2 is the main phase in all samples. Unreacted Mg is also present in all samples with a trace of MgO. The relatively low heat

treatment temperature (650 ^{O}C), is the reason for the presence unreacted Mg. Traces of unreacted Mg in MgB_2 is beneficial in improving in-field J_C [26, 38]. Also, the smaller grains resulting from lower sintering temperature provide more grain boundaries which are very good flux pinners [39, 40]. An impurity phase of Ni, namely $MgNi_3B_2$ is found in both Ni and monel sheathed wires. Its peaks are much more intense in monel sample wherein small quantities of another impurity phase, namely $MgCu_2$ is also present. Hence Fe, SS and Nb sheathed samples are relatively phase pure compared to Ni and monel sheathed samples. SEM images of transverse cross sections of mono wires in different sheaths are shown in figure (4.12). Here, the interface between sheath and core is highlighted. Clearly an interface layer is observed in

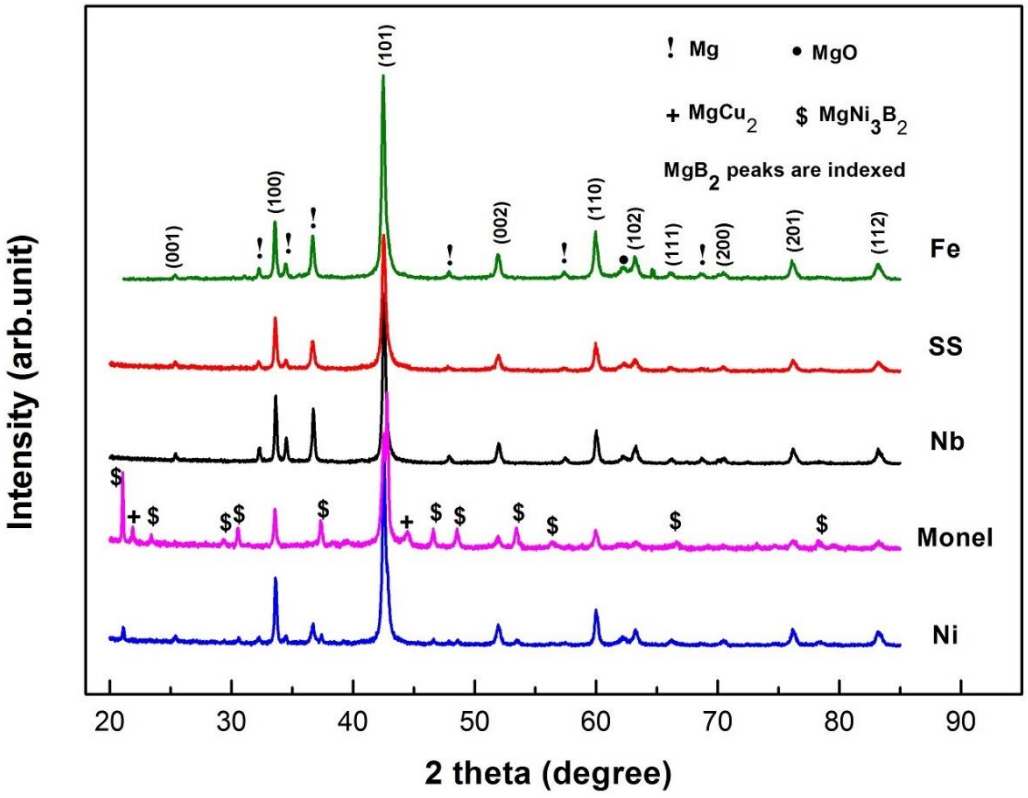

Fig (4.11) Powder XRD patterns of samples prepared in different sheaths.

Ni and monel wires. From XRD analysis it can be corroborated that the layer formed is mainly $MgNi_3B_2$ phase. Obviously this interface layer will act as a barrier for current transport from the sheath to core. The presence of such insulating layers will increase the current transfer length and causes the current to travel more distance through the resistive sheath resulting in joule heating [41]. The effect will be more intense in practical multifilamentary wires where the metal-core interface area is relatively more than that in monofilametary wires.

Figure (4.13) shows the R-T plots of the monofilamentary wires in the temperature range 10 to 300 K. All samples show good superconducting transitions. Fe, SS, and Nb based samples which were found to have better phase purity exhibit higher T_Cs of 38.6 K, 38.8 K, and 38.5 K respectively. Ni and monel sheathed samples show lower T_Cs of 37.7 K and 37.2 K respectively due to the presence of the impurity phases. Figure (4.14) shows a comparison of T_C values of the monofilamentary wires in different sheaths. The variation of transport critical current density of all the samples with respect to magnetic field in the range from 3 to 8 T at

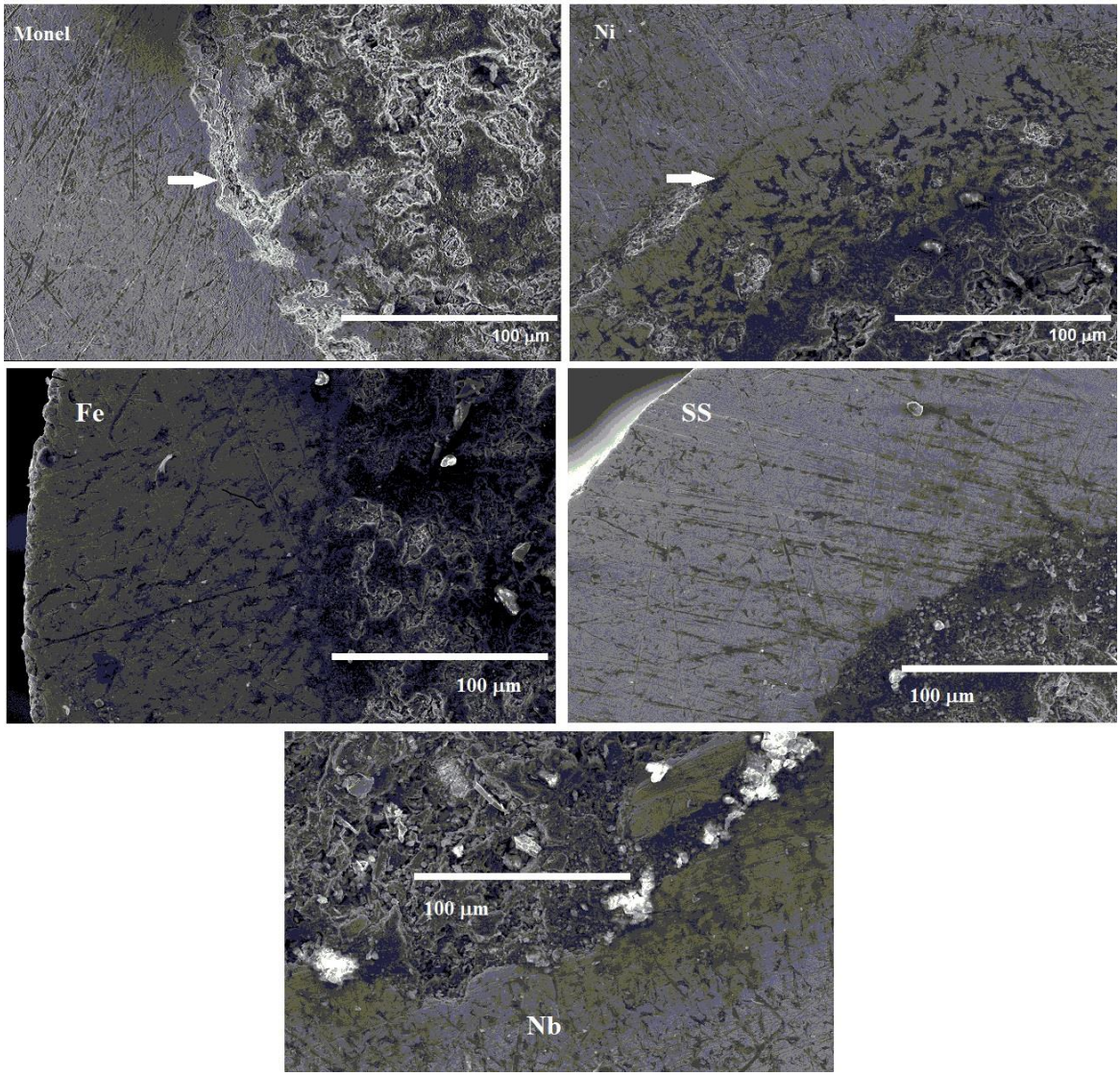

Fig (4.12) SEM images of the cross section the wires in different sheaths.

4.2 K is shown in figure (4.15). The Fe, Nb and SS sheathed wires show distinctly higher J_Cs than the Ni and monel sheathed samples with almost the same kind of variation in the entire field range. Fe sheathed sample show a J_C of 2.1×10^5 A/cm^2 at 4.2 K and 3 T, while Nb and

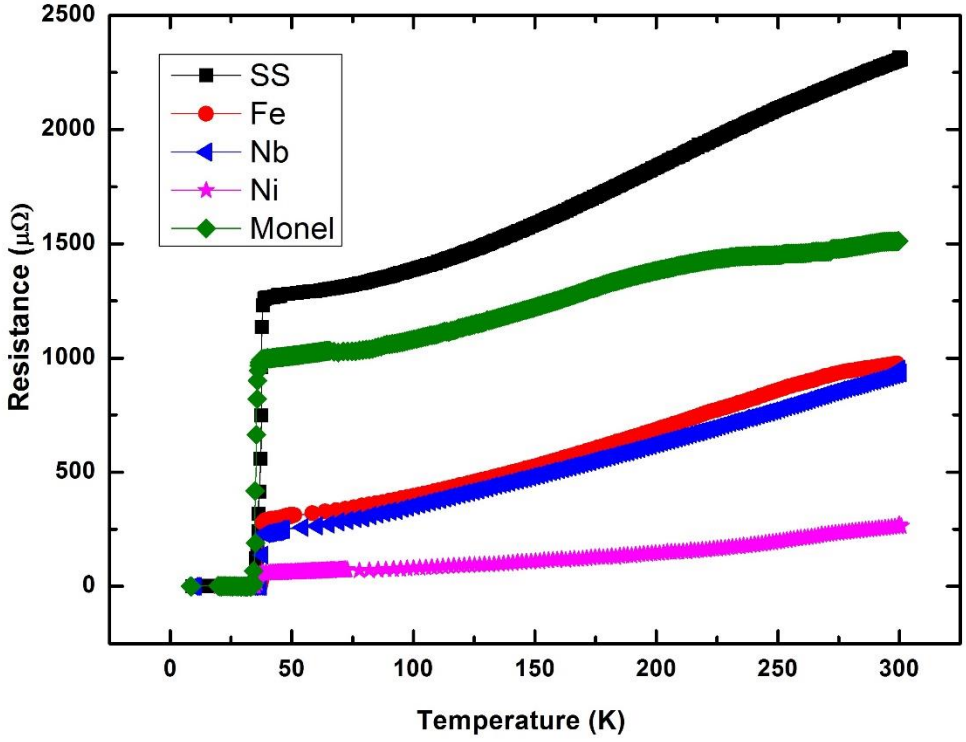

Fig (4.13) R-T Plots of monofilamentary wires in different sheaths.

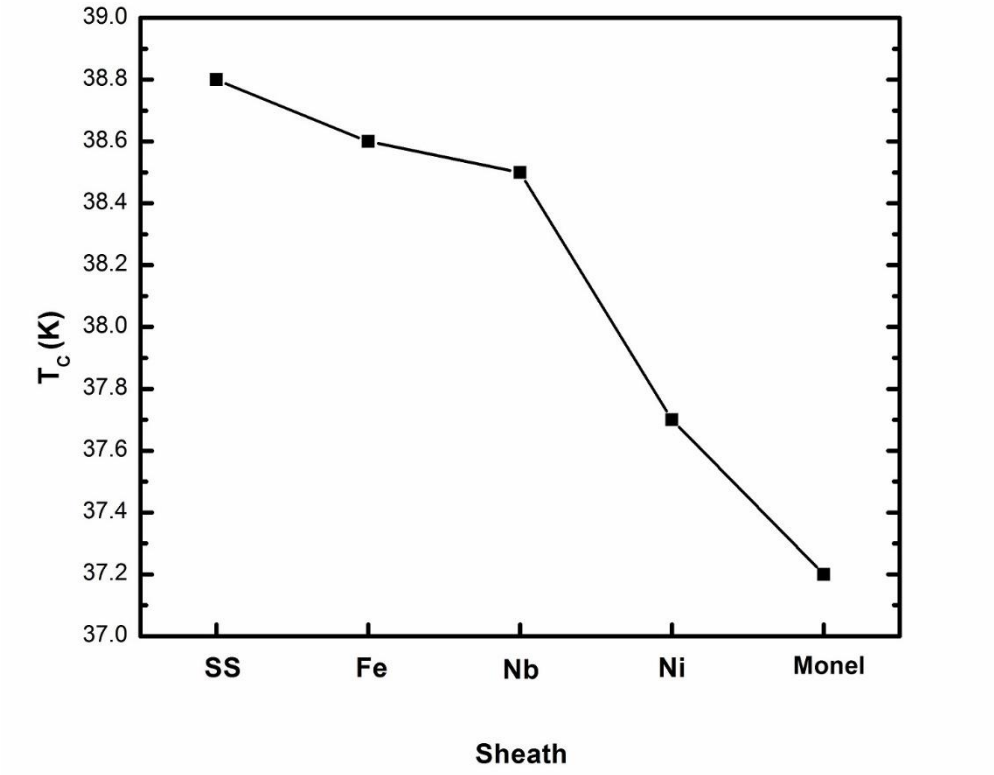

Fig (4.14) Comparison of T_Cs of monofilamentary wires in different sheathes.

SS based samples have J_Cs of 1.2×10^5 A/cm^2 and 1.0×10^5 A/cm^2 respectively at the same conditions. Since these were relatively pure samples except for the presence of a small fraction of Mg and a trace of MgO, the J_Cs of these samples decreased significantly as the field increased. At 8 T, the Fe sheathed sample shows the highest J_C of 4.6×10^3 A/cm^2, which is slightly higher than the J_C (3.1×10^3 A/cm^2) shown by Nb. The SS sheathed sample shows a still lower J_C of 2.4×10^3 A/cm^2 at 8 T. The flux pinning in all these samples is provided by grain boundaries only since no additional pinning centres were introduced into the superconducting matrix through chemical doping or other means. The secondary phases formed in Ni and monel sheathed samples only contributed to reducing the superconducting core and they are located at the sheath-core interface rather than distributed in the

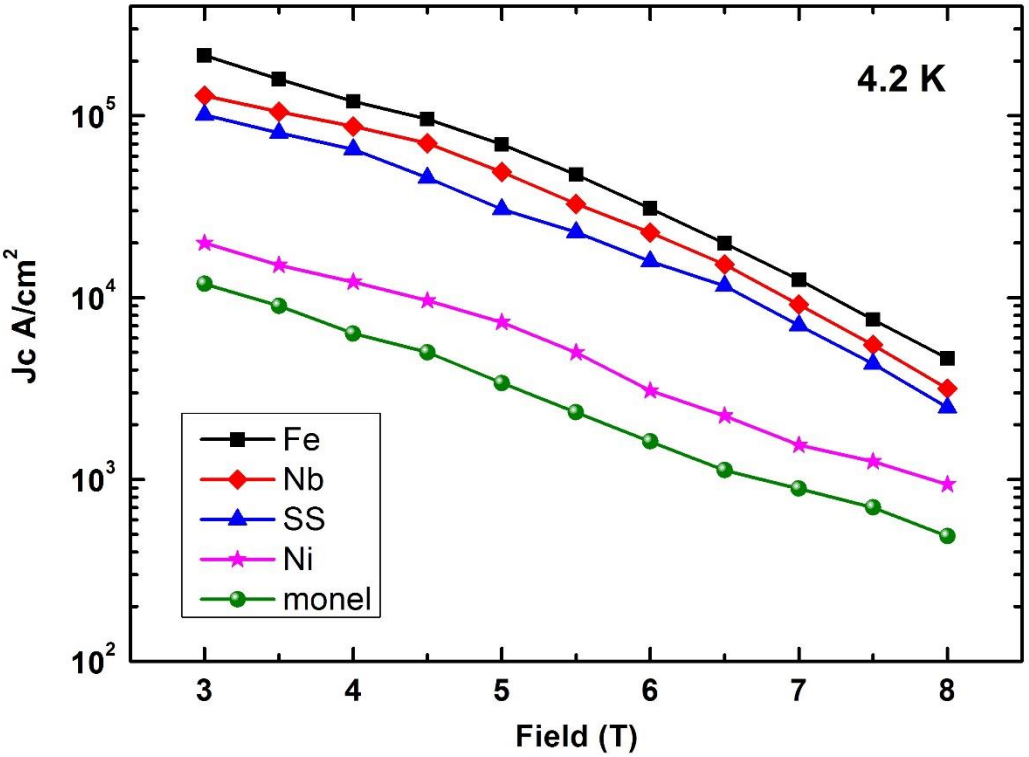

Fig (4.15) Variation of transport J_C of monofilamentary wires in different sheaths with applied magnetic field at 4.2 K.

superconducting matrix to contribute to flux pinning. Hence the self-field and in-field J_Cs of Ni and monel based samples are considerably lower. The superior performance of Fe, Nb and SS sheathed wires is due to the better phase purity of the samples or in other words their non-reactivity with Mg and B at the reaction temperature.

In many of the applications especially for magnets, electric motors, fault current limiters etc. the superconducting wires are wound into coils. It is important to study the effect of bending strain on the transport J_C of the wires before they are put into practical applications. In order to assess the behaviour of J_C during bending, we prepared all the above metal sheathed wires in multifilamentary configuration and measured the deterioration of J_C with respect to bending strain. In each case same metal was used as the barrier material and the outer sheath. For example, in the case of Fe based multifilamentary wires, the monofilamentary wires were prepared in an iron sheath and these wires were packed in another Fe tube and rolled down to the desired diameter. In all samples, the filament number was fixed at 4 and 5 Cu wires of 0.75 mm diameter were used as thermal stabilizers. In one of our earlier studies [42] on bend-strain tolerance of Fe sheathed MgB_2 wires, we identified that wires heat treated after bending, i.e. bent and reacted (B&R) wires retained much higher fraction of the J_C of the straight wire compared to the reacted and bent (R&B) wires [main results of that work is summarized in figure (4.16)]. Hence in the present work, we limited our studies only to B&R wires. Figure (4.17) shows the variation of transport J_C of the wires when subjected to different bending strain. Bending strain, ξ was calculated using the equation, $\xi = [d / (D + d)] \times 100$. Here d is the diameter of the multifilamentary wire and D is the bending diameter. The plots show that the J_C of all samples decreases with increase in bending strain and the rate of deterioration is found to increase with the increase in bending strain. Multifilamentary wires prepared in Fe when bent to 10 cm diameter show a decrease of around 15 % in J_C when measured at 30 K and self-field. While Ni, SS, Nb and monel show a decrease of 15 %, 19 %, 16 % and 14 % respectively under the same conditions. The advantage of B&R approach is that the cracks formed in the core during bending will be healed to a good extent during heat treatment followed. The various samples studied have retained 81 to 86 % of the straight wire J_C for the bending diameter of 10 cm which corresponds to a bending strain of 1.6 %. This can further be improved by increasing the filament number as discussed in our previous work [42]. Even though the difference in J_C retention is not very large the mechanical workability of these materials greatly differs. It was difficult to bend as rolled SS and monel samples and often they broke into pieces for lower bending diameters. Also, Nb wires when heat treated in air formed a thick oxide layer on the surface due to its high oxygen affinity and this made wires very brittle. Therefore Nb sheathed wires required an inert atmosphere heat treatment. Ni wires while rolled to longer lengths produced thin scales on the surface. While Fe wires were devoid of many of these problems and being a ductile material it was suitable for making long wires

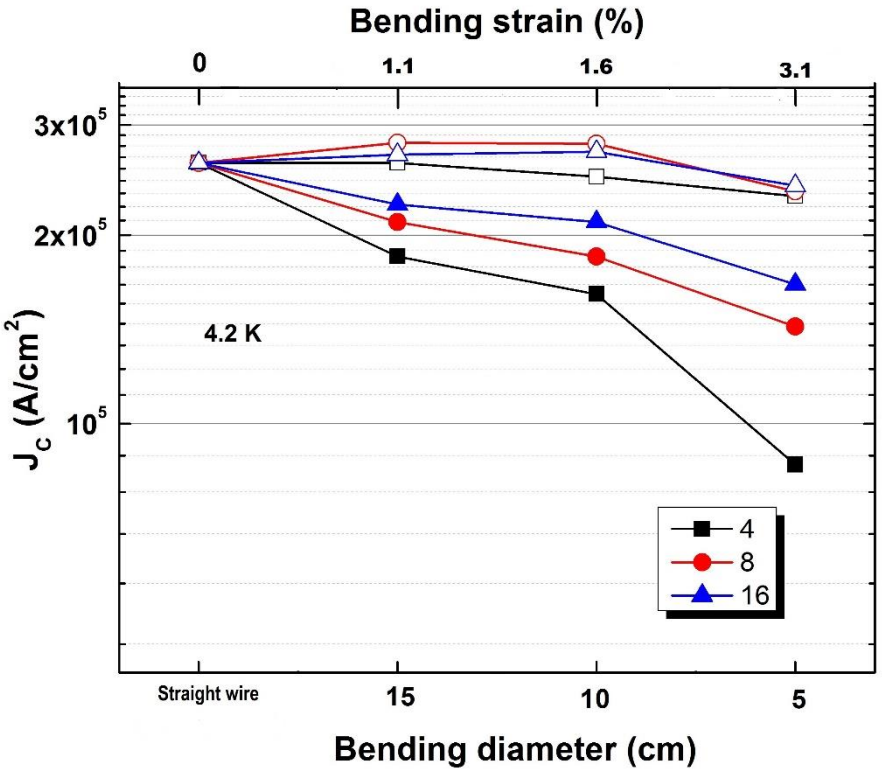

Fig (4.16) Variation of J_C with bending diameters and strain in 4, 8, and 16 filamentary MgB_2 multiwires for both B&R (open) and R&B (closed) sets at 4.2 K.

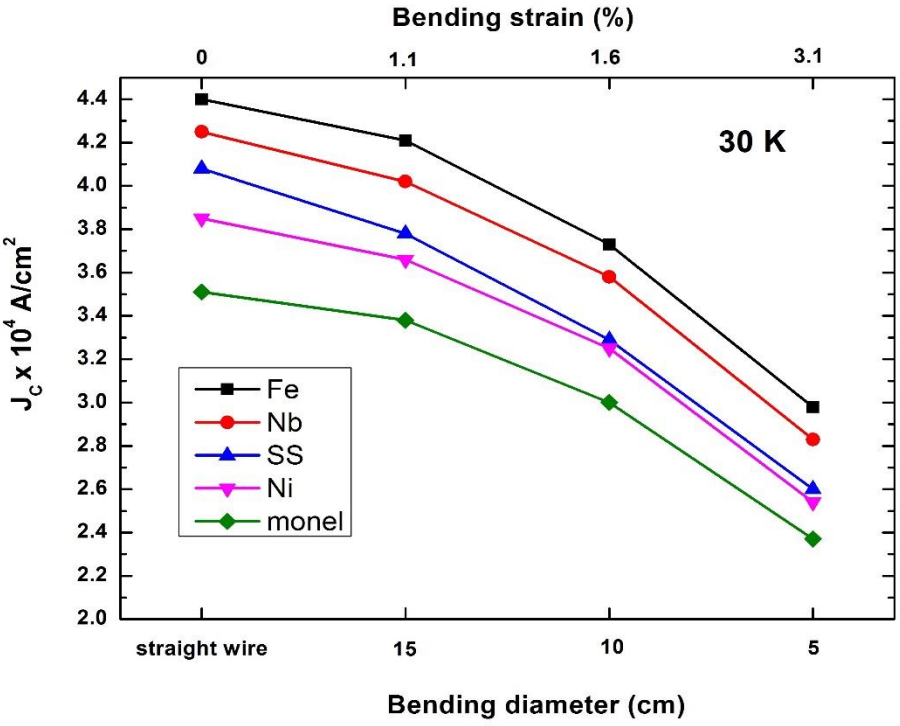

Fig (4.17) Variation of transport J_C of multifilamentary wires in different sheaths with bending diameter/bending strain at 30 K.

and also for bending. The physical condition of the wires after heat treatment is also important. While we used a heat treatment technique in the air for our samples, SS, monel and Ni showed the least oxidation on the surface. Fe formed a thin oxide coating on the surface whereas Nb was completely destroyed by heat treatment in the air as mentioned earlier.

Table 4.2 Important characteristics of MgB_2 superconducting wires prepared using different sheaths

Sheaths used	Impurity phases formed other than MgO	T_C onset (K)	Transport J_C at 4.2 K (A/cm^2)		Retention % of straight wire J_C at 30 K		
					Bending Diameter / Bending Strain		
			3 T $\times 10^5$	8 T $\times 10^3$	15 cm/ 1.1 %	10 cm/ 1.6 %	5 cm/ 3.1 %
Fe	----	38.6	2.1	4.6	95.7	84.8	67.7
Ni	$MgNi_3B_2$	37.7	0.2	0.9	95.1	84.4	66.0
SS	----	38.8	1.0	2.4	92.7	80.6	63.8
Nb	----	38.5	1.2	3.1	94.6	84.2	66.6
Monel	$MgNi_3B_2$, $MgCu_2$	37.2	0.1	0.5	96.3	85.5	67.5

4.2.3 Conclusion

A systematic investigation was made to identify the most suitable sheath material candidates for MgB_2 mono and multifilamentary wires for potential application in magnets, motors, fault current limiters etc. Among the commonly used sheath metals, Fe, Ni, SS, Nb, and monel were selected for the study. Mono and multifilamentary wires were prepared by PIT and WIT techniques. Monel and Ni were found to react with Mg even at 650 ^{O}C and formed

an interface layer of $MgNi_3B_2$ between the sheath and superconducting core. Among all the samples considered Fe, Nb and SS sheathed wires showed higher T_C values and superior in-field transport J_C values compared to the others. Of these, the Fe sheathed wires yielded the best transport J_C and superior strain tolerance. Multifilamentary wires prepared in Fe when bent to 10 cm diameter retained 85 % of the straight wire J_C. Also, the mechanical workability of Fe is much better than other sheath materials considered. The important factors such as no reactivity with Mg and B at elevated temperatures, good mechanical workability, higher transport J_C both at self and in-fields, retention of adequate fraction of J_C under bend mode, possibility of heat treatment directly in air, easy availability and low cost make Fe one of the best sheath materials for PIT processing of MgB_2 based mono and multifilamentary wires. The important characteristics of MgB_2 superconducting wires prepared using different sheath materials are summarised in table (4.2).

4.3 Summary

The chapter details the second stage of our research plan towards the development of MgB_2 superconducting wires with enhanced in-field critical current density. MgB_2 wires in mono and multifilamentary geometry, suitable for cryogen free operation, were developed using PIT and WIT techniques. Heat treatment conditions play important roles in the performance of MgB_2 conductors. The effects of heat treatment temperature on structural and superconducting properties of MgB_2 monofilamentary wires were studied. Iron sheathed wires were subjected to heat treatment temperatures in the range 600-850 ^{O}C for 2 hours. MgB_2 formation just started at 600 ^{O}C and MgB_2 was the main phase in XRD patterns from 650 ^{O}C onwards. Peaks of unreacted Mg diminished at higher temperatures. Better phase purity, improved crystallinity and fewer defects were attained at higher temperatures. Variations of FWHM of MgB_2 peaks, strain and T_Cs of samples supported this inference. Formation of voids in the matrix due to the volume reduction associated with MgB_2 formation has limited the transport current flow through the wires at higher heat treatment temperatures. 650 ^{O}C heat treatment has given the best J_C value among the samples studied. Keeping 650 ^{O}C as the optimum heat treatment temperature, duration of heat treatment was varied from 15 minutes to 5 hours. The variation in I_C values of all these samples falls within a range of 10 A, showing that the heat treatment duration didn't seriously affect the performance of the conductors at this heat treatment temperature.

In the second section, a comparison of the various sheath materials used with magnesium diboride superconducting wires prepared by PIT method has been done with a view to identifying the most suitable candidates. The wires with sheath metals such as Fe, Ni, SS, Nb and monel were studied for their reactivity with the precursor at heat treatment temperature (650 ^{O}C), influence on self-field and in-field superconducting properties and transport critical current density under bend mode. X-Ray diffraction analysis has shown that Ni and monel reacted with Mg and formed $MgNi_3B_2$, which appeared as a layer between the sheath and core as evident from SEM images. All samples except Ni and monel sheathed wires have exhibited good critical temperatures close to 39 K. The Fe, Nb and SS sheathed wires have also shown much higher transport J_Cs at 4.2 K in the entire field range from 3 to 8 T compared to Ni and monel sheathed wires and of these the Fe sheathed wire has exhibited the highest. Measurement of J_C of multifilamentary wires under different bending strain has shown that Fe and monel sheathed wires retained marginally higher fractions of straight wire J_C compared to others. At a strain of 1.6 %, these wires retained around 85 % straight wire J_C. Mechanical workability and cost of the sheaths have also been considered for selecting the most suitable candidates. Iron satisfied most of the requirements and found to be a suitable sheath material for MgB_2 superconducting wires.

Reference

1. Bessette, D., Mitchell, N., Zapretilina, E., Takigami, H.: Conductors of the ITER magnets. IEEE Trans. Appl. Supercond. **11**(1), 1550-1553 (2001). doi:10.1109/77.920072

2. Fiscarelli, L., Auchmann, B., Bermudez, S.I., Bordini, B., Dunkel, O., Karppinen, M., Loffler, C., Russenschuck, S., Savary, F., Smekens, D., Willering, G.: Magnetic Measurements and Analysis of the First 11-T Nb_3Sn Dipole Models Developed at CERN for HL-LHC. IEEE Trans. Appl. Supercond. **26**(4) (2016). doi:10.1109/tasc.2016.2530743

3. Mitchell, N., Devred, A., Libeyre, P., Lim, B., Savary, F., Div, I.M.: The ITER Magnets: Design and Construction Status. IEEE Trans. Appl. Supercond. **22**(3) (2012). doi:10.1109/tasc.2011.2174560

4. Nishijima, G., Matsumoto, S., Hashi, K., Ohki, S., Goto, A., Noguchi, T., Sakai, S., Shimizu, T.: Operation of 1020-MHz NMR Superconducting Magnet. IEEE Trans. Appl. Supercond. **26**(4) (2016). doi:10.1109/tasc.2016.2519259

5. Oguro, H., Watanabe, K., Awaji, S., Hanai, S., Ioka, S., Sugimoto, M., Tsubouchi, H.: Performance of a 14-T CuNb/Nb_3Sn Rutherford coil with a 300mm wide cold bore. Supercond. Sci. Technol. **29**(8) (2016). doi:10.1088/0953-2048/29/8/084004

6. Watanabe, K., Awaji, S., Sakuraba, J., Watazawa, K., Hasebe, T., Jikihara, K., Yamada, Y., Ishihara, M.: 11 T liquid helium-free superconducting magnet. Cryogenics **36**(12), 1019-1025 (1996). doi:10.1016/s0011-2275(96)00091-4

7. Patel, D., Al Hossain, M.S., See, K.W., Qiu, W.B., Kobayashi, H., Ma, Z.Q., Kim, S.J., Hong, J.G., Park, J.Y., Choi, S., Maeda, M., Shahabuddin, M., Rindfleisch, M., Tomsic, M., Dou, S.X., Kim, J.H.: Evaluation of persistent-mode operation in a superconducting MgB_2 coil in solid nitrogen. Supercond. Sci. Technol. **29**(4) (2016). doi:10.1088/0953-2048/29/4/04lt02

8. Patel, D., Al Hossain, M.S., Motaman, A., Barua, S., Shahabuddin, M., Kim, J.H.: Rational design of MgB_2 conductors toward practical applications. Cryogenics **63**, 160-165 (2014). doi:10.1016/j.cryogenics.2014.04.016

9. Kumakura, H., Matsumoto, A., Nakane, T., Kitaguchi, H.: Fabrication and properties of powder-in-tube-processed MgB_2 tape conductors. Physica C **456**(1-2), 196-202 (2007). doi:10.1016/j.physc.2006.12.017

10. Pan, A.V., Zhou, S.H., Liu, H.K., Don, S.X.: Properties of superconducting MgB_2 wires: in situ versus ex situ reaction technique. Supercond. Sci. Technol. **16**(5), 639-644 (2003). doi:10.1088/0953-2048/16/5/317

11. Yamamoto, A., Tanaka, H., Shimoyama, J., Ogino, H., Kishio, K., Matsushita, T.: Towards the Realization of Higher Connectivity in MgB_2 Conductors: In-situ or Sintered Ex-situ? Jpn. J. Appl. Phys. **51**(1) (2012). doi:10.1143/jjap.51.010105

12. Kovac, P., Husek, I., Melisek, T., Martinez, E., Dhalle, M.: Properties of doped ex and in situ MgB_2 multi-filament superconductors. Supercond. Sci. Technol. **19**(10), 1076-1082 (2006). doi:10.1088/0953-2048/19/10/016

13. Kovac, P., Melisek, T., Dhalle, M., den Ouden, A., Husek, I.: Critical currents of MgB_2 wires prepared in situ and ex situ subjected to axial stress. Supercond. Sci. Technol. **18**(10), 1374-1379 (2005). doi:10.1088/0953-2048/18/10/022

14. Alknes, P., Hagner, M., Bjoerstad, R., Scheuerlein, C., Bordini, B., Sugano, M., Hudspeth, J., Ballarino, A.: Mechanical Properties and Strain-Induced Filament Degradation of Ex Situ and In Situ MgB_2 Wires. IEEE Trans. Appl. Supercond. **26**(3) (2016). doi:10.1109/tasc.2015.2509166

15. Devadas, K.M., Rahul, S., Thomas, S., Varghese, N., Vinod, K., Syamaprasad, U., Pradhan, S., Chattopadhyay, M.K., Roy, S.B.: Transport properties of sealed MgB_2/Fe/Ni multifilamentary wires heat treated in air. J. Alloy. Compd. **509**(31), 8038-8041 (2011). doi:10.1016/j.jallcom.2011.04.147

16. Liu, C.F., Yan, G., Du, S.J., Xi, W., Feng, Y., Zhang, P.X., Wu, X.Z., Zhou, L.: Effect of heat-treatment temperatures on density and porosity in MgB_2 superconductor.

Physica C-Superconductivity and Its Applications **386**, 603-606 (2003). doi:10.1016/s0921-4534(02)02170-6

17. Tan, K.S., Kim, N.K., Kim, Y.J., Jun, B.H., Kim, C.J.: Influence of magnesium powder and heat treatment on the superconducting properties of MgB_2/Fe wires. Superconductor Science & Technology **21**(1) (2008). doi:10.1088/0953-2048/21/01/015015

18. Giunchi, G.: High density MgB_2 obtained by reactive liquid Mg infiltration. International Journal of Modern Physics B **17**(4-6), 453-460 (2003). doi:10.1142/s0217979203016091

19. Giunchi, G., Ceresara, S., Ripamonti, G., Di Zenobio, A., Rossi, S., Chiarelli, S., Spadoni, M., Wesche, R., Bruzzone, P.L.: High performance new MgB_2 superconducting hollow wires. Supercond. Sci. Technol. **16**(2), 285-291 (2003). doi:10.1088/0953-2048/16/2/328

20. Hur, J.M., Togano, K., Matsumoto, A., Kumakura, H., Wada, H., Kimura, K.: Fabrication of high-performance MgB_2 wires by an internal Mg diffusion process. Supercond. Sci. Technol. **21**(3) (2008). doi:10.1088/0953-2048/21/3/032001

21. Togano, K., Hur, J.M., Matsumoto, A., Kumakura, H.: Fabrication of seven-core multi-filamentary MgB_2 wires with high critical current density by an internal Mg diffusion process. Supercond. Sci. Technol. **22**(1) (2009). doi:10.1088/0953-2048/22/1/015003

22. Jie, H., Qiu, W.B., Billah, M., Mustapic, M., Patel, D., Ma, Z.Q., Gajda, D., Morawski, A., Cetner, T., Shahabuddin, M., Yanmaz, E., Rindfleisch, M., Kim, J.H., Hossain, M.S.A.: Superior transport Jc obtained in in-situ MgB_2 wires by tailoring the starting materials and using a combined cold high pressure densification and hot isostatic pressure treatment. Scr. Mater. **129**, 79-83 (2017). doi:10.1016/j.scriptamat.2016.09.042

23. Flukiger, R., Hossain, M.S.A., Kulich, M., Senatore, C.: Technical aspects of Cold High Pressure Densification (CHPD) on long lengths of in situ MgB_2 wires with enhanced Jc values. In: Balachandran, U. (ed.) Advances in Cryogenic Engineering, Vol 58, vol. 1435. AIP Conference Proceedings, pp. 353-362. Amer Inst Physics, Melville (2012)

24. Hossain, M.S.A., Senatore, C., Fluekiger, R., Rindfleisch, M.A., Tomsic, M.J., Kim, J.H., Dou, S.X.: The enhanced Jc and B_{irr} of in situ MgB_2 wires and tapes alloyed with $C_4H_6O_5$ (malic acid) after cold high pressure densification. Supercond. Sci. Technol. **22**(9) (2009). doi:10.1088/0953-2048/22/9/095004

25. Zeng, R., Lu, L., Li, W.X., Wang, J.L., Shi, D.Q., Horvat, J., Dou, S.X., Bhatia, M., Sumption, M., Collings, E.W., Yoo, J.M., Tomsic, M., Rindfleisch, M.: Excess Mg addition MgB_2/Fe wires with enhanced critical current density. Journal of Applied Physics **103**(8) (2008). doi:10.1063/1.2909203

26. Zeng, R., Lu, L., Wang, J.L., Horvat, J., Li, W.X., Shi, D.Q., Dou, S.X., Tomsic, M., Rindfleisch, M.: Significant improvement in the critical current density of in situ MgB_2

by excess Mg addition. Supercond. Sci. Technol. **20**(8), L43-L47 (2007). doi:10.1088/0953-2048/20/8/l01

27. Kumar, R.G.A., Vinod, K., Varghese, N., Syamaprasad, U.: Reactivity of sheath materials with Mg/B in MgB_2 conductor fabrication. Supercond. Sci. Technol. **20**(3), 222-227 (2007). doi:10.1088/0953-2048/20/3/018

28. Varghese, N., Vinod, K., Kumar, R.G.A., Syamaprasad, U., Sundaresan, A.: Influence of reactivity of sheath materials with Mg/B on superconducting properties of MgB_2. J. Appl. Phys. **102**(4) (2007). doi:10.1063/1.2773696

29. Katagiri, K., Takaya, R., Kasaba, K., Tachikawa, K., Yamada, Y., Shimura, S., Koshizuka, N., Watanabe, K.: Stress-strain effects on powder-in-tube MgB_2 tapes and wires. Supercond. Sci. Technol. **18**(12), S351-S355 (2005). doi:10.1088/0953-2048/18/12/021

30. Kovac, P., Husek, I., Dobrocka, E., Melisek, T., Haessler, W., Herrmann, M.: MgB_2 tapes made of mechanically alloyed precursor powder in different metallic sheaths. Supercond. Sci. Technol. **21**(1) (2008). doi:10.1088/0953-2048/21/01/015004

31. Kovac, P., Husek, I., Melisek, T., Strbik, V.: Basic properties of rectangular MgB2/FeNiCo and MgB_2/Fe wires made in situ. Supercond. Sci. Technol. **18**(6), 856-860 (2005). doi:10.1088/0953-2048/18/6/011

32. Feng, Y., Yan, G., Zhao, Y., Liu, C.F., Fu, B.Q., Zhou, L., Cao, L.Z., Ruan, K.Q., Li, X.G., Shi, L., Zhang, Y.H.: Superconducting properties of MgB_2 wires and tapes with different metal sheaths. Physica C **386**, 598-602 (2003). doi:10.1016/s0921-4534(02)02169-x

33. Grasso, G., Malagoli, A., Ferdeghini, C., Roncallo, S., Braccini, V., Siri, A.S., Cimberle, M.R.: Large transport critical currents in unsintered MgB_2 superconducting tapes. Appl. Phys. Lett. **79**(2), 230-232 (2001). doi:10.1063/1.1384905

34. Kovac, P., Husek, I., Melisek, T., Kulich, M., Strbik, V.: MgB_2 composite wires with Fe, Nb and Ta sheaths. Supercond. Sci. Technol. **19**(6), 600-605 (2006). doi:10.1088/0953-2048/19/6/031

35. Zhou, S.H., Pan, A.V., Ionescu, M., Liu, H.K., Dou, S.X.: Influence of Ag, Cu and Fe sheaths on MgB_2 superconducting tapes. Supercond. Sci. Technol. **15**(2), 236-240 (2002). doi:10.1088/0953-2048/15/2/310

36. Kovac, P., Birajdar, B., Husek, I., Holubek, T., Eibl, O.: Stabilized in situ rectangular MgB_2 wires: the effect of B purity and sheath materials. Supercond. Sci. Technol. **21**(4) (2008). doi:10.1088/0953-2048/21/4/045011

37. Grovenor, C.R.M., Goodsir, L., Salter, C.J., Kovac, P., Husek, I.: Interfacial reactions and oxygen distribution in MgB_2 wires in Fe, stainless steel and Nb sheaths. Supercond. Sci. Technol. **17**(3), 479-484 (2004). doi:10.1088/0953-2048/17/3/030

38. Zhang, H., Zhao, Y., Zhang, Y.: The Effects of Excess Mg Addition on the Superconductivity of MgB_2. J. Supercond. Nov. Magn **28**(9), 2711-2714 (2015). doi:10.1007/s10948-015-3120-8

39. Xu, H.L., Feng, Y., Xu, Z., Li, C.S., Yan, G., Mossang, E., Sulpice, A.: Effect of sintering temperature on properties of MgB_2 wire sheathed by low carbon steel tube. Physica C **419**(3-4), 94-100 (2005). doi:10.1016/j.physc.2004.01.004

40. Kim, J.H., Dou, S.X., Wang, J.L., Shi, D.Q., Xu, X., Hossain, M.S.A., Yeoh, W.K., Choi, S., Kiyoshi, T.: The effects of sintering temperature on superconductivity in MgB_2/Fe wires. Supercond. Sci. Technol. **20**(5), 448-451 (2007). doi:10.1088/0953-2048/20/5/007

41. Vinod, K., Varghese, N., Rahul, S., Devadas, K.M., Thomas, S., Gurusamy, P., Kedia, S., Pradhan, S., Syamaprasad, U.: On the current transfer length and current sharing in short length MgB_2 wires. Supercond. Sci. Technol. **23**(10) (2010). doi:10.1088/0953-2048/23/10/105002

42. Thomas, S., Varghese, N., Rahul, S., Devadas, K.M., Vinod, K., Syamaprasad, U.: Enhancement of bending strain tolerance and current carrying property of MgB_2 based multifilamentary wires. Cryogenics **52**(12), 767-770 (2012). doi:10.1016/j.cryogenics.2012.07.007

Chapter 5

Development of MgB_2 superconducting wires with enhanced in-field critical current density

Since the discovery of superconductivity in MgB_2 with a distinctly higher transition temperature (T_C) of 39 K there have been attempts to develop it as an alternative to the low temperature superconductors (LTS) with the added advantage of operation at a higher temperature in the range 20–30 K [1-4]. A comparison of the superconducting properties of MgB_2 with those of LTS shows that MgB_2 is at par or even superior in many of the critical properties [5-9]. Moreover, there is great scope for further improvement in the in-field critical current density [$J_C(H)$] and hence MgB_2 has been identified as a promising candidate for future high-field, 'cryogen free magnets'. The mechanism of superconductivity in MgB_2 is well understood now and efforts are still going on to improve the $J_C(H)$. Due to weak flux pinning and low upper critical field, the critical current density (J_C) of pristine MgB_2 drops rapidly in an applied magnetic field. Improving the in-field properties is very important in making MgB_2 competitive with other practical superconductors. Chemical doping is successfully employed by many groups to improve $J_C(H)$ of MgB_2, especially those causing C substitution for B in the boron plane of MgB_2 [10-28]. Substitution of C modifies the σ and π band scattering and enhances H_{C2} [29-31]. The lattice defects and strain caused by C addition enhance the flux pinning and thus J_C at higher fields. We have successfully employed chemical doping to improve the transport critical current density of MgB_2 Powder In Tube (PIT) wires at higher fields. We found that n C, n SiC and Burned Rice Husk (BRH) can effectively introduce more flux pinners into the MgB_2 lattice and enhance the in-filed properties. The results are discussed in detail in this chapter [32].

5.1 A comparative study on the effects of n C, n SiC and BRH on the structural and superconducting properties of MgB_2 PIT wires

The success of n SiC in improving the in-field properties of MgB_2 was a breakthrough in the efforts to tailor this superconductor for practical applications. SiC causes considerable C substitution for B and reacts with Mg to form Mg_2Si [18-21]. This dual effect of C substitution and inclusion of reacted secondary phases is one among the most effective methods to improve $J_C(H)$ of MgB_2 [33]. Our group has previously explored an alternative source of Si and C, BRH

and achieved excellent results [34, 35]. BRH contains amorphous silica (SiO_2) in a matrix of friable carbon. In the present work, we have done a comparative study on the effects of the above three potential additives namely, n C, n SiC and BRH on the structural and superconducting properties of MgB_2 PIT wires.

5.1.1 Preparation and characterisation

Sample composition chosen was MgB_2 + x wt % of (n C or n SiC or BRH), where x = 2.5, 5 and 7.5. Mg (-325 mesh, 99.8%), amorphous B (-325 mesh, 99%), n C (< 50 nm, 99 +%), n SiC (< 100 nm, 97.5 +%) and raw rice husk heat treated at 300 ^{O}C for 1 hour were the starting powders. Table (5.1) details the composition of the samples and sample codes. Stoichiometric weights of powders were homogeneously mixed and ground thoroughly using an agate mortar and pestle. PIT method was used for preparing monofilamentary wires. The mixture was filled in seamless Fe tubes of length 5 cm, outside diameter (OD) 6 mm and inside diameter (ID) 4 mm and mechanically compacted. Ends of the tubes were plugged using brass studs. The composite tubes were groove rolled down to wires of diameter 1.47 mm. Samples of length 10 cm were cut from the middle of the rolled wires and their ends were sealed using a simple capping technique [36]. All the samples were heat treated in air at 800 ^{O}C for 2 hours in a muffle furnace at a ramp rate of 2 ^{O}C per minute and furnace cooled. Phase analysis of the samples was done using an X-ray diffractometer. X'pert Highscore Plus software supported by the ICDD-PDF-2 database was used for phase identification. A Scanning Electron Microscope was used for microstructural examination. The resistance versus temperature measurements were carried out in a closed cycle cryocooler integrated cryostat by DC four probe resistive method. Keithley 220 current source and Keithley 2182A nano voltmeter were used for R-T measurements. Transport critical current (I_C) in the applied magnetic field (from 0-8 T) was measured in an AMI LHe cooled magnet system (9 T, 75 mm bore). 1μV/cm criterion was used for determining I_C. Wire samples of length around 3 cm were used for the R-T and I-V measurements. The current and voltage leads were taken from the Fe sheath by soldering OFHC wires with the help of phosphoric acid flux.

5.1.2 Results and discussion

Looking at the XRD patterns, figure (5.1), it is clear that MgB_2 is the main phase in undoped and n C, n SiC and BRH added samples. The secondary phases formed vary with respect to their nature and quantity depending on the dopants added. Minor quantities of MgO are formed in n C added samples and also in the undoped and lightly doped SiC and BRH

Table 5.1 Sample code, weight % of dopants, semi-quantitative phase analysis, C substitution for B and strain in undoped and doped samples

Sample name	Dopant	Wt % of dopant	Volume % of				x in $MgB_{2-x}C_x$	Strain (%)
			MgB_2	Mg_2Si	MgO	MgB_2C_2		
MB	-	-	99.4	-	0.6	-	-	0.44
MBC 2.5	n C	2.5	98.6	-	1.4	-	0.034	0.84
MBC 5		5	98.4	-	1.6	-	0.04	1.74
MBC 7.5		7.5	88.3	-	2.0	9.7	0.046	2.95
MBSC 2.5	n SiC	2.5	92.4	7.0	0.6	-	0.026	0.84
MBSC 5		5	85.5	14.5	-	-	0.034	0.94
MBSC 7.5		7.5	72.4	27.6	-	-	0.044	1.04
MBRH 2.5	BRH	2.5	97.8	-	2.2	-	0.024	0.64
MBRH 5		5	92.1	7.9	-	-	0.034	0.83
MBRH 7.5		7.5	90.3	9.7	-	-	0.041	1.35

samples. Heavily C doped sample (7.5 wt %) shows peaks of MgB_2C_2. A semi-quantitative phase analysis is done from the peak intensities of XRD patterns and tabulated in table (5.1). All the n SiC added samples show peaks of Mg_2Si. The volume % of Mg_2Si increases with increasing doping concentration of SiC. Due to the formation of significant quantities of Mg_2Si, the volume fraction of MgB_2 in SiC added samples is less than the corresponding n C and BRH added samples. Mg_2Si peaks in BRH doped samples are not as intense as in SiC doped samples. Mg_2Si peak is absent in 2.5 wt % BRH added sample. While 5 wt % and 7.5 wt % BRH added samples have 7.9 % and 9.7 % Mg_2Si in its matrix. So a glance of XRD patterns shows that we have MgB_2 in our samples in different quantities plus some secondary phases, a few of which are expected to enhance the superconducting current transfer and others may mar it depending on their size and nature of the distribution.

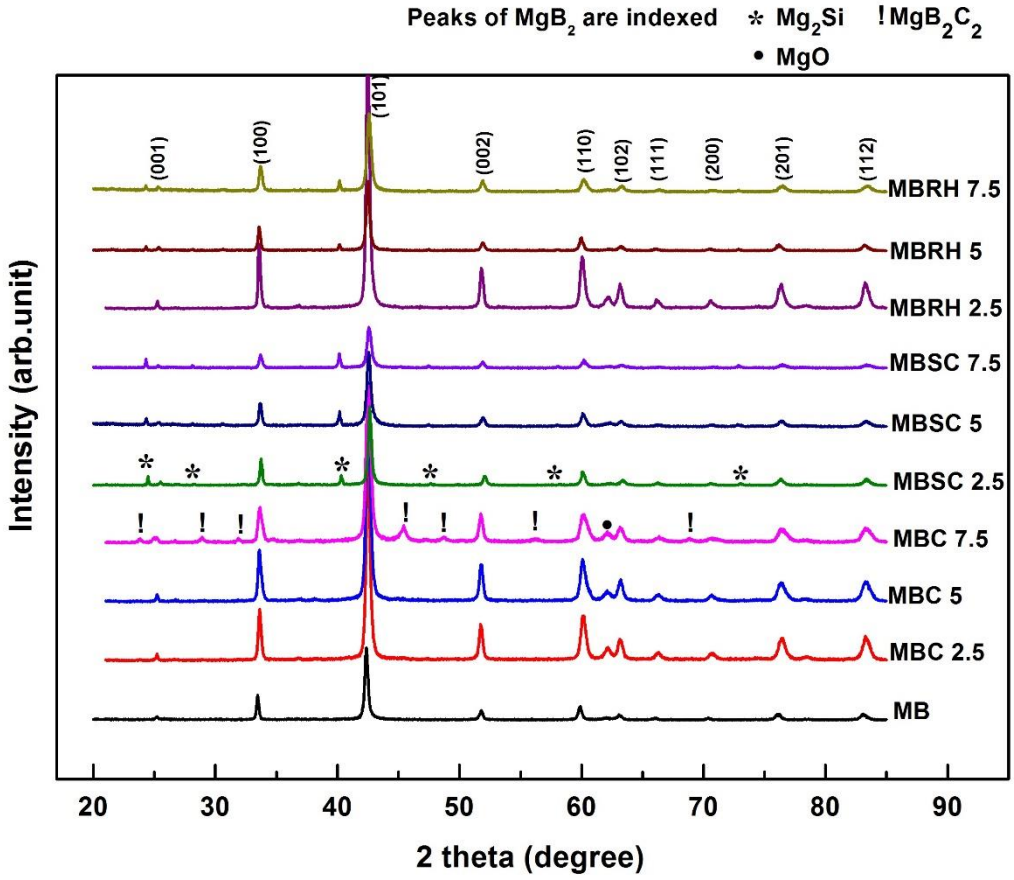

Fig (5.1) XRD patterns of the undoped and doped samples.

Analysing the XRD patterns it is observed that (100) and (110) peaks of doped samples have slightly shifted towards higher angles whereas (002) peaks have maintained the same positions in both doped and undoped samples. The peak shift indicates a decrease in in-plane

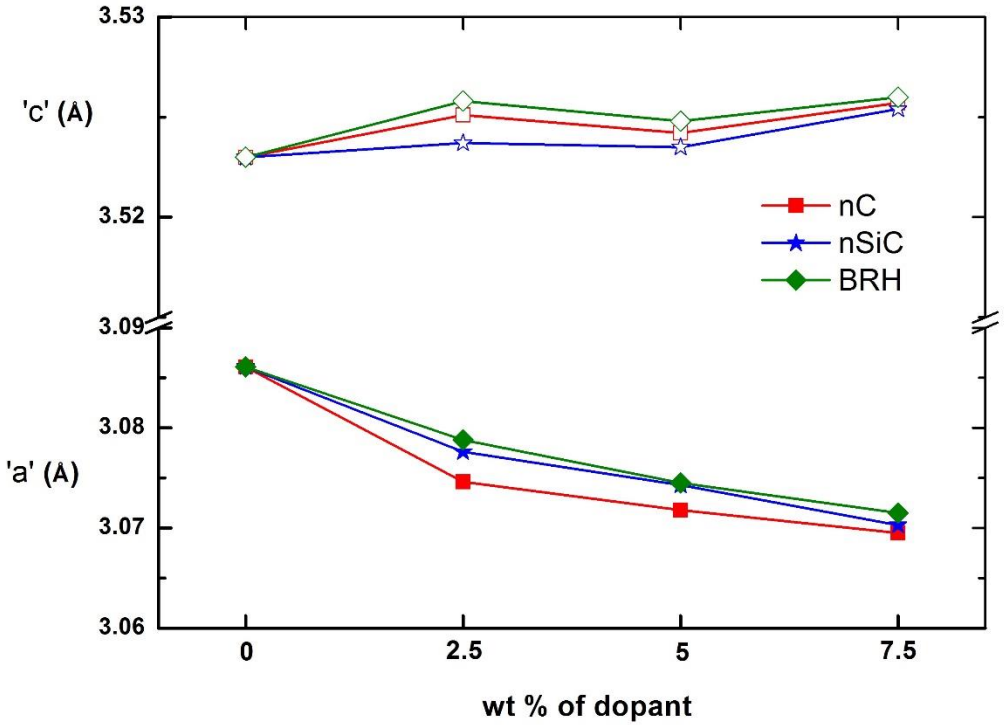

Fig (5.2) Variation of lattice parameters 'a' and 'c' with doping.

lattice constant 'a'. The variation of lattice constants 'a' and 'c' with doping is shown in figure (5.2). The lattice constant 'c' has not changed significantly with doping but 'a' consistently decreased with increasing doping concentration. All the three dopants studied in this work are causing carbon substitution at boron sites. Carbon which has a smaller covalent radius than boron causes contraction of the in-plane lattice. The secondary phases present in the doped samples, mainly Mg_2Si in n SiC and BRH doped samples and MgB_2C_2 in heavily C doped sample cause lattice distortions and play a minor part in decreasing 'a'. Compared to bulk samples, the secondary phases have a much more significant influence on lattice parameters in thin films of MgB_2. In thin films, the grains are oriented preferentially whereas in bulk the random orientation of grains belittles the effect of secondary phases. MgB_2C_2 in heavily C doped thin films play a major role in modifying the structural and superconducting properties [37-39]. From the variations in 'a' lattice parameter, approximate C substitution for B (x in $MgB_{2-x}C_x$) is estimated [30] and tabulated in table (5.1). In order to understand the effect of different dopants on lattice strain and grain size the full width at half maximum (FWHM) of selected peaks of the XRD patterns are calculated and are shown in figure (5.3). The (002) peak is least affected by doping, as evident from the figure the FWHM values of this peak haven't

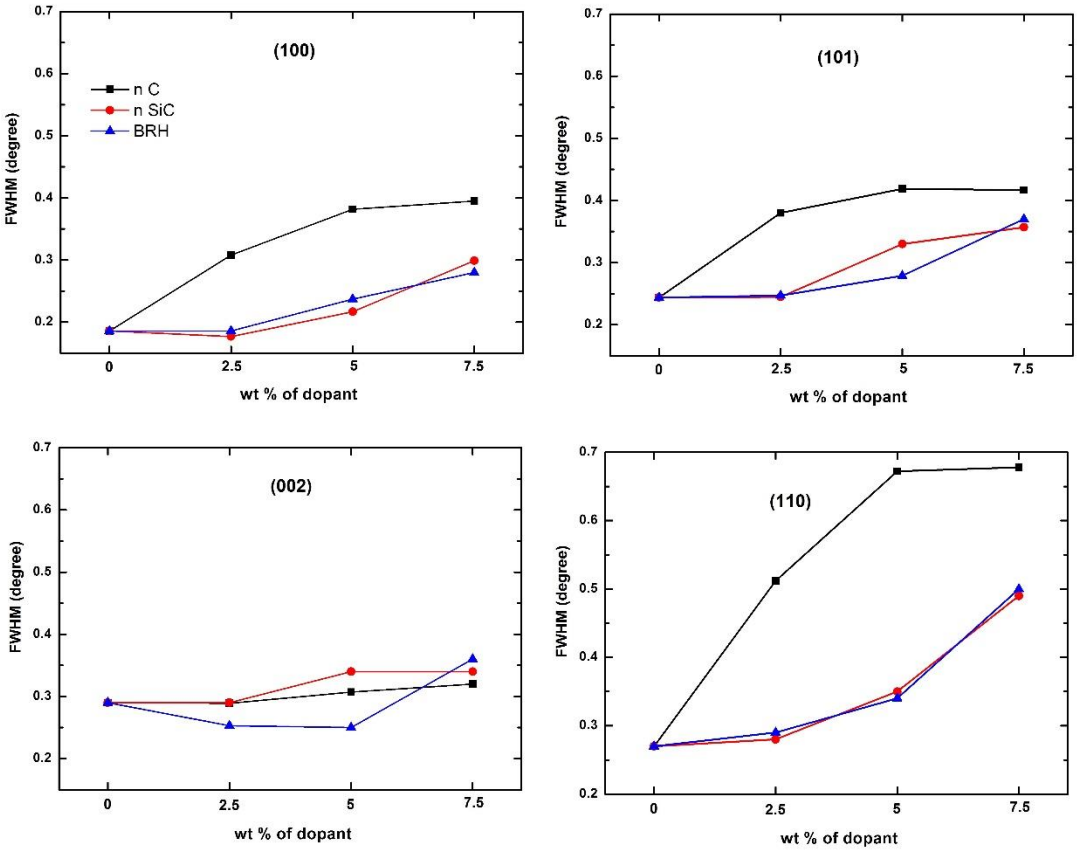

Fig (5.3) FWHM of selected peaks of the undoped and doped samples.

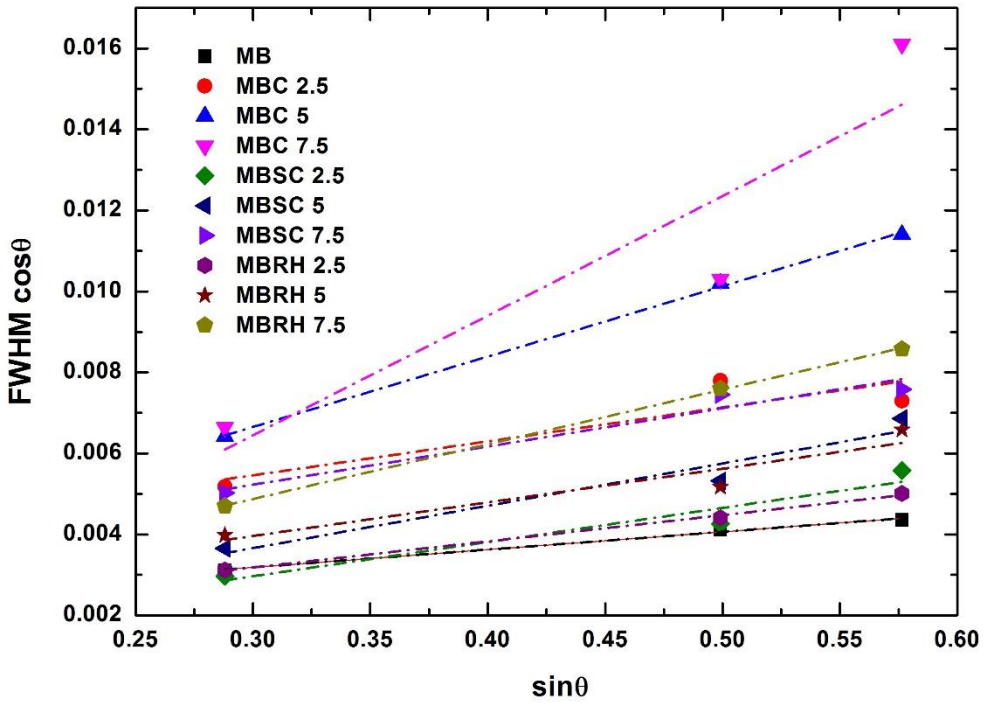

Fig (5.4) Williamson – Hall plots of (hk0) peaks of the undoped and doped samples.

changed much with doping. There is significant variation in the FWHM of other peaks and the (hk0) peaks show maximum peak broadening. Compared to the pure sample, the (101) peaks of doped samples show a slight increase in FWHM with doping concentration. The variation is even greater in (100) and (110) peaks. Comparing the dopants, n C is found to have a greater influence in broadening peaks compared to n SiC and BRH. Carbon substitution at boron sites is mainly responsible for broadening of peaks. The strain caused by the inclusion of secondary phase (Mg_2Si) present in n SiC and BRH added samples also contributes to peak broadening. Of course the MgB_2C_2 phase present in heavily carbon doped sample plays its part too. Higher FWHM indicates smaller grain size and higher lattice strain. The lattice strain is calculated from Williamson- Hall plots of (hk0) peaks, figure (5.4). The slopes of the plots represent the lattice strain. All the doped samples show higher strain values compared to the undoped sample. The strain induced by n C doping is higher than that of n SiC and BRH doping and the strain increased systematically with doping concentration. Variation of strain among the SiC doped samples is less compared to the other two sets of doped samples. Lattice strain values of all samples are tabulated in table (5.1). Carbon substitution for boron is the main reason for increased lattice strain in the doped samples.

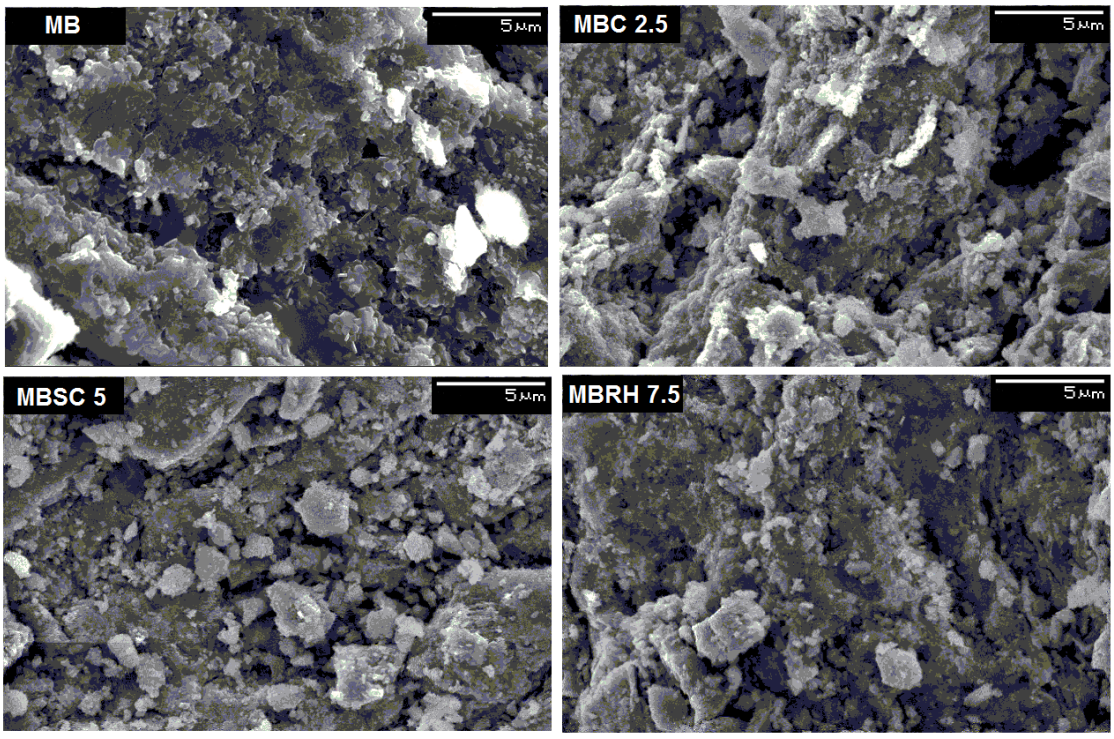

Fig (5.5) SEM images of the fractured surfaces of selected samples.

Typical SEM images of the undoped and doped samples are shown in figure (5.5). MgB_2 grains comprising agglomerates of hexagonal crystallites are visible in the undoped sample. At several places, grain boundaries are not clearly distinguishable and the grains appear to have fused together. Among the three sets of doped samples, the ones which exhibited the best J_C values at higher magnetic fields in each set (discussed in the following section) are shown here. The MgB_2 grains are not easily distinguishable in the doped samples. On closer examination much smaller grains than the undoped sample could be spotted. We have seen a broadening trend in FWHM analysis of the doped samples and this agrees with this microstructure. In MgB_2, the grain boundaries are good flux pinners, smaller grains provide more of them and this will help to enhance the in-field performance of doped samples.

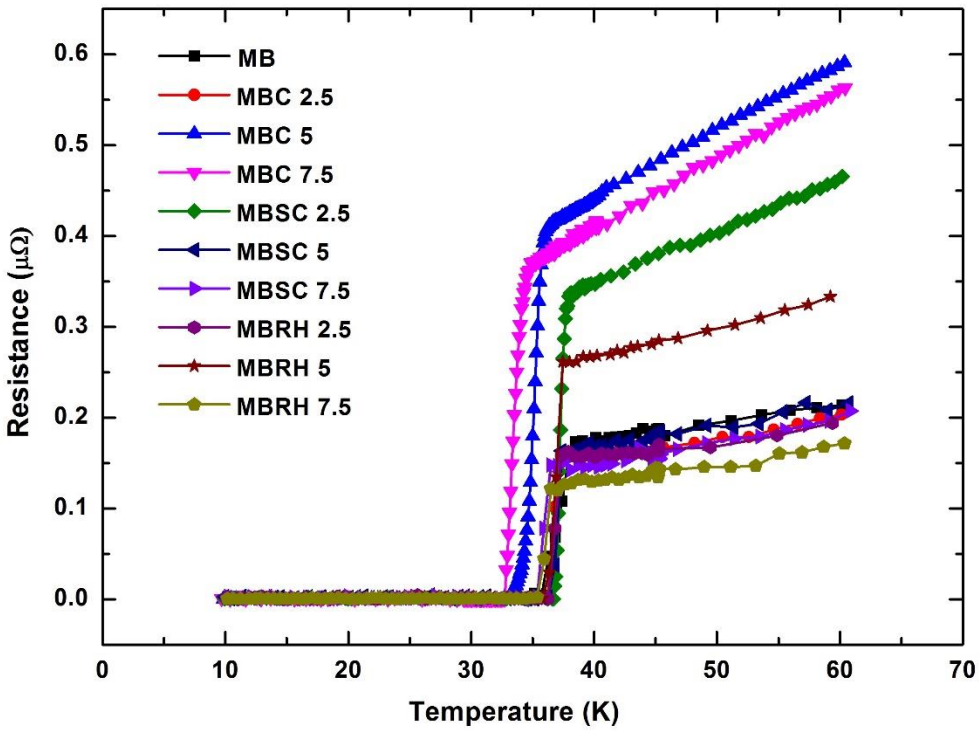

Fig (5.6) R-T plots of undoped and doped monofilamentary wires in the temperature range from 10 K to 60 K.

Figure (5.6) shows the R-T plots of undoped and doped monofilamentary wires. All samples show sharp superconducting transition. The undoped sample, MB, has the highest critical temperature of 38.5 K. All the three dopants have lowered the T_C compared to the pure sample and the T_C values decreased with increasing dopant concentration. Nano C reduces the

T_C more than that of n SiC and BRH. The T_C decreased from 37.3 K to 34.6 K for 2.5 to 7.5 wt % n C doping. The reduction in hole concentration due to C substitution for B is the main reason for T_C reduction in C containing samples [40]. Heavily carbon doped sample MBC 7.5 has an impurity phase (MgB_2C_2) in the matrix and this sample with high C substitution and low phase purity has the lowest T_C (34.6 K) among all the samples studied. Nano SiC and BRH have similar T_Cs for similar doping concentrations. The addition of n SiC and BRH in the range from 2.5 to 7.5 wt % lowers the T_C from 37.9 K to 36.4 K and from 37.9 K to 36.5 K respectively. Carbon substitution and the presence of a non-superconducting phase Mg_2Si are the reasons for T_C reduction in n SiC and BRH doped samples. Examining the T_C values it is clear that n SiC and BRH have only a lighter effect on T_C compared to n C. Transition temperatures of all samples are tabulated in table (5.2).

Table 5.2 Transition temperature and critical current density of undoped and doped samples

Sample name	T_C (K)	J_C at 4.2 K ($\times 10^4$ A/cm^2)		J_C at 20 K ($\times 10^4$ A/cm^2)	
		0 T	8 T	0 T	4 T
MB	38.5	11.68	0.37	4.79	1.61
MBC 2.5	37.3	10.27	1.45	4.36	1.63
MBC 5	36.0	9.22	0.63	3.42	1.26
MBC 7.5	34.6	8.78	0.53	3.19	1.17
MBSC 2.5	37.9	9.89	1.59	3.92	1.41
MBSC 5	37.4	9.26	2.41	3.47	1.54
MBSC 7.5	36.4	8.86	1.36	3.25	1.30
MBRH 2.5	37.9	9.69	1.01	3.75	1.28
MBRH 5	37.4	8.80	1.38	3.26	1.29
MBRH 7.5	36.5	8.77	2.09	3.17	1.42

The non-superconducting phases in the matrix can reduce the grain connectivity and obstruct the transport current flow. Assuming that self-field J_C is independent of doping, the current carrying fraction, (1/F) of the cross sectional area of the sample could be roughly estimated from the reduction in self-field critical current density of doped samples. $1/F = J_C/J_{C0}$,

where J_{C0} is the self-field J_C of the pure sample having perfectly connected grains [37]. Figure (5.7) shows the variation of 1/F with doping concentration for various samples. Self-field J_C values at 4.2 K in table (5.2) are used for the calculation. For the highest dopant concentration connectivity reduces by approximately 25 % for all samples compared to the undoped sample.

The variation of transport critical current density of the samples with applied magnetic field from 0 - 8 T at 4.2 K is shown in figure (5.8). At lower fields, pure sample MB shows the best J_C values. At 0 T MB has the highest J_C of 11.68 $\times 10^4$ A/cm^2 at 4.2 K [At lower fields the critical current values were very high, which results in heating up the samples instantly for a short period during the I_C measurement. The Cu wires connecting sample to the current source were heated up slightly and this, in turn, increased the sample temperature. This sample heating has slightly underestimated J_C at lower fields]. Among the doped samples, the ones with lighter doping concentration show better results at lower fields. Trend remains the same at higher temperatures also, at 20 K and 0 T pure sample MB has shown the highest J_C of 4.79 $\times 10^4$ A/cm^2. Samples with better phase purity and grain connectivity have the maximum current carrying ability at lower fields. As the field increases, J_C of pure sample drops rapidly. Above 5 T its J_C values are much lower than the doped samples. At higher fields, SiC and BRH doped samples give the best J_C values. The sample MBSC 5 shows the best J_C of 2.41 $\times 10^4$ A/cm^2 at 4.2 K and 8 T which is closely followed by MBRH 7.5 with a J_C of 2.09 $\times 10^4$ A/cm^2 at the same conditions. In n C doped samples the best result is given by MBC 2.5 (1.45 $\times 10^4$ A/cm^2 at 4.2 K and 8 T). Higher pinning force in the doped samples which arrests the movement of flux vortices is the reason for the better performance of doped samples at higher fields. All the three types of dopants we tried in this work cause C substitution at B sites. In addition to this, SiC and BRH form Mg_2Si which will be distributed within the grains [34, 35, 41]. The defects caused by C substitution and the intra-grain Mg_2Si particles act as good flux pinners. Also, we have seen from SEM images that the doped samples consist of smaller grains and thereby providing more grain boundaries which are very good flux pinners. At 8 T the samples which have shown the best $J_C(H)$ performance are MBSC 5, MBRH 7.5 and MBSC 2.5, then only comes the first n C sample MBC 2.5 which is closely followed by the samples MBRH 5 and MBSC 7.5. This shows the significance of the dual effect of carbon substitution and inclusion of reacted secondary phases in the MgB_2 matrix in enhancing J_C at higher fields. But the heavily C doped sample MBC 7.5 which contained a reacted phase MgB_2C_2 is the worst among all the doped samples. It should be noted that not all inclusions have a positive effect on improving J_C at higher fields. Intragrain inclusions of the size comparable to the coherence length of

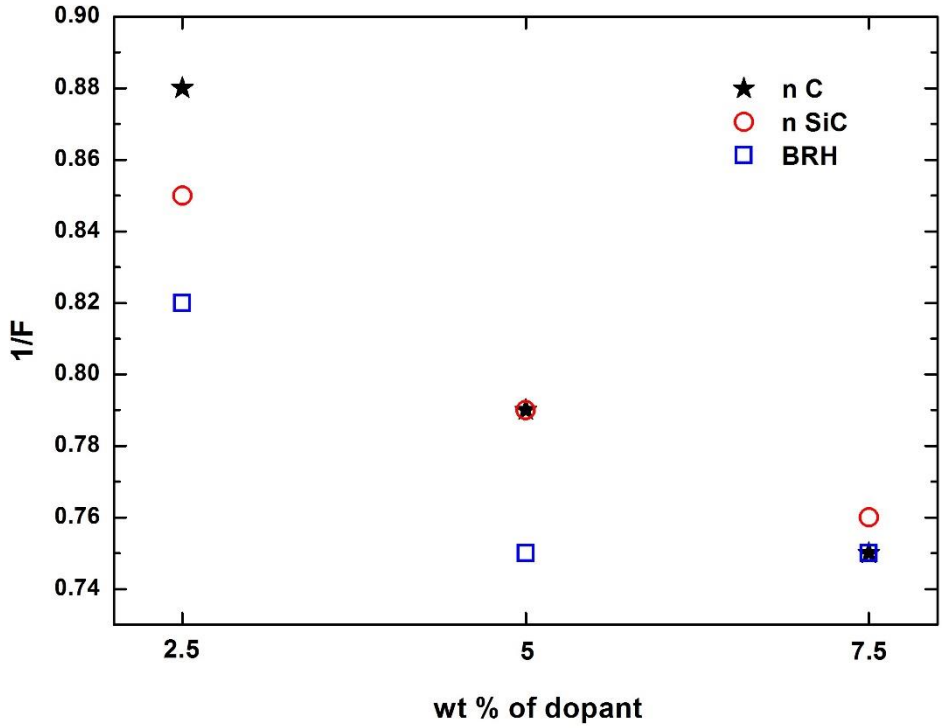

Fig (5.7) Variation in the current carrying fraction with doping concentration for n C, n SiC and BRH doped samples.

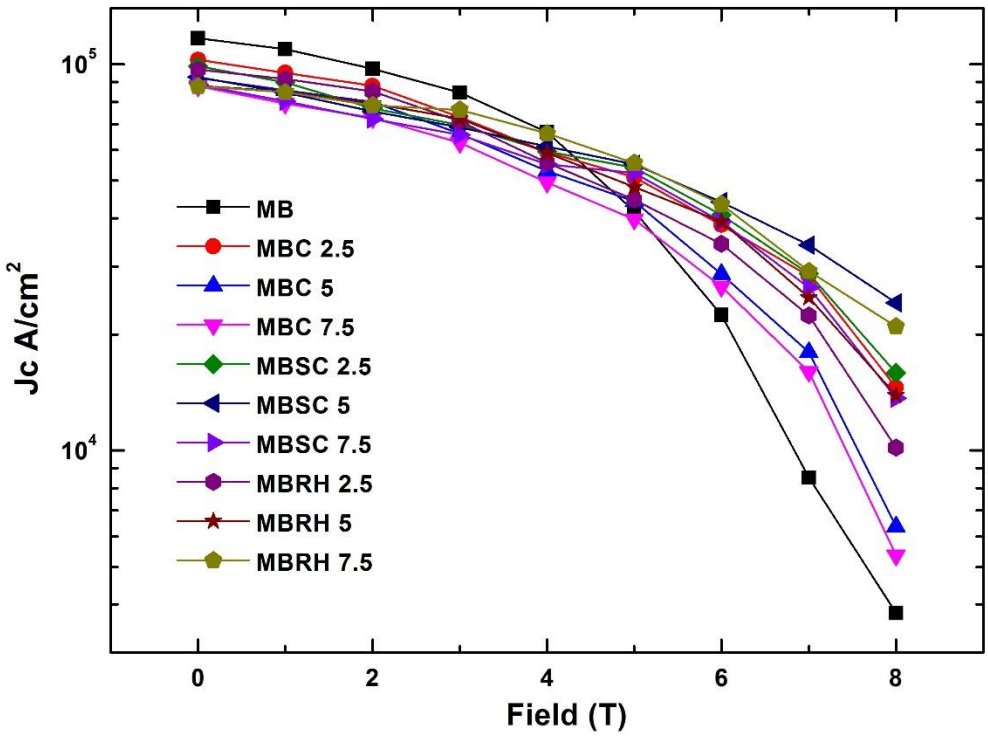

Fig (5.8) Variation of transport critical current density of the wire samples with applied magnetic field from 0 to 8 T at 4.2 K.

cooper pairs will have a more positive impact on improving J_C. Also, the competitiveness of BRH deserves special mention. SiC is considered among the best dopants to enhance the critical current density of MgB_2 at higher fields and is set as a benchmark [18-21, 41]. In our study BRH addition has improved J_C to as higher values as n SiC addition. Rice Husk, being a very cheap and easily available raw material, could be used as an alternative for SiC. The critical current density of all samples at selected temperatures and fields are listed in table (5.2).

5.1.3 Conclusion

A detailed study of the effects of three dopants (n C, n SiC and BRH) on the structural and superconducting properties of PIT processed MgB_2 monofilamentary wires is done and presented in this chapter. XRD analysis shows the formation of Mg_2Si in both n SiC and BRH doped samples, its inclusion in the superconductor matrix is known to enhance J_C at high fields. All the three dopants cause C substitution at B sites and as a result 'a' lattice parameter decreases in doped samples. FWHM of the (hk0) peaks of doped samples shows systematic broadening with increasing doping concentration. Smaller grains in SEM images of doped samples justify the peak broadening. Doping reduces T_C of all samples with n C dropping T_C to much lower values compared to n SiC and BRH. In heavily doped SiC and BRH samples the T_C drops by around 2 K and in the case of n C it drops by almost 4 K. Best critical current density results at higher fields are achieved by n SiC and BRH doping, which cause carbon substitution as well as inclusion of Mg_2Si phase in the superconductor matrix. The combined flux pinning force provided by the lattice defects from C substitution and Mg_2Si inclusions is better than that provided by C substitution alone in n C doped samples. The best doped samples have J_Cs improved by an order compared to the undoped sample at 4.2 K and 8 T. The competitiveness of BRH shows that it is a cheaper alternative for n SiC.

5.2 Summary

The chapter details the third phase of our research plan towards the development of MgB_2 superconducting wires with in-field transport critical current densities on a par with the best samples reported internationally. We have successfully employed chemical doping to improve the $J_C(H)$ of MgB_2 wires which could be put into operation using a cryogen free cooling mechanism. A comparative study on the structural and superconducting properties of MgB_2 PIT wires doped with various weight percentage of nano carbon, nano SiC and Burned Rice Husk has been carried out. X-Ray diffraction patterns of n SiC and BRH doped samples

showed peaks of Mg_2Si which is a useful intragrain inclusion for flux pinning. The Lattice parameter 'a' decreased with increasing doping concentration for all the doped samples, the maximum being for n C, indicating C substitution for B. The FWHM of (hk0) peaks of all samples increased with doping. Doping caused a reduction in grain size and SEM images showed tightly packed smaller grains containing hexagonal crystallites in all the three types of doped samples. All the dopants reduced the transition temperature of the undoped sample and the effect was severe for n C doping. Unlike the pure sample, the transport critical current density of the doped samples didn't fall rapidly at high fields; but retained large fractions depending on the dopants. The best results were obtained for n SiC and BRH doped samples with BRH closely matching the performance of n SiC. Rice Husk, which is cheap and easily available, has the potential to be developed as an alternative dopant for SiC. Improvement in critical current density for these samples was about an order higher than the undoped sample at 4.2 K and 8 T.

Reference

1. Dimitrov, I.K., Zhang, X., Solovyov, V.F., Chubar, O., Li, Q.: Rapid and Semi-analytical Design and Simulation of a Toroidal Magnet Made With YBCO and MgB_2 Superconductors. IEEE Trans. Appl. Supercond. **25**(5) (2015). doi:10.1109/tasc.2015.2448455

2. Ling, J.Y., Voccio, J.P., Hahn, S., Kim, Y., Song, J.B., Bascunan, J., Iwasa, Y.: Construction and Persistent-Mode Operation of MgB_2 Coils in the Range 10-15 K for a 0.5-T/240-mm Cold Bore MRI Magnet. IEEE Trans. Appl. Supercond. **25**(3) (2015). doi:10.1109/tasc.2014.2370105

3. Mine, S., Xu, M.F., Bai, Y., Buresh, S., Stautner, W., Immer, C., Laskaris, E.T., Amm, K.: Development of a 3 T-250 mm Bore MgB_2 Magnet System. IEEE Trans. Appl. Supercond. **25**(3) (2015). doi:10.1109/tasc.2014.2364396

4. Yao, W.J., Bascunan, J., Kim, W.S., Hahn, S., Lee, H., Iwasa, Y.: A solid nitrogen cooled MgB_2 "Demonstration" coil for MRI applications. IEEE Trans. Appl. Supercond. **18**(2), 912-915 (2008). doi:10.1109/tasc.2008.920836

5. Ma, Z.Q., Liu, Y.C.: Low-temperature synthesis of MgB_2 superconductors. Int. Mater. Rev. **56**(5-6), 267-286 (2011). doi:10.1179/1743280411y.0000000002

6. Xi, X.X.: Two-band superconductor magnesium diboride. Rep. Prog. Phys. **71**(11) (2008). doi:10.1088/0034-4885/71/11/116501

7. Collings, E.W., Sumption, M.D., Bhatia, M., Susner, M.A., Bohnenstiehl, S.D.: Prospects for improving the intrinsic and extrinsic properties of magnesium diboride

superconducting strands. Supercond. Sci. Technol. **21**(10) (2008). doi:10.1088/0953-2048/21/10/103001

8. Eisterer, M.: Magnetic properties and critical currents of MgB_2. Supercond. Sci. Technol. **20**(12), R47-R73 (2007). doi:10.1088/0953-2048/20/12/r01

9. Vinod, K., Kumar, R.G.A., Syamaprasad, U.: Prospects for MgB_2 superconductors for magnet application. Supercond. Sci. Technol. **20**(1), R1-R13 (2007). doi:10.1088/0953-2048/20/1/r01

10. Kazakov, S.M., Puzniak, R., Rogacki, K., Mironov, A.V., Zhigadlo, N.D., Jun, J., Soltmann, C., Batlogg, B., Karpinski, J.: Carbon substitution in MgB_2 single crystals: Structural and superconducting properties. Phys. Rev. B **71**(2) (2005). doi:10.1103/PhysRevB.71.024533

11. Wong, D.C.K., Yeoh, W.K., De Silva, K.S.B., Kondyurin, A., Bao, P., Li, W.X., Xu, X., Peleckis, G., Dou, S.X., Ringer, S.P., Zheng, R.K.: Microscopic unravelling of nano-carbon doping in MgB_2 superconductors fabricated by diffusion method. J. Alloy. Compd. **644**, 900-905 (2015). doi:10.1016/j.jallcom.2015.05.082

12. Barua, S., Al Hossain, M.S., Ma, Z.Q., Patel, D., Mustapic, M., Somer, M., Acar, S., Kokal, I., Morawski, A., Cetner, T., Gajda, D., Dou, S.X.: Superior critical current density obtained in MgB_2 bulks through low-cost carbon-encapsulated boron powder. Scr. Mater. **104**, 37-40 (2015). doi:10.1016/j.scriptamat.2015.04.003

13. Liu, Y.C., Lan, F., Ma, Z.Q., Chen, N., Li, H.J., Barua, S., Patel, D., Shahriar, M., Hossain, A., Acar, S., Kim, J.H., Dou, S.X.: Significantly enhanced critical current density in nano-MgB_2 grains rapidly formed at low temperature with homogeneous carbon doping. Supercond. Sci. Technol. **28**(5) (2015). doi:10.1088/0953-2048/28/5/055005

14. Varghese, N., Vinod, K., Rahul, S., Anees, P., Devadas, K.M., Thomas, S., Shipra, Sundaresan, A., Roy, S.B., Syamaprasad, U.: Effect of Carbon Substitution on the Superconducting Properties of Nanocarbon-, Nanodiamond- and Nano-SiC-Doped MgB_2. J. Am. Ceram. Soc. **94**(4), 1133-1137 (2011). doi:10.1111/j.1551-2916.2010.04163.x

15. Kim, J.H., Oh, S., Heo, Y.U., Hata, S., Kumakura, H., Matsumoto, A., Mitsuhara, M., Choi, S., Shimada, Y., Maeda, M., MacManus-Driscoll, J.L., Dou, S.X.: Microscopic role of carbon on MgB_2 wire for critical current density comparable to NbTi. NPG Asia Mater. **4** (2012). doi:10.1038/am.2012.3

16. Rahul, S., Varghese, N., Vinod, K., Devadas, K.M., Thomas, S., Anees, P., Chattopadhyay, M.K., Roy, S.B., Syamaprasad, U.: Combined addition of nano diamond and nano SiO_2, an effective method to improve the in-field critical current density of MgB_2 superconductor. Mater. Res. Bull. **46**(11), 2036-2040 (2011). doi:10.1016/j.materresbull.2011.07.005

17. Hossain, M.S.A., Senatore, C., Flukiger, R., Rindfleisch, M.A., Tomsic, M.J., Kim, J.H., Dou, S.X.: The enhanced Jc and B-irr of in situ MgB_2 wires and tapes alloyed with

$C_4H_6O_5$ (malic acid) after cold high pressure densification. Supercond. Sci. Technol. **22**(9) (2009). doi:10.1088/0953-2048/22/9/095004

18. Dou, S.X., Shcherbakova, O., Yoeh, W.K., Kim, J.H., Soltanian, S., Wang, X.L., Senatore, C., Flukiger, R., Dhalle, M., Husnjak, O., Babic, E.: Mechanism of enhancement in electromagnetic properties of MgB_2 by nano SiC doping. Phys. Rev. Lett. **98**(9) (2007). doi:10.1103/PhysRevLett.98.097002

19. Varghese, N., Vinod, K., Syamaprasad, U., Roy, S.B.: Doping effect of nano-SiC on structural and superconducting properties of MgB_2 bulks prepared by PIST method in air. J. Alloy. Compd. **484**(1-2), 734-738 (2009). doi:10.1016/j.jallcom.2009.05.028

20. Susner, M.A., Sumption, M.D., Bhatia, M., Peng, X., Tomsic, M.J., Rindfleisch, M.A., Collings, E.W.: Influence of Mg/B ratio and SiC doping on microstructure and high field transport Jc in MgB_2 strands. Physica C **456**(1-2), 180-187 (2007). doi:10.1016/j.physc.2007.02.005

21. Ma, Z.Q., Liu, Y.C., Zhao, Q., Dong, Z.Z., Yu, L.M.: Mechanism analysis for the enhanced electromagnetic properties in nano-SiC-doped MgB_2 based on the discussion of the sintering process. Supercond. Sci. Technol. **22**(8) (2009). doi:10.1088/0953-2048/22/8/085015

22. Thomas, S., Rahul, S., Devadas, K.M., Varghese, N., Sundaresan, A., Syamaprasad, U.: Co-addition of nano-carbon and nano-silica: An effective method for improving the in-field properties of magnesium diboride superconductor. Mater. Chem. Phys. **148**(1-2), 190-194 (2014). doi:10.1016/j.matchemphys.2014.07.030

23. Kim, J.H., Zhou, S., Hossain, M.S.A., Pan, A.V., Dou, S.X.: Carbohydrate doping to enhance electromagnetic properties of MgB_2 superconductors. Appl. Phys. Lett. **89**(14) (2006). doi:10.1063/1.2358947

24. Xu, X., Dou, S.X., Wang, X.L., Kim, J.H., Stride, J.A., Choucair, M., Yeoh, W.K., Zheng, R.K., Ringer, S.P.: Graphene doping to enhance the flux pinning and supercurrent carrying ability of a magnesium diboride superconductor. Supercond. Sci. Technol. **23**(8) (2010). doi:10.1088/0953-2048/23/8/085003

25. Shcherbakova, O.V., Pan, A.V., Wang, J.L., Shcherbakov, A.V., Dou, S.X., Wexler, D., Babic, E., Jercinovic, M., Husnjak, O.: Sugar as an optimal carbon source for the enhanced performance of MgB_2 superconductors at high magnetic fields. Supercond. Sci. Technol. **21**(1) (2008). doi:10.1088/0953-2048/21/01/015005

26. Vajpayee, A., Awana, V.P.S., Bhalla, G.L., Bhobe, P.A., Nigam, A.K., Kishan, H.: Superconducting properties of adipic-acid-doped bulk MgB_2 superconductor. Supercond. Sci. Technol. **22**(1) (2009). doi:10.1088/0953-2048/22/1/015016

27. Bohnenstiehl, S.D., Susner, M.A., Yang, Y., Collings, E.W., Sumption, M.D., Rindfleisch, M.A., Boone, R.: Carbon doping of MgB_2 by toluene and malic-acid-in-toluene. Physica C **471**(3-4), 108-111 (2011). doi:10.1016/j.physc.2010.12.005

28. Zhang, X.P., Ma, Y.W., Gao, Z.S., Wang, D.L., Wang, L., Liu, W., Wang, C.R.: Strongly enhanced current-carrying performance in MgB_2 tape conductors by C_{60} doping. J. Appl. Phys. **103**(10) (2008). doi:10.1063/1.2936917

29. Senkowicz, B.J., Giencke, J.E., Patnaik, S., Eom, C.B., Hellstrom, E.E., Larbalestier, D.C.: Improved upper critical field in bulk-form magnesium diboride by mechanical alloying with carbon. Appl. Phys. Lett. **86**(20) (2005). doi:10.1063/1.1920428

30. Wilke, R.H.T., Bud'ko, S.L., Canfield, P.C., Finnemore, D.K., Suplinskas, R.J., Hannahs, S.T.: Systematic effects of carbon doping on the superconducting properties of $Mg(B_{1-x}C_x)_2$. Phys. Rev. Lett. **92**(21) (2004). doi:10.1103/PhysRevLett.92.217003

31. Angst, M., Bud'ko, S.L., Wilke, R.H.T., Canfield, P.C.: Difference between Al and C doping in anisotropic upper critical field development in MgB_2. Phys. Rev. B **71**(14) (2005). doi:10.1103/PhysRevB.71.144512

32. Rahul, S., Devadas, K.M, Thomas, S., Varghese, N., Paulose, A.P., Varma, M.R., Syamaprasad, U.: A comparative study on the effects of n C, n SiC and BRH on the structural and superconducting properties of MgB_2 PIT wires. Materials Chemistry and Physics **200**, 395-401 (2017). doi: 10.1016/j.matchemphys.2017.08.009

33. Yeoh, W.K., Dou, S.: Enhancement of H_{C2} and Jc by carbon-based chemical doping. Physica C **456**(1-2), 170-179 (2007). doi:10.1016/j.physc.2007.01.024

34. Varghese, N., Vinod, K., Shipra, Sundaresan, A., Syamaprasad, U.: Burned Rice Husk: An Effective Additive for Enhancing the Electromagnetic Properties of MgB_2 Superconductor. J. Am. Ceram. Soc. **93**(3), 732-736 (2010). doi:10.1111/j.1551-2916.2009.03438.x

35. Vinod, K., Varghese, N., Sundaresan, A., Syamaprasad, U.: Highly enhanced in-field critical current density of MgB_2 superconductor by combined addition of burned rice husk and nano Ho_2O_3. Solid State Sci. **12**(4), 610-616 (2010). doi:10.1016/j.solidstatesciences.2010.01.012

36. Devadas, K.M., Rahul, S., Thomas, S., Varghese, N., Vinod, K., Syamaprasad, U., Pradhan, S., Chattopadhyay, M.K., Roy, S.B.: Transport properties of sealed MgB_2/Fe/Ni multifilamentary wires heat treated in air. J. Alloy. Compd. **509**(31), 8038-8041 (2011). doi:10.1016/j.jallcom.2011.04.147

37. Dai, W.Q., Ferrando, V., Pogrebnyakov, A.V., Wilke, R.H.T., Chen, K., Weng, X.J., Redwing, J., Bark, C.W., Eom, C.B., Zhu, Y., Voyles, P.M., Rickel, D., Betts, J.B., Mielke, C.H., Gurevich, A., Larbalestier, D.C., Li, Q., Xi, X.X.: High-field properties of carbon-doped MgB_2 thin films by hybrid physical-chemical vapor deposition using different carbon sources. Supercond. Sci. Technol. **24**(12) (2011). doi:10.1088/0953-2048/24/12/125014

38. Zhu, Y., Pogrebnyakov, A.V., Wilke, R.H., Chen, K., Xi, X.X., Redwing, J.M., Zhuang, C.G., Feng, Q.R., Gan, Z.Z., Singh, R.K., Shen, Y., Newman, N., Rowell, J.M., Hunte, F., Jaroszynski, J., Larbalestier, D.C., Baily, S.A., Balakirev, F.F., Voyles, P.M.:

Nanoscale disorder in pure and doped MgB_2 thin films. Supercond. Sci. Technol. **23**(9) (2010). doi:10.1088/0953-2048/23/9/095008

39. Saengdeejing, A., Saal, J.E., Wang, Y., Liu, Z.K.: Effects of carbon in MgB_2 thin films: Intrinsic or extrinsic. Appl. Phys. Lett. **90**(15) (2007). doi:10.1063/1.2717569

40. Kortus, J., Dolgov, O.V., Kremer, R.K., Golubov, A.A.: Band filling and interband scattering effects in MgB_2: Carbon versus aluminum doping. Phys. Rev. Lett. **94**(2) (2005). doi:10.1103/PhysRevLett.94.027002

41. Vinod, K., Varghese, N., Roy, S.B., Syamaprasad, U.: Significant enhancement of the in-field critical current density of the MgB_2 superconductor through codoping of nano-TiC with nano-SiC. Supercond. Sci. Technol. **22**(5) (2009). doi:10.1088/0953-2048/22/5/055009

Chapter 6

Summary, conclusion and future directions

6.1 Summary

The prospects of MgB_2 based cryogen free magnets replacing the classical LTS magnets are bright. In commercial applications, price–performance ratio of a superconductor decides its suitability. Low density and low cost of raw materials are favourable factors for MgB_2. If the in-field engineering current density could be improved beyond that of LTS, MgB_2 could become the wire of choice for future high field magnets. In multifilamentary MgB_2 wires, only about 10-15 % of the cross sectional area is occupied by the superconductor and the remaining is consumed by the barrier, stabilizer and outer sheath. Thus it is necessary to improve the transport critical current density under high magnetic fields to make MgB_2 competitive for practical applications. In this work, the main objective was to develop MgB_2 superconducting wires suitable for cryogen free operation and having enhanced transport critical current density under external magnetic field [$J_C(H)$]. To achieve this objective a three stage research plan was drawn. In the first stage, chemical doping was successfully employed to improve the $J_C(H)$ of MgB_2 in bulk form. Combined addition of nano diamond (n D) and nano SiO_2 (n SiO_2) was found to be very effective in enhancing the $J_C(H)$ of MgB_2. Conventional methods like mortar-pestle, ball milling etc. used to mix nano additives in chemical doping do not guarantee their homogeneous distribution in the superconductor matrix, thus compromising their effect on enhancing superconducting properties. To address this issue we have developed a novel processing route. By using Mg-Si cast alloy we were able to tackle the agglomeration of Mg_2Si nano particles in the superconductor matrix. The homogeneous distribution of the secondary phase was found to be more effective in improving flux pinning and thus $J_C(H)$ in MgB_2.

In the second stage, MgB_2 mono and multifilamentary wires were developed. Effects of heat treatment temperature and duration on structural and superconducting properties of undoped mono-wires were studied. Heat treatment of the wires at a temperature in the range 650 to 700 ^{O}C for 1 to 2 hours was found to give the best J_C values under self-field. A comparison of commonly used sheath materials regarding their reactivity with the precursor powder, influence on superconducting properties, strain tolerance, mechanical workability and cost were done. Iron was found to be one of the best sheath materials for MgB_2 PIT wires. The

enhancement in magnetic $J_C(H)$ achieved through chemical doping in bulk was successfully replicated in transport $J_C(H)$ of wire samples in the third stage. We compared the effectiveness of n C, n SiC and Burned Rice Husk (BRH) in introducing flux pinners into the MgB_2 matrix and enhancing transport critical current density. A critical analysis was also made on the usefulness of BRH, an indigenously developed dopant by our group as a cheaper alternative for n SiC.

6.2 Conclusions

- The dual mechanism of carbon substitution for boron and incorporation of secondary phases in the MgB_2 matrix was successfully employed to improve the magnetic as well as transport J_C of MgB_2 bulk and wire samples at higher magnetic fields. Nano diamond and nano SiO_2 effectively caused C substitution and introduced nanometre sized Mg_2Si particles in the MgB_2 matrix. The lattice defects caused by C substitution and Mg_2Si particles acted as good flux pinners. The flux pinning capabilities of the codoped samples were found to be better than that of solo doped samples and they improved the J_C of the undoped sample by an order at 5 K and 8 T.

- Agglomeration of nano dopants is a major issue which compromises the effectiveness of chemical doping in MgB_2. We have successfully tackled the agglomeration of Mg_2Si particles in MgB_2 by using 'Mg-Si' cast alloy as one of our starting materials instead of pure Mg. Comparison of results showed that the uniformly distributed flux pinners were more effective than the agglomerated flux pinners resulting from normal route of preparation.

- Heat treatment conditions play important roles in the development of suitable microstructure in the superconducting core for obtaining the best performance in the PIT processed MgB_2 wires. The volume shrinkage associated with the formation of MgB_2 caused formation of voids in the superconducting core. The size of the voids was found to increase with increase in the heat treatment temperature and duration of the wire samples. These voids limited the transport current flow through the samples. Heat treatment temperatures in the range 650-700 ^{O}C and duration in the range 1–2 hours gave the best J_C values for undoped wires under self-field.

- Sheath materials play an important role in the development of MgB_2 based wires and coils. A comparison of commonly used sheath materials with MgB_2 was done. Attributes like no reactivity with Mg and B at elevated temperatures, good mechanical workability, higher transport J_C both at self and in-fields, retention of adequate fraction of J_C under bend mode, possibility of heat treatment directly in air, easy availability and low cost make Fe one of the best sheath materials for PIT processing of MgB_2 based mono and multifilamentary wires.

- Transport critical current densities more than 10^4 A/cm^2 at 4.2 K and 8 T or at 20 K and 4 T were achieved in Fe sheathed MgB_2 wires, through chemical doping of n C, n SiC and BRH, which are on a par with the best results reported internationally. SiC and BRH were more effective in enhancing the J_C, besides being light on T_C. It was found that BRH, an indigenously developed dopant by our group has the potential to be a cheaper alternative for SiC.

6.3 Future directions

From an application point of view, it is necessary to improve the $J_C(H)$ of MgB_2 still further. We are yet to tap the full potential of chemical doping in MgB_2. Using cast Mg-Si alloy, we were able to tackle the agglomeration of Mg_2Si dopant in MgB_2 and this was found to have an instant effect on $J_C(H)$. However, in the same work we added n C to the mixture by solid state mixing only. No matter how much care we take, physical methods of mixing either manual or with machines will not give the same homogeneity of the dopants as in the case of melting and casting. We could not assess the level of homogeneity of C in our samples. The effectiveness of C substitution for B is the main factor determining the success of chemical doping in MgB_2. So it is necessary to ensure the uniform distribution of C in the MgB_2 matrix to maximise its effect. To develop a method that can uniformly distribute C in MgB_2 is an important next step that we would like to undertake.

Due to the porous nature of MgB_2, we could usually attain only 50 % of the theoretical density in samples prepared through PIT and PIST methods. Results discussed in chapter 4 clearly suggests the importance of densifying the core of MgB_2 conductors. Studying the influence of multistage heat treatment, multistage rolling and addition of pre-reacted MgB_2 powder, on the core density of PIT processed wires is the next step in our development of wires. MgB_2 has the potential to have a major impact on MRI magnet industry, provided persistent superconducting joints are developed. A superconducting joint for MgB_2 conductors using

NbTi was tried by some groups but with limited success. Also when NbTi was used as the joint, the operating temperature was limited below 9 K. To operate an MgB_2 based cryogen free magnet at 20-30 K range, the joining process should also be based on MgB_2 or any high T_C superconductor. Development of MgB_2 superconducting joint is a very significant step to be pursued in future.

Details of publications

List of papers published in SCI journals

1. **Rahul, S**., Devadas, K. M, Thomas, S., Varghese, N., Paulose, A.P., Varma, M.R., Syamaprasad, U.: A comparative study on the effects of n C, n SiC and BRH on the structural and superconducting properties of MgB_2 PIT wires. Materials Chemistry and Physics **200**, 395-401 (2017). doi: 10.1016/j.matchemphys.2017.08.009

2. **Rahul, S**., Thomas, S., Devadas, K.M., Varghese, N., Paulose, A.P., Varma, M.R., Syamaprasad, U.: Tackling the agglomeration of Mg_2Si dopant in MgB_2 superconductor using cast Mg-Si alloy. Materials Research Bulletin **93**, 296-302 (2017). doi:10.1016/j.materresbull.2017.05.022

3. Thomas, S., **Rahul, S**., Devadas, K.M., Varghese, N., Sundaresan, A., Syamaprasad, U.: Co-addition of nano-carbon and nano-silica: An effective method for improving the in-field properties of magnesium diboride superconductor. Mater. Chem. Phys. **148**(1-2), 190-194 (2014). doi:10.1016/j.matchemphys.2014.07.030

4. Devadas, K.M., **Rahul, S**., Thomas, S., Varghese, N., Pradhan, S., Syamaprasad, U.: An Effort Toward Development of MgB_2-Based Current Leads With 2000-A Rating. IEEE Trans. Appl. Supercond. **24**(4) (2014). doi:10.1109/tasc.2014.2311413

5. Thomas, S., Varghese, N., **Rahul, S**., Devadas, K.M., Vinod, K., Syamaprasad, U.: Enhancement of bending strain tolerance and current carrying property of MgB_2 based multifilamentary wires. Cryogenics **52**(12), 767-770 (2012). doi:10.1016/j.cryogenics.2012.07.007

6. **Rahul, S**., Varghese, N., Vinod, K., Devadas, K.M., Thomas, S., Anees, P., Chattopadhyay, M.K., Roy, S.B., Syamaprasad, U.: Combined addition of nano diamond and nano SiO_2, an effective method to improve the in-field critical current density of MgB_2 superconductor. Mater. Res. Bull. **46**(11), 2036-2040 (2011). doi:10.1016/j.materresbull.2011.07.005

7. Devadas, K.M., **Rahul, S**., Thomas, S., Varghese, N., Vinod, K., Syamaprasad, U., Pradhan, S., Chattopadhyay, M.K., Roy, S.B.: Transport properties of sealed MgB_2/Fe/Ni multifilamentary wires heat treated in air. J. Alloy. Compd. **509**(31), 8038-8041 (2011). doi:10.1016/j.jallcom.2011.04.147

8. Varghese, N., Vinod, K., **Rahul, S**., Anees, P., Devadas, K.M., Thomas, S., Shipra, Sundaresan, A., Roy, S.B., Syamaprasad, U.: Effect of Carbon Substitution on the Superconducting Properties of Nanocarbon-, Nanodiamond- and Nano-SiC-Doped MgB_2. J. Am. Ceram. Soc. **94**(4), 1133-1137 (2011). doi:10.1111/j.1551-2916.2010.04163.x

9. Varghese, N., Vinod, K., **Rahul, S**., Devadas, K.M., Thomas, S., Pradhan, S., Syamaprasad, U.: Influence of nano-Cu additive on MgB_2 phase formation, processing

temperature, and transport properties. J. Appl. Phys. **109**(3) (2011). doi:10.1063/1.3544067

10. Vinod, K., Varghese, N., **Rahul, S**., Devadas, K.M., Thomas, S., Gurusamy, P., Kedia, S., Pradhan, S., Syamaprasad, U.: On the current transfer length and current sharing in short length MgB_2 wires. Supercond. Sci. Technol. **23**(10) (2010). doi:10.1088/0953-2048/23/10/105002

11. Vinod, K., Varghese, N., **Rahul, S**., Syamaprasad, U.: Preparation of in situ MgB_2/Fe superconducting tapes with highly densified core by hot pressing of electrically self-heated PIT wires. Mater. Sci. Eng. B-Adv. Funct. Solid-State Mater. **164**(2), 131-134 (2009). doi:10.1016/j.mseb.2009.08.008

Communicated

1. **Rahul S**, Devadas K M, Thomas S, Varghese N, Varma M R and Syamaprasad U:"Superconducting and Bending Strain Properties of MgB_2 PIT Wires with Fe, Ni, SS, Nb and Monel Sheaths."; communicated to "Applied Physics A".

List of papers presented in conferences

1. "Transport properties of MgB_2 based multifilamentary wires heat treated in air". **Rahul Sugathan**, Devadas Kavazhikathu Mohandas, Syju Thomas, Neson Varghese,Vinod Krishnankutty, Subrata Pradhan, Maulindu Kumar Chattopadhyay, Sindhunil Barman Roy, and Syamaprasad Upendran. Presented at the Asian Conference on Applied Superconductivity & Cryogenics 2011 (ACASC 2011), New Delhi, November 16- 18, 2011.

2. "Enhancement of bending strain tolerance and current carrying property of MgB_2 based multifilamentary wires". Syju Thomas, Neson Varghese, **Rahul Sugathan,** Devadas Kavazhikath Mohandas, Vinod Krishnankutty and Syamaprasad Upendran. Presented at the Asian Conference on Applied Superconductivity & Cryogenics 2011 (ACASC 2011), New Delhi, November 16- 18, 2011.

3. "Development of MgB_2 based conduction cooled current leads with 1000 A rating". K M Devadas, Neson Varghese, **S Rahul**, Syju Thomas, S Pradhan, P Guruswamy and U Syamaprasad. Presented at the Asian Conference on Applied Superconductivity & Cryogenics 2011 (ACASC 2011), New Delhi, November 16- 18, 2011.

4. "A comparative study on the structural and superconducting properties of carbon variants doped MgB_2". Neson Varghese, **S Rahul**, K M Devadas, Syju Thomas, A Sundaresan, S B Roy and U Syamaprasad. Presented at the Asian Conference on Applied Superconductivity & Cryogenics 2011 (ACASC 2011), New Delhi, November 16- 18, 2011.

5. "Nano diamond and nano SiO_2 – An effective combination to improve the in-field properties of MgB_2 superconductor". **S. Rahul**, Neson Varghese, K. Vinod, K. M. Devadas, Syju Thomas, P. Anees, M. K. Chattopadhyay, S. B. Roy, R. P. Aloysius and U. Syamaprasad. Presented at the 55th DAE Solid State Physics Symposium (DAE

SSPS 2010), Manipal, December 26 – 30, 2010. (Published in **AlP** Conf. Proc. 1349, 909)

6. "Enhanced superconducting properties of MgB_2 by carbon substitution using carbon containing nano additives". K. M. Devadas, Neson Varghese, K. Vinod, **S. Rahul**, Syju Thomas, J. B. Anooja, A. Sundaresan, S.B. Roy and U. Syamaprasad. Presented at the 55th DAE Solid State Physics Symposium (DAE SSPS 2010), Manipal, December 26 – 30, 2010. (Published in AlP Conf. Proc. 1349,913-914)

7. "Lowering the sintering temperature of MgB_2/Fe wires with high transport current by nano Cu doping". Neson Varghese, K. Vinod**, S. Rahul**, K. M. Devadas, Syju Thomas, P. M. Aswathy, S. Pradhan and U. Syamaprasad. Presented at the 55th DAE Solid State Physics Symposium (DAE SSPS 2010), Manipal, December 26 – 30, 2010. (Published in AlP Conf. Proc. 1349, 891-892)

8. Combined effect of burned rice husk and nano Ho_2O_3 on the in-field critical current density of MgB_2 superconductor. **S. Rahul**, G. R. Anuraghi, K. T. Jakson, Neson Varghese, K. Vinod and U. Syamaprasad, Presented at the International Conference on Advanced Functional Materials (ICAFM 2009), held at NIIST, Trivandrum on December 09-10, 2009. (Also published in the proceedings: page 51-52).

9. Hot pressing of electrically self-heated MgB_2/Fe PIT wires. K. Vinod, Neson Varghese, **S. Rahul** and U. Syamaprasad, Presented at the 53rd DAE Solid State Physics Symposium (DAE SSPS 2008), held at BARC on December 16- 20,2008.(Also published in the proceedings: vol 53 page 919-920).